NASA Contractor Report 180853
Flow Research Report No. 425

NASA-CR-180853
19880016473

Direct Simulations of Chemically Reacting Turbulent Mixing Layers—Part II

Ralph W. Metcalfe, Patrick A. McMurtry, Wen-Huei Jou, James J. Riley, and Peyman Givi

Flow Research Company
Kent, Washington

June 1988

Prepared for
Lewis Research Center
Under Contract NAS3-24229

National Aeronautics and
Space Administration

CONTENTS

1. SUMMARY

The objectives of this work are to continue the application of direct numerical simulation techniques to combustor flows and to use the simulations to develop a better understanding of the effects of turbulence on reactions. This work has involved three major tasks. First, we have performed simulations of chemical reactions without heat release in three dimensions to extend the results of our previous successful simulations. Second, we have performed high-resolution two and three-dimensional simulations of chemical reactions with heat release. These results have been compared with our previous calculations to determine the effects of heat release on reaction rate and flow field evolution. Finally, we have performed a series of simulations of three-dimensional turbulence decay for Dr. R. G. Deissler at NASA Lewis. We have designed, written, and debugged a code capable of performing simulations of three-dimensional reacting flows, and this code has been delivered to Mr. Russ Claus and Dr. Deissler at NASA Lewis to enhance the center's computational capability. The work on this contract has been an important component of the basic combustion research being conducted at the NASA Lewis Research Center.[1]

The extension of the three-dimensional work from Part I of this report[2] included some comparisons with laboratory data which showed good agreement in such quantities as average reactant concentration, rms fluctuating reactant concentration, rms fluctuating product concentration, and concentration correlations. Since there was no ad hoc modeling or adjustable parameters in these simulations, they have given strong evidence that this direct numerical simulation technique can accurately represent much of the important physics of this problem.

This technique was next extended to the study of reacting flows with chemical heat release. This problem was solved using both the fully compressible equations as well as an approximate set of equations that is asymptotically valid for low Mach number flows. These latter equations have the computational advantage that high-frequency acoustic waves have been filtered out, allowing much larger time steps to be taken. The two-dimensional simulation results showed that the rate of chemical product formed, the thickness of the

mixing layer, and the amount of mass entrained into the layer all decrease with increasing rates of heat release.

The subsequent three-dimensional simulations with heat release showed that, in agreement with previous laboratory experiments, the heat release is observed to lower the rate at which the mixing layer grows and to reduce the rate at which chemical products are formed. The baroclinic torque and thermal expansion in the mixing layer were found to produce changes in the flame vortex structure that act to produce more diffuse vortices than in the constant density case, resulting in lower rotation rates of fluid elements. Previously unexplained anomalies observed in the mean velocity profiles of reacting jets and mixing layers were shown to result from vorticity generation by baroclinic torques. The density reductions also lowered the generation rates of turbulent kinetic energy and the turbulent shear stresses, resulting in less turbulent mixing of fluid elements.

Calculations of the energy in the various wave number modes showed that the heat release has a stabilizing effect on the growth rates of individual modes. A linear stability analysis of a simplified model problem confirmed this, showing that low-density fluid in the mixing region will result in a shift of the frequency of the unstable modes to lower wave numbers. The growth rates of the unstable modes decrease, contributing to the slower growth of the mixing layer.

Finally, an overall assessment of the status of the direct numerical simulation approach to the study of turbulent, reacting flows was made. While the strong constraints of spatial and temporal resolution of these methods will not be overcome in the near future, a great deal of useful information about the physics of such flows is available from these simulations, and the development of better subgrid-scale models will permit the implementation of the large eddy simulation technique to flows in more complex geometries.

2. *SIMULATIONS OF A THREE-DIMENSIONAL, COLD, REACTING MIXING LAYER*

The results of the numerical simulations begun in the previous contract period were further analyzed and compared with experimental data. The simulations agree very well with the predictions of self-similarity theory, yielding approximately linear growth rates of various computed length scales, including the mean velocity half-width, the mean vorticity thickness, and the mean product thickness. In addition, mean profiles of the average reactant concentrations, the rms fluctuating reactant concentrations, the concentration correlations, the average product concentrations, and the rms fluctuating product concentrations collapsed in a manner consistent with self-similarity theory. This was not an artifact of the initial conditions, since the initial concentration fields were not in the self-similar form, and the self-similarity was maintained over a time in which the width of the layer grew by a factor of 5. Simulation results also compared reasonably with laboratory data. Computed profiles that were qualitatively similar to corresponding laboratory profiles were obtained for the average reactant concentrations, the rms fluctuating product concentrations, and the concentration correlations. Computed profiles of average product concentrations were in approximate agreement with laboratory data.

In the course of this work, a detailed analysis was made of the accuracy of these techniques when applied to the simulation of chemically reacting flows. When the reaction rate is large relative to the species diffusivity, steep gradients can develop in the concentration fields during the course of the simulation, even though the initial fields are smooth. Thus, the accuracy of a simulation can decrease with time until significant errors develop. Some test calculations were performed in which the exact analytical solution was known so that the resulting numerical errors could be quantitatively estimated. These simulations showed that in the limit as the time stepping errors approached zero, the superalgebraic convergence (or infinite order accuracy) characteristic of spectral methods could be maintained.

The results of this work are described in much greater detail in the two papers reproduced in two papers by Riley et al.[3] [4]

3. *TWO-DIMENSIONAL MIXING LAYERS WITH HEAT RELEASE*

The purpose of this aspect of the work was to begin an investigation into the interactions between chemical heat release and fluid dynamics in a mixing layer. This is an extension of the previous work in which the chemical reaction was a passive process, and thus did not affect the fluid motion. In a reacting flow with heat release, the dynamics of the fluid motion are coupled with the chemical reaction through the inhomogeneous density distribution caused by the thermal expansion. This problem can be attacked by solving the compressible Navier-Stokes equations with heat production, together with the species transport equations. This set of equations contains the vorticity, entropy and acoustic modes, which can be of greatly different frequencies. In particular, for low subsonic fluid motion, the acoustic modes are in frequency bands much higher than the other two modes. Due to this high frequency, the acoustic fluctuations do not interact effectively with either the vorticity mode or the entropy mode. From the computational point of view, tracking the acoustic fluctuations requires extremely small time steps, thus decreasing the efficiency of the computation. To mitigate this constraint, a set of approximate equations was derived, asymptotically valid for small Mach number flows.

The validity of the low Mach number approximation in the parameter range of the simulations performed here was tested by solving the exact, fully compressible equations for a reacting mixing layer with a Mach number of 0.2. Vorticity contours obtained from solutions of the exact and approximate equations showed that although acoustic waves propagate throughout the flow field, they apparently have no influence on the vorticity dynamics. Simulations of the two-dimensional mixing layer undergoing vortex rollup showed that the effect of heat release was to reduce significantly the amount of product produced in the layer. Because of the decrease in density caused by exothermic chemical reactions, the heat release and resulting density changes act to decrease the rate of mass entrainment into the layer, since the overall layer growth is approximately unchanged from the cold flow case. This is in qualitative agreement with the experimental findings of Wallace,[5] who conducted an experimental study of mixing layers that included a chemical reaction with weak heat release.

The variations in density permit a major new source of vorticity generation in the form of

baroclinic torques. This tends to reduce the vorticity near the outer edges of the layer, inhibiting the rollup process. Another effect of heat release is to raise the viscosity of the flow. This can also have a stabilizing effect on the flow.

An important result of this aspect of the work was to demonstrate the effectiveness of the direct numerical simulation approach as a predictive tool in studying complex reacting flows with heat release. This clearly suggested the importance of extending this computational capability to three-dimensional flows. A detailed discussion of the derivation of the low Mach number approximation equations, the numerical solution procedure and results of the simulations are given in the paper reproduced in Appendix A.[6]

4. HEAT RELEASE IN CHEMICALLY REACTING TURBULENT MIXING LAYERS

The results of the two-dimensional simulations with heat release showed that the presence of heat release produced a stabilizing effect on the flow field. However, in fully turbulent mixing layers, other secondary modes of instability are present which could change this situation. In order to investigate this possibility, a fully three-dimensional code was developed to simulated reacting flows under the following conditions. First, to ease time stepping stability constraints, low Mach number approximation equations were used to filter out acoustic waves. Second, a single binary, irreversible reaction between two species to form a product was used. The reaction rate was independent of the temperature. Third, the viscosity, thermal and molecular diffusivities and the specific heats were taken to be temperature- independent constants. Finally, the amount of heat release was restricted in order to ensure that large velocities would not be generated by the reaction to violate the low Mach number approximation.

The computational domain was chosen to be large enough to contain the most unstable mode and its subharmonic. The velocity field was initialized by adding a hyperbolic tangent velocity profile to a low- level, three-dimensional, broad-band background perturbation field. In addition, in the "forced" simulations, an additional perturbation in the form of the most unstable mode and its subharmonic was added. These forced simulations are analogous to laboratory experiments in which well-defined harmonic perturbations are introduced into the flow at, or upstream of, the splitter plate. The chemical reactant fields were initially two-dimensional and consisted of two species fields that were offset so that there was initially no overlap between them.

In three spatial dimensions, an additional secondary instability mechanism comes into play. At large amplitudes, it is manifest as streamwise, counter-rotating vortex tubes on the braids between the vortex cores. The effect of these structures on the flow field is to induce a velocity field that acts to pump fluid between the two layers, thereby further convoluting the reaction interface. This tends to increase mixing between the two streams and enhance the chemical reaction rate.

In spite of these additional instabilities, the effect of heat release on the chemical product

formation is very much similar to the two-dimensional results. Heat release tends to reduce the product generation, again by inhibiting the mixing between the two streams. When the flow is forced, by including the two-dimensional most unstable mode and its subharmonic, the product generation is greater than without forcing but is still significantly less than in the comparable run without heat release. However, the three-dimensional modes do enhance the product generation compared to the strictly two-dimensional runs by providing an additional mechanism for wrinkling the flame front and increasing the intercomponent mixing. For the growth of the mixing layer thickness, there is a small initial enhancement, followed by a decrease in the layer growth rate. These results are qualitatively similar to those obtained experimentally by Wallace[5] and Hermanson[7] and are consequences of lower rates of fluid entrainment into the mixing region when exothermic chemical reactions occur.

An analysis of the turbulent kinetic energy equation for these simulations showed that the most important effects of heat release are significant reductions in the turbulence production and turbulent transport. In the case of the production term, the lower density resulting from the combustion is directly responsible for most of this change. Transport by the fluctuating motion decreases in the heat release runs simply because the turbulence levels are lower. The heat release results in a production of turbulent kinetic energy along the center of the mixing layer through the expansion part of the velocity-pressure gradient correlation. However, the production is small in these simulations compared with the decrease in the exchange of energy with the mean flow, yielding an overall lower turbulent kinetic energy profile. As heat release is increased, there can be a significantly greater conversion of internal energy to kinetic energy. With much higher heat release, this could possibly result in an overall increase in the kinetic energy.

The reduction in mixing layer growth and turbulence production observed in the simulations with heat release is also consistent with the results of a simplified linear analysis based on linear profile approximations to the mean velocity density fields. This analysis shows that, in the presence of heat release, there is a shift of the most unstable wave number to a lower value and a decrease in the value of the largest wave number that is still unstable, and there is also a decrease in the growth rate of the most unstable mode. The precise effect of these stabilizing

factors depends on the relative time scales involved in the manifestation of the primary instabilities and the time scales over which the density decreases develop. However, the net result of this analysis is to show that heat release can be strongly stabilizing, both in the linear as well as in the nonlinear regime.

A more complete analysis of these simulations is given in a paper by McMurtry et al.[8] and the paper provided in Appendix B,[9] as well as in the Ph.D. thesis of McMurtry.[10]

5. *FURTHER ANALYSIS OF THREE-DIMENSIONAL SIMULATIONS*

5.1 Computation of Probability Density Functions

We have employed results of direct numerical simulations to construct the probability density function of a conserved scalar variable in a perturbed three-dimensional temporally evolving mixing layer. Calculations have been performed to a time just before mixing transition, and the results are comparable to experimental data obtained in the same region. Some additional simulations were performed to explore the possibility of extending the simulation procedure to larger domains.

Probability density functions have proven useful in the theoretical treatment of turbulent reacting flows since the early work of Hawthorn et al.[11] An approach based on the single-point probability density function of the scalar variables has the advantage that the effects of chemical reactions appear in closed form, eliminating the need for any turbulence modeling associated with the scalar-scalar correlations. However, models are needed for the closure of the molecular mixing term and also the turbulent convection.

In previous work,[12] [13] [14] the pdf approach was employed in a variety of turbulent reacting shear flows, and the results were compared with available experimental data under similar hydrochemical conditions. In this work, the effects of the molecular mixing term were modeled by a coalescence/dispersion model, and the turbulent flux of the pdf was modeled by a simple gradient diffusion approximation.

As far as the first few moments are concerned, the results obtained from the pdf transport equation are in reasonable agreement with experimental data. However, a major difference between the calculated and measured shape of the pdf was observed in the two-stream plane mixing layer calculations.

The experimentally observed shape of the pdf is dependent on the streamwise location, where the pdf is measured. Measurements of Konrad[16] and Koochesfahani[16] in nonreacting mixing layers indicate that below the mixing transition point, the concentration field consists of pure

unmixed fluid originating from either the high- or low-speed stream, and mixed fluid is found only at the thin interface separating the two fluids. Under these conditions, the shape of the pdf is rather simple. It has spikes only at values corresponding to the free stream concentrations and is negligible at other concentration values. Above the point of mixing transition, the experimental measurements indicate that there is a change in the shape of the pdf. It still consists of the two spikes at the concentration values corresponding to the free stream concentrations. However, a third peak in the mixing region of the shear layer is observed (Figure 1). The asymmetry of this peak indicates the excess of high-speed fluid species in the mixing core of the layer. Furthermore, experimental measurements show that the functional form of the pdf (including the position of the third peak) changes very little as the mixing layer is transversed.

Calculations based on a modeled pdf transport equation by Givi et al.[14] do not predict the shape of the pdf consistent with experimental observations. The predicted results indicate that the location of the pdf peak, with respect to the concentration coordinate, changes as the layer is transversed. The major reason for this discrepancy is due to the shortcomings associated with the gradient diffusion modeling of the turbulent flux of the pdf. It has been mentioned by Givi et al.[14] that in a mixing layer the inner turbulent region is often interrupted by the presence of irrotational surrounding flow. Therefore, a simple gradient diffusion assumption, which is a reasonable model for fully turbulent flows, would not be expected to result in plausible predictions in a highly intermittent flow such as the mixing layer.

With direct numerical simulation, it is possible to simulate the mixing layer directly without any need for additional modeling, as is usually required if the equations are statistically averaged. The results of the direct numerical simulations can be analyzed in order to obtain useful statistical information about the important vector and scalar variables. Comparison of such statistical quantities with experimental data is very useful in obtaining a better understanding of the important physical phenomena that occur in turbulent flows. The probability density function of a conserved scalar is constructed directly from the flow fields generated by the direct numerical simulations. The following results have been obtained for

the pre-transitional region of the mixing layer.

The initialization of the mean flow and the velocity perturbation fields is consistent with the RUN R simulations reported by Metcalfe et al.[17] The initial small amplitude random perturbations are superimposed on a mean hyperbolic tangent velocity profile. These linear perturbations grow as time progresses, and, as a result, the initially smooth flow experiences a period of transition before it reaches a fully turbulent state.

One way of determining whether the flow is in the pre- or post-transitional domain is to examine the growth of the vorticity thickness and the product thickness. Vorticity thickness is defined by

$$\delta\omega = \frac{\Delta U}{(\frac{\partial U}{\partial Y})_{max}}$$

The product thickness is a measure of the degree of mixing in the core of the mixing layer. One way of measuring the degree of mixing, experimentally, is to inject reactants on two sides of the mixing layer and measure the amount of product resulting from the chemical reaction between the two reactants. The reactants selected must have very fast chemical kinetics so that the amount of product formed is proportional to the amount of mixing. In such a system, the product thickness is defined by

$$\delta p = \frac{1}{(C_{B)_\infty}} \int_{-\infty}^{\infty} C_p dy$$

where C_p is the concentration of product and $(C_{B)_\infty}$ refers to the concentration in one of the streams.

Experimental evidence[18] indicates that, before mixing transition, both product thickness and vorticity thickness increase in the streamwise direction, while the ratio between the two remains more or less constant until the transitional point. Beyond this point, there is an abrupt increase in product formation and, therefore, a sharp increase in the ratio of the product thickness to the vorticity thickness. In one simulation, the product thickness and the

vorticity thickness, as well as the ratio between the two, are calculated directly from the instantaneous velocity and scalar fields. The product concentration is calculated by employing a fast chemistry model (flame sheet approximation[13]). This approximation relates the product concentration to the concentration of a conserved Shvab-Zeldovich scalar variable.

A plot of the normalized product thickness, normalized vorticity thickness, and the ratio between the two is presented as a function of time in Figure 2. Note that both thicknesses increase while the ratio between the two remains constant. At the time of $t^* = 160$, boundary effects become important, so this calculation was not continued beyond this point. The flow at this time is still in the pre-transitional mixing region, since there has not been a sharp increase in the ratio of the product thickness to the vorticity thickness.

The probability density function of a conserved scalar variable at the time of $t^* = 160$ is presented in Figure 3. The instantaneous free stream value of the concentration is equal to zero in the top stream and equal to 1 in the bottom stream. Analysis of this figure suggests that the mechanism of mixing before mixing transition is fairly simple in that the fluid across the shear layer width is essentially composed only of the fluid originating from the two streams. The experimental measurements of Koochesfahani[16] also show the same behavior for the pdf in the pre-transitional region. In this region, the fluid is either from the top stream or from the bottom stream, and strong mixing has not yet occurred.

5.2 Simulations on Larger Domains

In an attempt to carry the above simulations beyond the mixing transition regime, some studies were made as to the feasibility of reinitializing the code at the pre-transition point but on a larger domain. The basic procedure involved doubling the size of the computational domain in all three dimensions. The regions above and below the mixing layer were extended uniformly based on the values of the computational variables at the top and bottom boundaries. In the streamwise and spanwise directions, the periodicity length was doubled and the initial data were prescribed by retaining only alternate data points in the original calculation but repeating the sequence twice. Both calculations were then continued in time

so that they could be compared.

Figure 4 shows a three-dimensional perspective plot of the species concentration field C_B at a time of $t^* = 90$. This is after the first pairing and at the beginning of the second pairing on a domain of side 8π. The state of this field at $t^* = 120$ is shown in Figure 5, at which time the second pairing is taking place. The corresponding plots for the larger 16π domain are shown in Figures 6 and 7. This computation is then carried on further to $t^* = 150$ as shown in Figure 8.

While the perspective plots indicate strong similarities between the original and expanded simulations, a more quantitative analysis can be undertaken by examining the evolution of some of the low-order modes in the two simulations. Figure 9 shows the evolution of the energies in the mean flow and the second and third subharmonics for the original simulation. Note that the second subharmonic (E_{SH_2}) saturates by about $t^* = 80$, while the third subharmonic saturates by about $t^* = 130$. The behaviors of these modes in the simulations on the expanded domain from $t^* = 90$ to $t^* = 150$ are shown in Figure 10. Note that while there are some differences, the basic trends are similar, especially considering the fact that boundary effects are becoming significant in the original run by $t^* = 150$.

Based on these simulations, this grid expansion technique appears to have significant potential as a tool to further the study of reacting mixing layer dynamics well into the mixing transition regime.

6. *CONCLUSIONS AND DISCUSSION*

This contract research work has provided the first major applications of the direct numerical simulation approach to reacting flows. In the first place, the possibility of employing high-resolution spectral numerical methods to reacting flows was examined and shown to be feasible through a series of test calculations. That the retention of the critical superalgebraic convergence property of spectral methods was possible when applied to the simulation of moderately fast reactions in a mixing layer undergoing nonlinear vortex pairing was demonstrated quantitatively. The three-dimensional simulations showed the relative importance of secondary instabilities in the flow and the role they have in mixing enhancement. Comparisons of the results of these simulations of a fully turbulent flow with experiments and self- similarity theory showed excellent agreement on a number of statistical quantities, especially considering that there were no adjustable parameters or ad hoc constants in the model.

The extension of this work to the more complex case with heat release was successfully undertaken. Initial simulations, involving the pairing of large-scale, two-dimensional vortical structures in the mixing layer, showed that heat release can have a strongly stabilizing effect on the flow, in agreement with laboratory experiments. An analysis of these and later three-dimensional simulations showed that this stabilization was due to both linear and nonlinear effects. The thermal expansion tends to reduce the growth rates of the unstable modes in a laminar mixing layer, as does the reduction in Reynolds stress production and generation of baroclinic torques in the nonlinear regime.

The principal advantages of the direct numerical simulation approach include the following: the flow can be examined in detail, since all quantities are known at each point in space and time; parameters can be easily varied and experimental conditions are easily controlled; large-scale structures are directly computed. The main disadvantage is in the limited spatial and temporal resolution available. For reacting turbulent flows at realistic Reynolds and Damkohler numbers, it is often necessary to include a subgrid-scale model. The development of accurate subgrid-scale models for such simulations [often referred to as large eddy simulations (LES) to distinguish them from the unmodeled full turbulence simulations (FTS)]

is one of the most critical issues that needs to be addressed in order to extend the power of these methods to more practical situations. Present subgrid-scale models for nonreacting flows rely on hypotheses regarding the nonlinear cascade of energy from large to small scales and the universality of motion at high wave numbers. For large Damkohler numbers, heat release and other chemical reaction effects could significantly modify such behavior. Thus, the development of accurate, physically derived subgrid-scale models is a very challenging task. One particularly promising approach is the application of renormalization group methods.[19] A more detailed comparison of the various approaches to the simulation of reacting turbulent flows is given in a paper by Jou and Riley.[20]

The simulations performed in this research work indicate that while there are limitations on Reynolds number and Damkohler number, important aspects of the physics are being properly represented and that the velocity and concentration fields being generated by these simulations provide a useful source of information about the dynamics of the reacting flow.

REFERENCES

1. Mularz, Edward J. and Claus, Russell W. (1985) *Combustion Research for Gas Turbine Engines*, presented at the **Seventh International Symposium on Air Breathing Engines,** Beijing, China, September 2 - 6.

2. Riley, James J., and Ralph W. Metcalfe (1984) Direct Simulations of Chemically Reacting Turbulent Mixing Layers, NASA Contractor Report 174640, 148 pp.

3. Riley, James J. and Metcalfe, Ralph W. (1985) **AIAA Paper AIAA-85-0321,** 14 pp.

4. Riley, James, J., Ralph W. Metcalfe, and Steven A. Orszag (1986) *Physics of Fluids*, **29:2** pp. 406-422.

5. Wallace, A. K. (1981) **Ph.D Thesis** University of Adelaide, Adelaide, Australia.

6. McMurtry, P. A., W. H. Jou, J. J. Riley, and R. W. Metcalfe (1985) **AIAA Paper AIAA-85-0143** 8 pp.

7. Hermanson, J. C. (1985) **Ph.D. Thesis** California Institute of Technology, Pasadena

8. McMurtry, P. A., J. J. Riley and R. W. Metcalfe (1986) **The American Institute of Chemical Engineers 1986 Annual Meeting,** Paper 148g. 32 pp.

9. McMurtry, P. A., J. J. Riley, and R. W. Metcalfe (1987) **AIAA Paper No. AIAA-87-0131,** 22 pp.

10. McMurtry, P. A. (1987) **Ph. D Thesis** University of Washington, Seattle.

11. Hawthorn, W. R., D. S. Wedell and H. C. Hottel (1949) in **Third Symposium (International) on Combustion,** pp. 266-268.

12. Givi, P., W. A. Sirignano and S. B. Pope (1984) **Combustion Science and Technology,** Vol. 37, pp. 59-78.

13. Givi, P., J. I. Ramos and W. A. Sirignano (1984) **Progress in Aeronautics and Astronautics,** Vol. 95, pp. 384-418.

14. Givi, P., J. I. Ramos and W. A. Sirignano (1985) **Journal of Non-Equilibrium Thermodynamics** Vol. 10, pp. 75-104.

15. Konrad, J. H. (1976) **Ph.D Thesis,** California Institute of Technology, Pasadena.

16. Koochesfahani, M. M. (1983) **Ph.D Thesis,** California Institute of Technology, Pasadena.

17. Metcalfe, R. W., A. K. M. F. Hussain, S. Menon and M. Hayakawa (1987) in **Turbulent Shear Flows 5,** Eds. Durst et al., Springer-Verlag, Berlin. pp. 110 - 123.

18. Breidenthal, R. E. (1978) **Ph.D Thesis** California Institute of Technology Pasadena.

19. Yakhot, V. and Orszag, S. A. (1986) *J. Sci. Comp.* Vol. 1. pp.3-51.

20. Jou, W. H. and Riley, J. J. (1987) **AIAA Paper No. AIAA-87-1324** 23 pp.

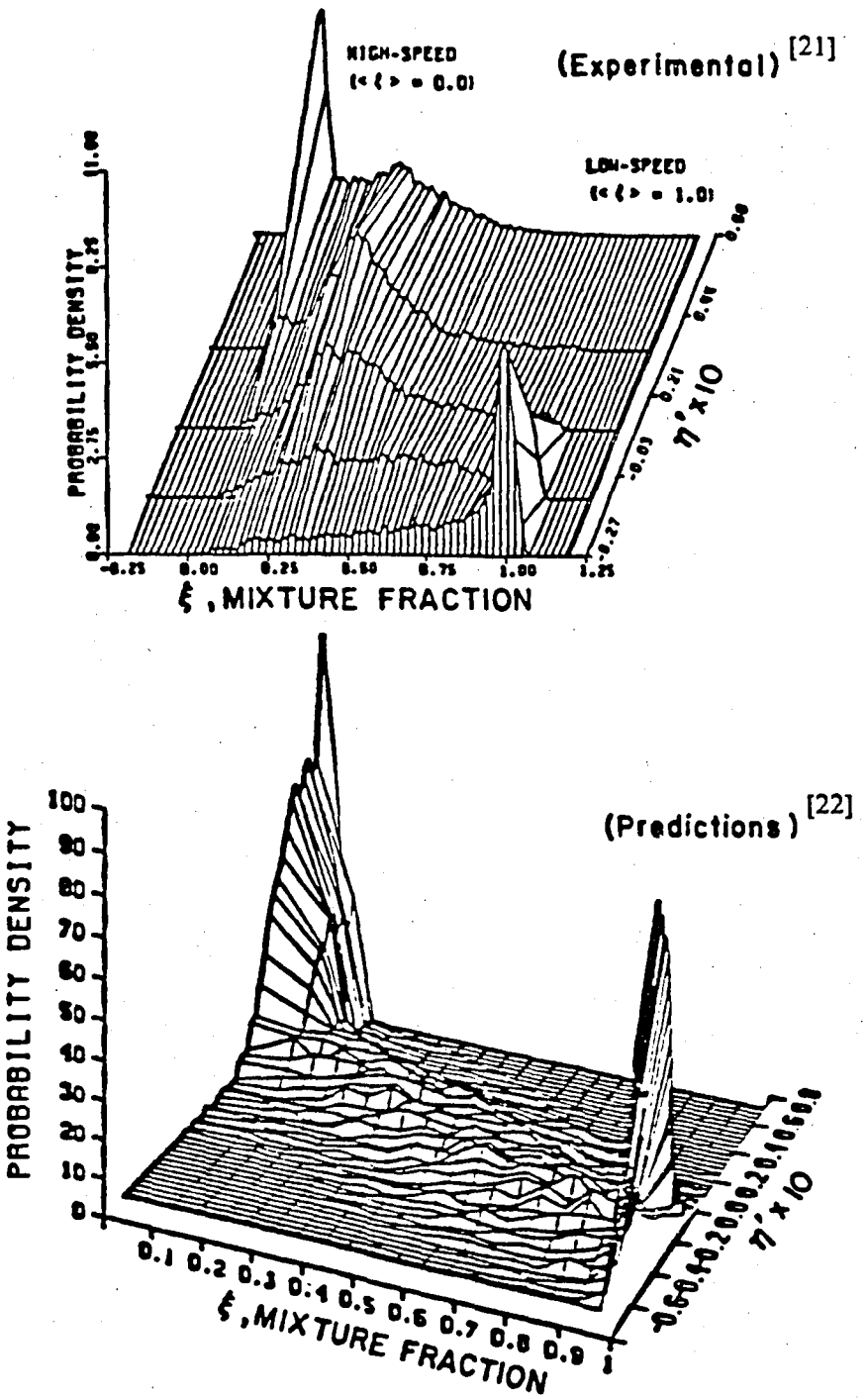

Figure 1. Comparison of measured and calculated pdf's of a normalized conserved scalar (the mixture fraction, ξ) at points across the mixing layer. The similarity coordinate, η', is the ratio of the cross-stream coordinate divided by the downstream distance from the virtual origin of the mixing layer. These pdf's represent conditions at a distance of $\approx$ 15 cm from the virtual origin.

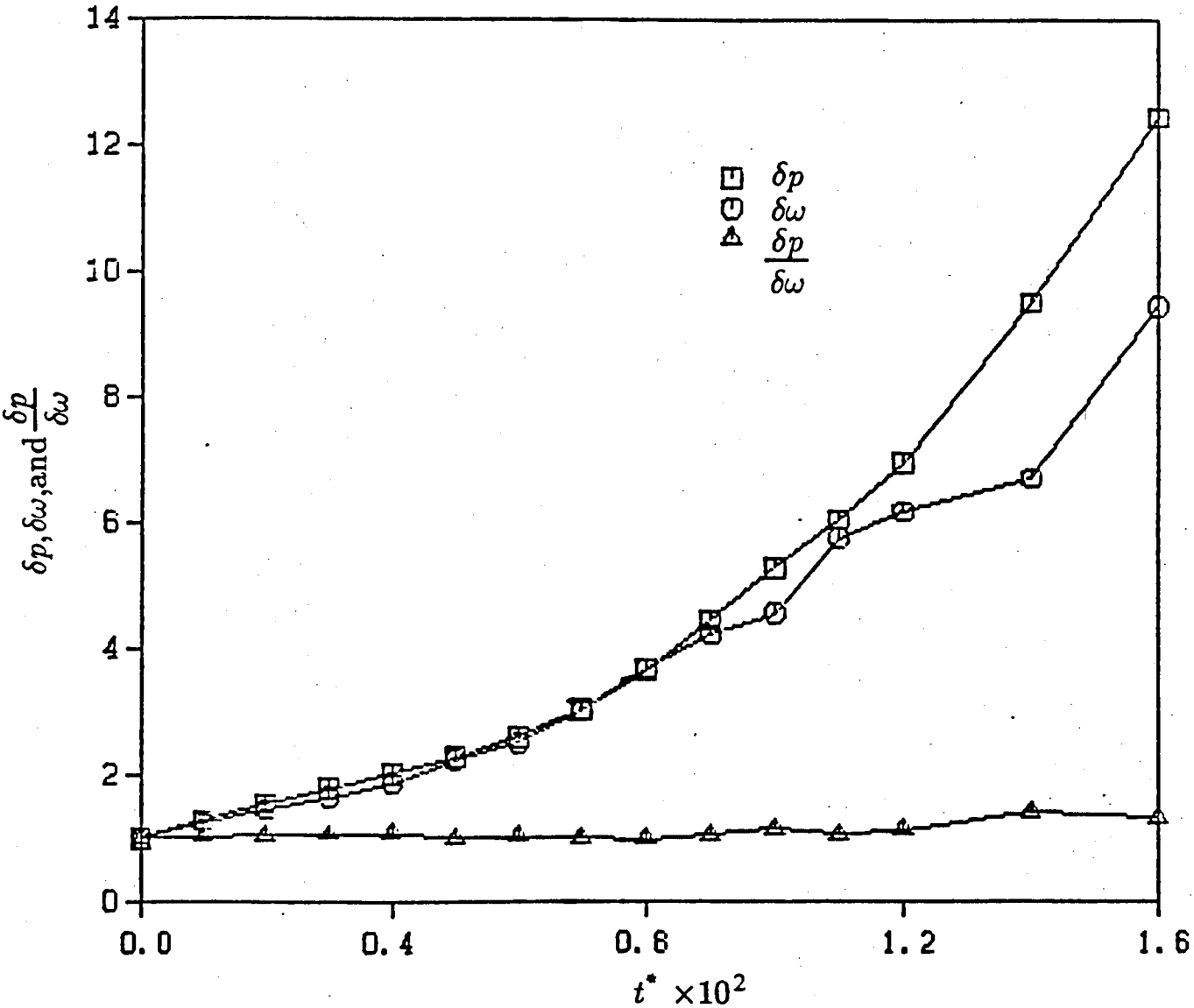

Figure 2. $\delta p, \delta\omega, \text{and} \frac{\delta p}{\delta\omega}$ vs. t^*.

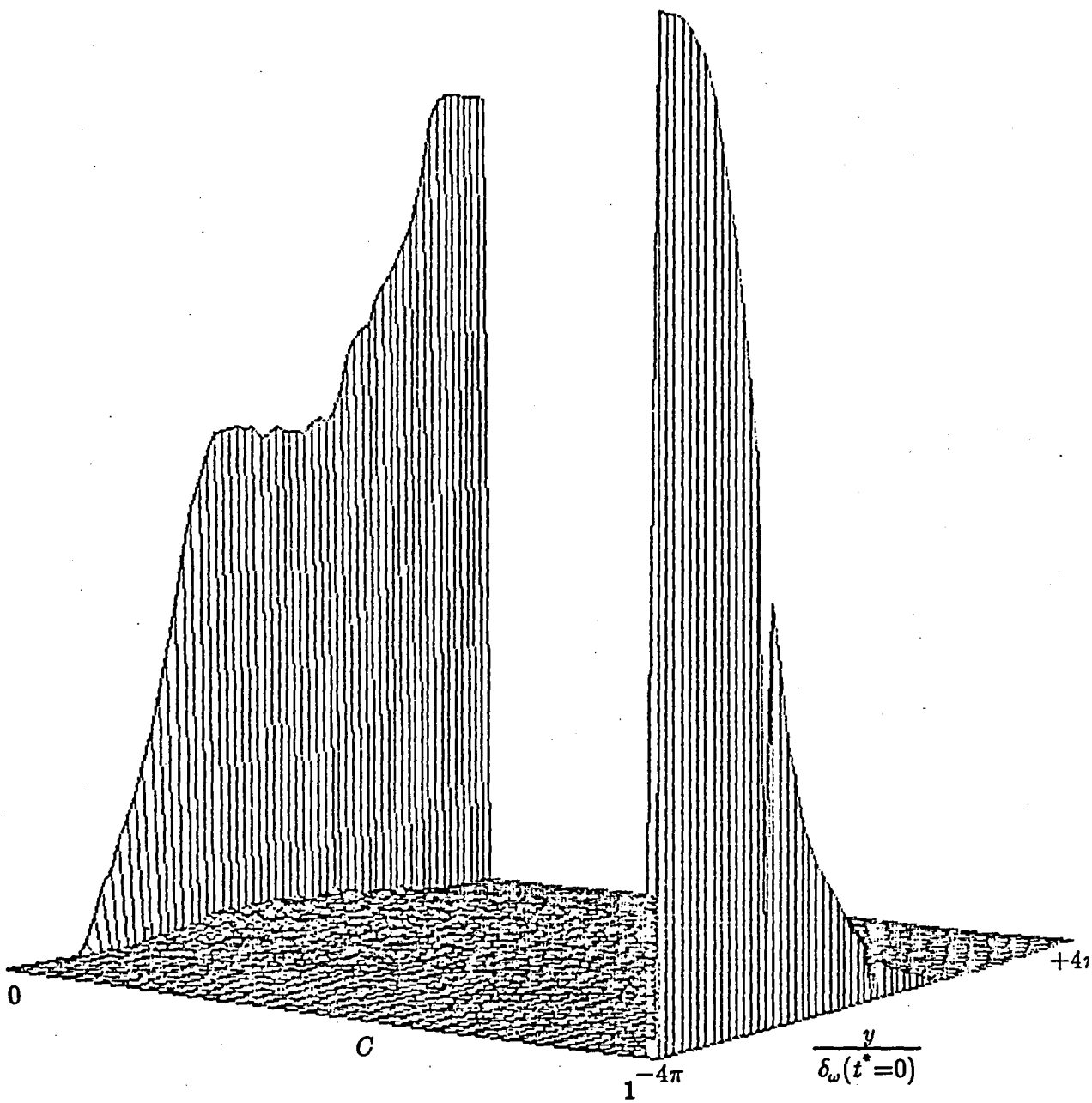

Figure 3. PDF of a conserved scalar **C** ($0 \leq C \leq 1$) as a function of y at $t^* = 160$.

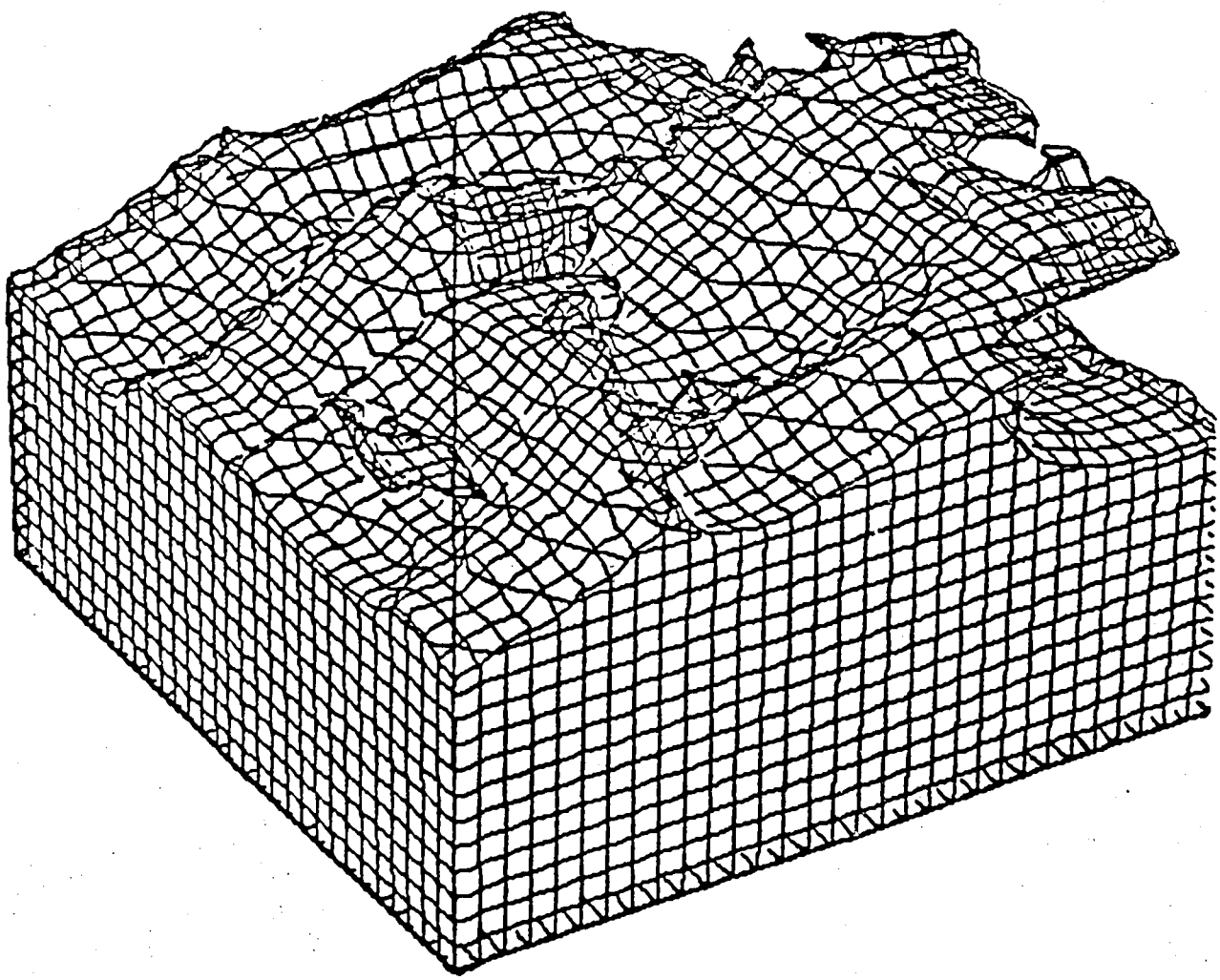

Figure 4. Three-dimensional perspective plot of species concentration field C_B at $t^* = 90$ on 8π domain.

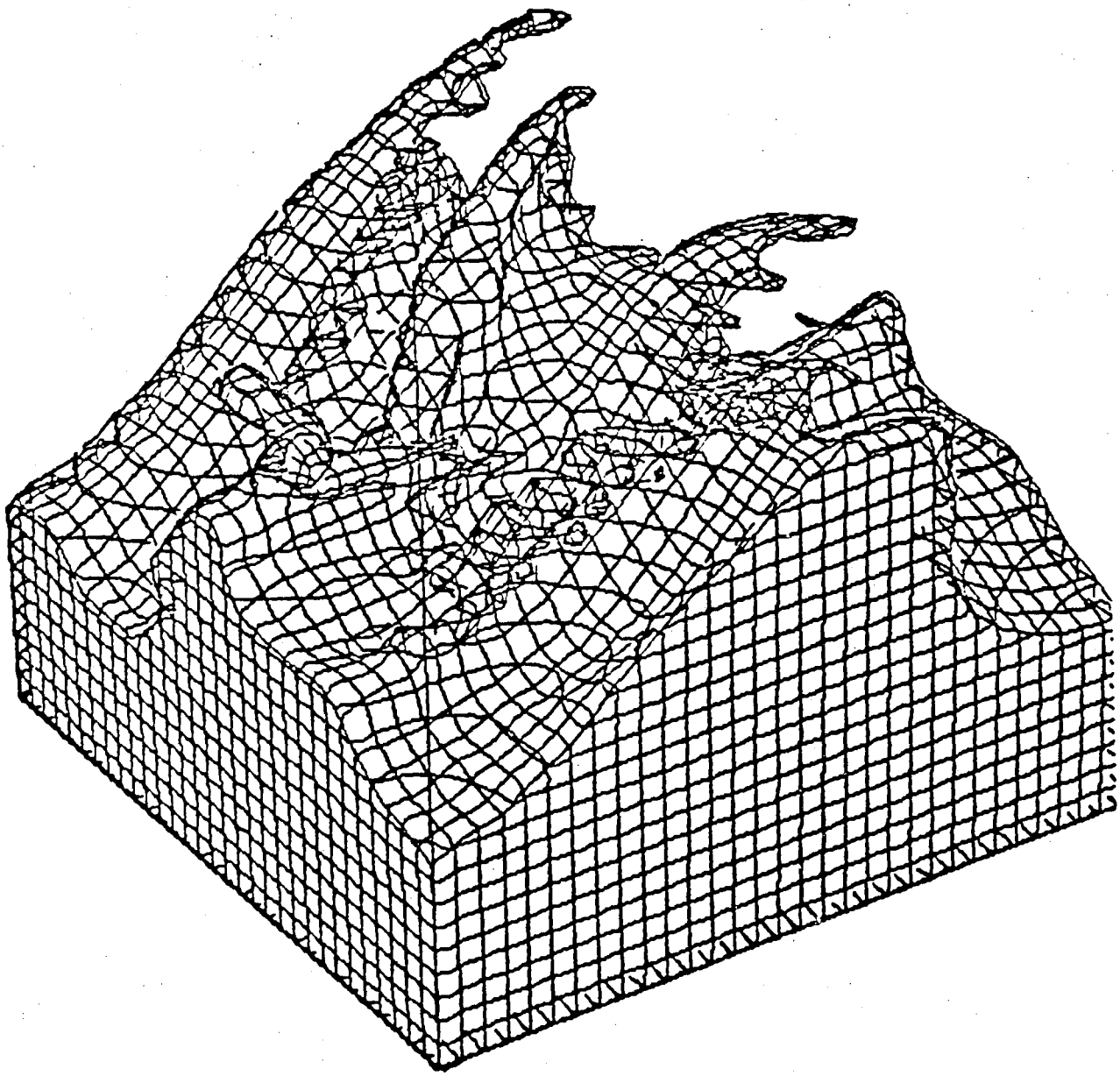

Figure 5. Three-dimensional perspective plot of species concentration field C_B at $t^* = 120$ on 8π domain.

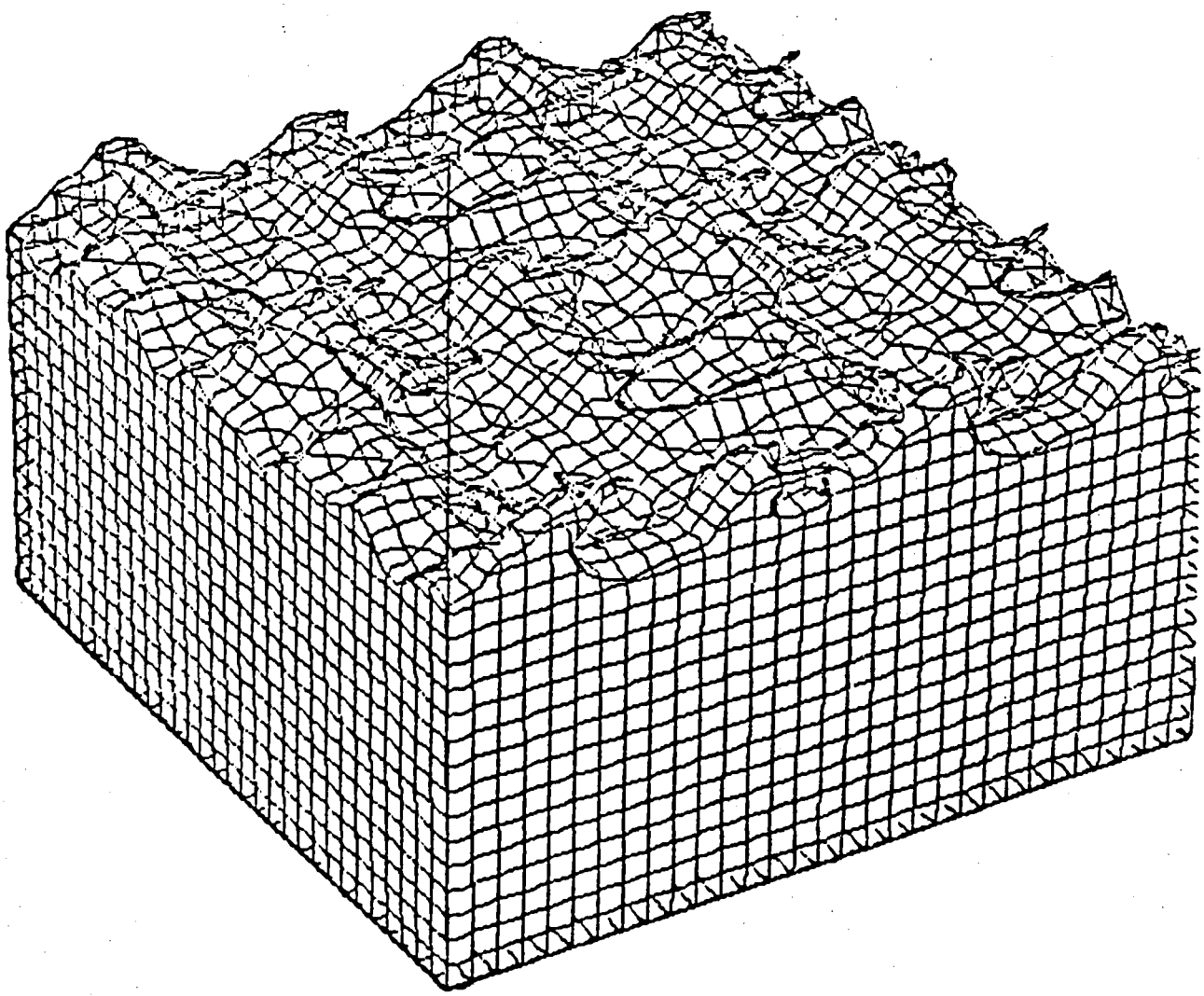

Figure 6. Three-dimensional perspective plot of species concentration field C_B at $t^* = 90$ on 16π domain.

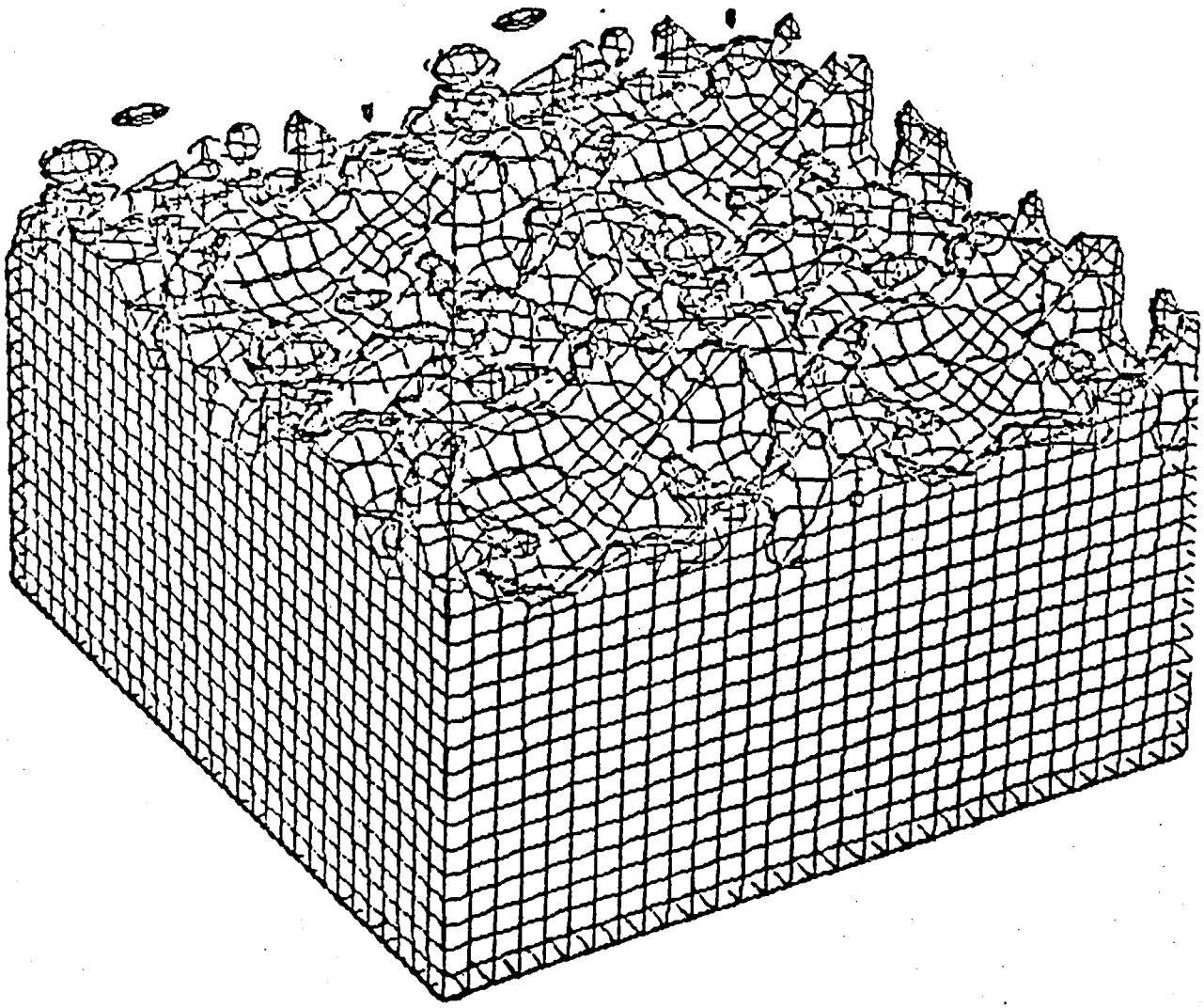

Figure 7. Three-dimensional perspective plot of species concentration field C_B at $t^* = 120$ on 16π domain.

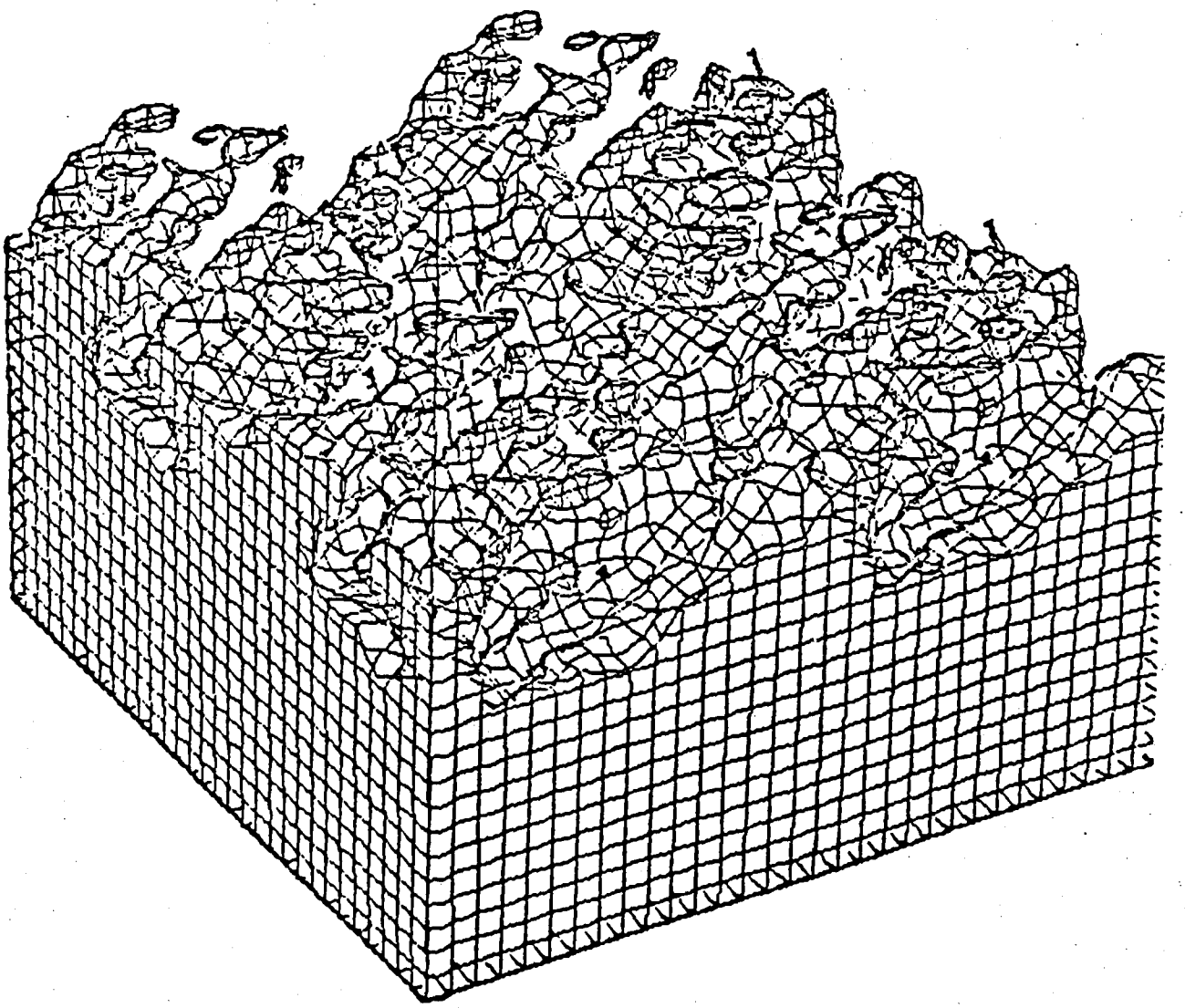

Figure 8. Three-dimensional perspective plot of species concentration field C_B at $t^* = 150$ on 16π domain.

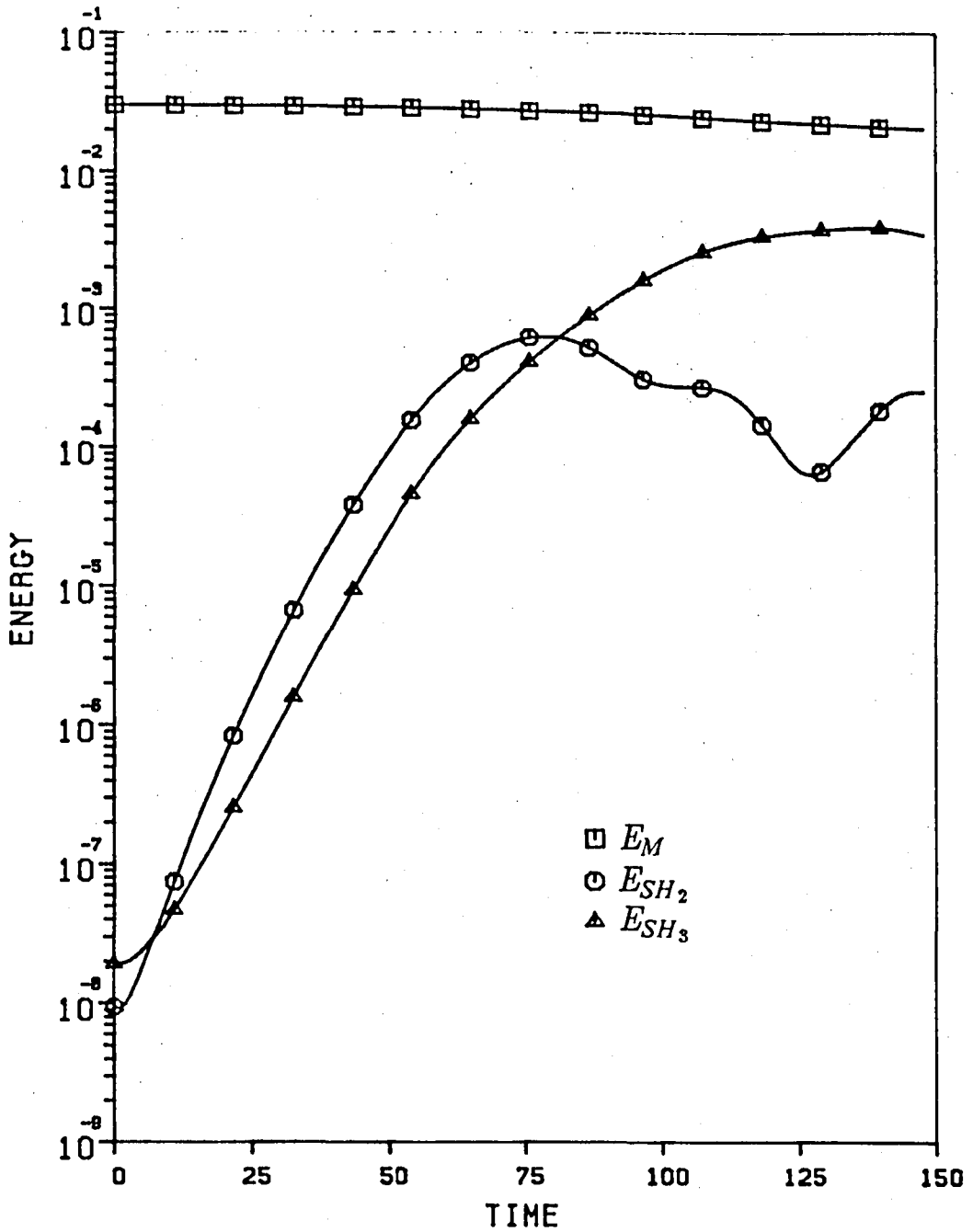

Figure 9. The evolution of the energies in the mean flow, E_M, and the second and third subharmonics, E_{SH_2},E_{SH_3}, for the turbulent mixing layer simulation in the 8π domain.

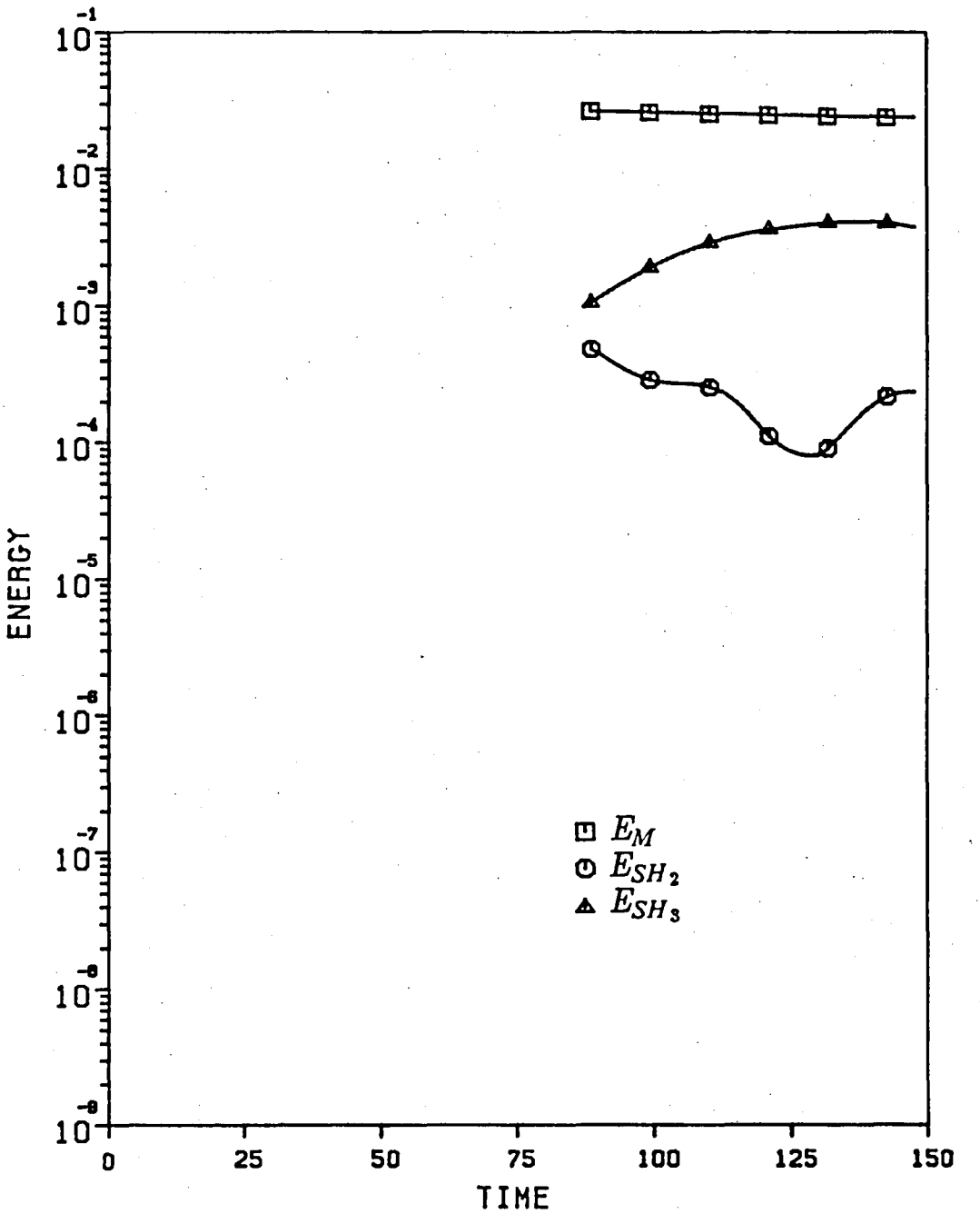

Figure 10. The evolution of the energies in the mean flow, E_M, and the second and third subharmonics, E_{SH_2},E_{SH_3}, for the turbulent mixing layer simulation in the 16π domain.

APPENDIX A

DIRECT NUMERICAL SIMULATIONS OF A REACTING MIXING LAYER WITH CHEMICAL HEAT RELEASE

P.A. McMurtry*, W.-H. Jou,**
J.J. Riley†, and R.W. Metcalfe††
Flow Industries, Inc.
Kent, Washington

Abstract

In order to study the coupling between chemical heat release and fluid dynamics, we have performed direct numerical simulations of a chemically reacting mixing layer with heat release. We have treated the fully compressible equations as well as an approximate set of equations that is asymptotically valid for low Mach number flows. These latter equations have the computational advantage that high frequency acoustic waves have been filtered out, allowing much larger time steps to be taken in the numerical solution procedure. A detailed derivation of these equations along with an outline of the numerical solution technique is given. Simulation results indicate that the rate of chemical product formed, the thickness of the mixing layer, and the amount of mass entrained into the layer all decrease with increasing rates of heat release.

Nomenclature

C_i - molar concentration of ith chemical species
Ce - nondimensional heat release parameter
C_v - specific heat at constant volume
Da - Damkölher number
e - internal energy
L_o - wavelength of fundamental perturbation mode
M - Mach number
p - pressure
p^0 - thermodynamic pressure
p^1 - dynamic pressure
$\dot{P}$ - dimensionless heat source
Pe - Peclet number
$\vec{q}$ - heat flux vector
Q - rate of heat release
R_i - rate of reaction of ith chemical species
Re - Reynolds number
t - time
T - temperature
U - velocity difference across mixing layer
v - magnitude of velocity
$\vec{v}$ - velocity vector
$\vec{x}$ - position vector
γ - ratio of specific heats
ε - γM^2
ρ - density
$\bar{\tau}$ - stress tensor

1. Introduction

The development of accurate combustion models relies on understanding more fully the fundamental interactions among the thermal, chemical, and fluid dynamical processes in reacting flow systems. The work reported here is directed at studying the interactions between chemical heat release and fluid dynamics, one of the least understood aspects of combustion. To achieve this purpose we have performed direct numerical simulations of a two-dimensional, temporally growing mixing layer, including a single step, irreversible chemical reaction between initially unmixed chemical species. The idea of direct numerical simulations is to use very accurate and efficient numerical methods to solve the governing equations for the detailed time evolution of the complex flow field. The appeal of this method is that no closure modelling is necessary and the complete flow field is known at every instant so that any statistical quantities of interest may be computed. The main disadvantage of this method is the limited range of spatial and temporal scales that can be resolved, restricting accurate numerical resolution to moderate Reynolds numbers. No turbulence or transport modelling has been attempted, limiting our study to the large scale features of the fluid motion. However, the large-scale motions play a significant role in the evolution of a mixing layer and do not depend strongly on the Reynolds number[1].

Previous direct numerical simulations of an incompressible reacting mixing layer without heat release[2] focused on how the turbulent flow field affects chemical reaction rates. This work has given physical insight into how the vortex rollup and three-dimensional turbulence affect the chemical reaction. Furthermore, from comparison of simulation results with laboratory data, this work has also led to increased confidence in the application of the direct numerical simulation methodology to this class of problems. However, because no heat was released, the chemical reaction was a passive process and did not influence the fluid motion. In a reacting flow with heat release, the dynamics of the fluid motion are coupled with the chemical reaction through the nonhomogeneous density distribution caused by the thermal expansion. The work presented here attempts to include coupling between the chemical reaction, the heat release, and the flow field.

To accomplish this goal, one may proceed to solve the compressible Navier-Stokes equation with heat production, together with the species transport equations. This set of equations contain the vorticity, entropy and acoustic modes from the linearized disturbance point of view.[3] In many practical cases, these modes are of greatly different frequency. Particularly, for low subsonic fluid motion, the acoustic modes are in frequency bands much higher than the other two modes. Since the frequency of these modes is high, the acoustic fluctuations do not interact effectively with either the vorticity mode or the entropy mode. From the computational point of view, tracking the acoustic fluctations requires extremely small time steps, thus decreasing the efficiency of the computation

* Graduate Student, Mechanical Engineering, University of Washington
** Senior Research Scientist, Member AIAA
† Associate Professor, Mechanical Engineering, University of Washington, Member AIAA
†† Senior Research Scientist

as far as the vortex/entropy dynamics are concerned. For these reasons, we have derived a set of approximate equations asymptotically valid for small Mach number flows. This derivation is given in Section 2.

In Section 3, a numerical solution procedure to solve the governing equations is outlined. The differences between the method used here and similar solution techniques for unsteady, imcompressible fluid flows are pointed out.

Although a turbulent mixing layer is inherently three-dimensional, the two-dimensional simulations discussed here reveal important information about some of the dominant features. Laboratory experiments have shown that, at least in its early stages, the mixing layer is dominated by large-scale, two-dimensional vortices, with the growth of the layer dominated by the pairing of these vortices.[4] Two-dimensional simulations have been shown to accurately portray the characteristic large-scale rollup and vortex pairing process of mixing layers.[5] Implications of heat releasing chemistry on this process can thus be meaningfully addressed with two-dimensional simulations. In Section 4, simulation results with and without heat releasing chemistry are presented.

2. Low Mach Number Approximation

Detailed numerical solutions to general combustion processes are prohibited by excessive computer storage requirements and unacceptable computational expense. This results in part from the wide range of time and space scales present in reacting flow problems. For example, accurate resolution of steep gradients of reacting species may require a grid spacing orders of magnitude finer than that necessary to resolve other characteristic flow structures. Similarly, time scales characterizing acoustic wave propagation may be orders of magnitude smaller than time scales characterizing convection processes. It is this last problem to which attention is directed here.

The existence of high frequency acoustic waves places a severe restriction on the time stepping increments used to numerically advance the fully compressible equations in time. To deal with this difficulty an approximate set of equations has been derived for low Mach number flows. These equations have the computational advantage that acoustic waves have been filtered out, relieving the above mentioned time stepping constraint. However, at the same time they allow density nonuniformities resulting from heat release to develop. In the following, we have started from the exact governing equations. By using a small Mach number expansion, a set of ordered approximate equations is obtained. A set of criteria on other non-dimensional parameters for the problem can also be obtained for the applicability of the approximation. The approach used is similar to that of Rehm and Baum,[6] who derived approximate equations for buoyantly driven flows with slow heat addition. Application of similar equations in subsonic reacting flows have been discussed by Oran and Boris[7], although the distinction between the lowest order pressure and the first order pressure was not pointed out. This distinction is essential in both a theoretical framework and the numerical procedure.

Governing Equations

The conservation equations of mass, momentum, energy, and chemical species may be written in the following form.

$$\frac{\partial \rho}{\partial t} + \nabla\cdot(\rho\vec{v}) = 0 \tag{1a}$$

$$\rho \frac{D\vec{v}}{Dt} = -\nabla p + \nabla\cdot\bar{\tau} \tag{1b}$$

$$\rho \frac{D}{Dt} E = -\nabla\cdot(p\vec{v}) - \nabla\cdot\vec{q} + \nabla\cdot(\bar{\tau}\cdot\vec{v}) + Q \tag{1c}$$

$$\frac{\partial C_i}{\partial t} + \nabla\cdot(C_i\vec{v}) = R_i + \nabla\cdot(D_i\nabla C_i) \ , \tag{1d}$$

where

$$E = e + \frac{1}{2} v^2 \ .$$

In a perfect gas in which the molecular weights of the individual species are approximately equal, the equation of state is

$$p = \rho RT \ . \tag{1e}$$

The variables are scaled by their respective reference quantities as

$$\begin{aligned} \rho &= \rho_o \rho' \\ \vec{v} &= U_o \vec{v}' \\ P &= (\rho_o R T_o) p' \\ e &= (C_v T_o) e' \\ \dot{Q} &= Q_o \dot{P} \\ \vec{x} &= L_o \vec{x}' \\ t &= \frac{L_o}{U_o} t' \ . \end{aligned} \tag{2}$$

In (2), the primed variables are dimensionless and the subscripted variables refer to the reference state. The resulting nondimensional equations, with the primes now dropped from the dimensionless variables, are

$$\frac{\partial \rho}{\partial t} + \nabla\cdot(\rho\vec{v}) = 0 \tag{3a}$$

$$\gamma M^2 \rho \frac{D\vec{v}}{Dt} = -\nabla p + \frac{\gamma M^2}{Re} \nabla\cdot\bar{\tau} \tag{3b}$$

$$\rho \frac{D}{Dt} E = -\nabla\cdot((\gamma-1)p\vec{v}) - \frac{1}{PrRe} \nabla\cdot\vec{q} + \frac{(\gamma-1)\gamma M^2}{Re} (\nabla\cdot(\bar{\tau}\cdot\vec{v})) + Ce\dot{P} \tag{3c}$$

$$\frac{\partial C_i}{\partial t} + \nabla\cdot(C_i\vec{v}) = Da\, R_i + \frac{1}{Pe} \nabla^2 C_i \tag{3d}$$

$$p = \rho T \tag{3e}$$

$$E = T + \frac{1}{2} \gamma(\gamma-1) M^2 v^2 \ .$$

To close this system of equations the following constitutive relations must be provided

$$R_i = R_i(C_i, T)$$
$$\dot{P} = \dot{P}(R_i)$$
$$\vec{q} = \vec{q}(\nabla T)$$
$$\tilde{\tau} = \tilde{\tau}(\nabla \vec{v}) \quad .$$

Pr, Re, Da, and Pe are the Prandtl, Reynolds, Damköhler, and Peclet numbers, respectively. The parameter Ce is given by

$$Ce = \frac{Q_o L_o}{U_o \rho_o C_v T_o} \quad .$$

For the validity of the low Mach number approximation, Q_o must be restricted such that Ce = o(1). If Ce >> 1, large velocities will be generated by the combustion, and the low Mach number approximation will not be valid.

Small Mach Number Expansion

Defining $\epsilon = \gamma M^2$ and assuming that $\epsilon << 1$, the dependent variables may be expanded as power series in ϵ:

$$\begin{aligned} \rho &= \rho^{(0)} + \epsilon\rho^{(1)} + \ldots \\ \vec{v} &= \vec{v}^{(0)} + \epsilon\vec{v}^{(1)} + \ldots \\ p &= p^{(0)} + \epsilon p^{(1)} + \ldots \\ T &= T^{(0)} + \epsilon T^{(1)} + \ldots \\ C_i &= C_i^{(0)} + \epsilon C_i^{(1)} + \ldots \end{aligned} \qquad (4)$$

Substituting equations (4) in (3) and collecting the zeroth order terms in ϵ results in the following lowest order equations:

$$\frac{\partial \rho^{(0)}}{\partial t} + \nabla\cdot\left[\rho^{(0)} \vec{v}^{(0)}\right] = 0 \qquad (5a)$$

$$\nabla p^{(0)} = 0 \qquad (5b)$$

$$\rho^{(0)} \frac{D^{(0)}}{Dt} T^{(0)} = -(\gamma-1) p^{(0)} \nabla\cdot\vec{v}^{(0)} + \frac{1}{PrRe} \nabla\cdot\vec{\gamma}^{(0)} + Ce\dot{P} \qquad (5c)$$

$$\frac{\partial C_i^{(0)}}{\partial t} + \nabla\cdot\left[C_i^{(0)} \vec{v}^{(0)}\right] = Da\, R_i + \frac{1}{Pe} \nabla^2 C_i^{(0)} \qquad (5d)$$

$$p^{(0)} = \rho^{(0)} T^{(0)} \quad . \qquad (5e)$$

It is observed from this last set of equations that the momentum equation has degenerated to describe the variation of the thermodynamic pressure $p^{(0)}$. To complete the description of the velocity field, $\vec{v}^{(0)}$, the first order momentum equation must be included and is given as

$$\rho^{(0)} \frac{D^{(0)}}{Dt} \vec{v}^{(0)} = -\nabla p^{(1)} + \frac{1}{Re} \nabla\cdot\tilde{\tau}^{(0)} \quad . \qquad (5f)$$

It should be noted that all dependent variables appear only to lowest order except pressure, in which both $p^{(0)}$ and $p^{(1)}$ appear. The superscripts will now be dropped except to distinguish $p^{(0)}$ and $p^{(1)}$. The lowest order momentum equation simply states that in the first approximation the thermodynamic pressure, $p^{(0)}$, is constant in space but may vary with time. In this approximation the sound speed is infinite so that any disturbances in thermodynamic pressure caused by combustion are felt instantaneously throughout the fluid. For combustion in an open domain, $p^{(0)} = p_\infty$, and the combustion is a constant pressure process. $p^{(1)}$ is the dynamic pressure associated with the fluid flow and, to the lowest order, does not participate in thermodynamic processes.

These equations may be stated in an alternate form that proves to be helpful in obtaining numerical solutions. Equations (5a) and (5c) can be combined to give

$$\nabla\cdot\vec{v} = \frac{1}{\gamma p^{(0)}} \left[\frac{\gamma\nabla\cdot\vec{q}}{PrRe} - \frac{dp^{(0)}}{dt} + Ce\dot{P}\right] \quad . \qquad (6)$$

In a closed domain with adiabatic walls or in a domain with periodic boundary conditions, equation (6) can be integrated to give

$$\frac{dp^{(0)}}{dt} = \frac{1}{\text{volume}} \iiint Ce\dot{P}\, dV \quad . \qquad (7)$$

Under these conditions the combustion is a constant volume process and the pressure in a closed domain increases due to the rate of chemical energy released in the chamber. Equations (6) and (7) are used to replace equations (5b) and (5c), giving the final set of equations. Note that if the heat release term, $\dot{P} = 0$, then $\nabla\cdot\vec{v} = 0$ and these equations reduce to those of a strictly incompressible fluid.

3. Numerical Solution Procedure

Equations (5a) and (5f) may be written in the following form:

$$\frac{\partial \rho}{\partial t} + \rho\nabla\cdot\vec{v} + \vec{v}\cdot\nabla\rho = 0 \qquad (8)$$

$$\frac{\partial}{\partial t}(\rho\vec{v}) = -\nabla p^{(1)} + A(x) \qquad (9)$$

Here A(x) represents the viscous and convective components of the momentum equation. The local density is obtained by substituting equation (6) into (8) and advancing the density ahead in time using a second order Adams-Bashforth time stepping scheme. The chemical species equations are also solved using an Adams-Bashforth scheme. All spatial derivitives are computed using pseudo-spectral methods. The pressure and velocity components are obtained by solving equation (9) in two stages. First equation (9) is advanced to an intermediate time step neglecting pressure effects:

$$\rho\vec{v}^{*} = \rho\vec{v}^{n-1} + \Delta t\left[\frac{3}{2} A(x)^n - \frac{1}{2} A(x)^{n-1}\right] \quad . \qquad (10)$$

The remaining pressure term gives:

$$\frac{(\rho\vec{v})^{n+1} - (\rho\vec{v})^{*}}{\Delta t} = -\nabla p^{(1)\,n+1/2} \qquad (11)$$

Note that adding equations (10) and (11) results in a second order accurate finite difference approximation to the time derivative of $\rho\vec{v}$. Taking the

divergence of equation (11) gives the following Poisson equation for pressure:

$$-\nabla^2 p^{(1)^{n+1/2}} = \frac{\nabla\cdot(\rho\vec{v})^{n+1} - \nabla\cdot(\rho\vec{v})^*}{\Delta t} \qquad (12)$$

Since we are treating a spatially periodic problem in this work (see Section 4), equation (12) is easily solved for $p^{(1)}$ by taking the Fourier transform of equation (12), solving for the transform of $p^{(1)}$, and then transforming back to physical space. The velocity components are obtained by using this value of $p^{(1)}$ in equation (11). This method is similar to numerical solution techniques for the incompressible, unsteady, Navier-Stokes equations as outlined by Peyret and Taylor[8]. The important difference is that the density is not constant and an approximation for $\nabla\cdot(\rho\vec{v})^{n+1}$ must be obtained directly from equation (5a) using computed values of ρ^{n+1}, ρ^n, and ρ^{n-1} to give a second order accurate estimate to $\frac{\partial\rho^{n+1}}{\partial t}$.

4. Simulation Results

In this section we discuss some preliminary results of our numerical simulations of the temporal development of a chemically reacting mixing layer with heat release. The computational domain is a rectangle with 64 x 64 equally spaced grid points. The flow is assumed periodic in the streamwise direction and free-slip, impermeable boundary conditions are employed at the transverse boundary. The initialization of the flow field is the same as used by Riley and Metcalfe[2] in their two-dimensional simulations of an incompressible reacting mixing layer without heat release. Namely, the velocity field was initialized with a hyperbolic tangent profile, and perturbations corresponding to the most unstable mode and its subharmonic as determined from linear stability theory[9]. The chemical reactant concentrations were set as follows:

$$C_1(\vec{x},o) = \frac{1}{y_o\sqrt{\pi}} \int_{-\infty}^{y} \exp(-\zeta^2/y_o^2)d\zeta$$

$$C_2(\vec{x},o) = 1 - C_1 \quad .$$

We are treating a constant volume combustion process and the chemical reaction studied here is a single step, irreversible reaction.

$$C_1 + C_2 \rightarrow \text{Product} + \text{Heat}$$

The reaction rate is taken to be a function only of the reactant concentrations and is not temperature dependent. Although we lose some important physical features of real reacting flows with this simplification, we are able to study details of the effects of heat release on the dynamics of reacting flows.

All simulations were run at a Reynolds number of 250, Peclet number of 100, and a Damköhler number of 1.5. Using the low Mach number approximation (LMA), three different cases have been run for different values of the heat release parameter, Ce, to study the effects of heat release on the flow. In addition, computer simulations involving the solution to the exact, fully compressible (FC) equations have been performed to examine the validity of the low Mach number approximation and the range of heat release over which the approximate equations will produce accurate results.

The validity of the low Mach number approximation in the parameter range of the simulations discussed here has been tested by solving the exact, fully compressible equations (equations 3a - 3f) for a reacting mixing layer with a Mach number of 0.2. Only a single rollup of the fundamental mode was computed because of the excessive computational costs associated with the solution of the fully compressible equations. Vorticity contours obtained from solutions of the exact and approximate equations are compared in Fig. 1. Although acoustic waves propagate throughout the flow field, they apparently have no influence on the vorticity dynamics. The pressure field, plotted in Fig. 2 shows the evidence of acoustic waves. These acoustic waves have a frequency much greater than the hydrodynamic frequency, so that as mentioned earlier, the hydrodynamics cannot respond to the acoustic fluctuations, indicating that only pressure averaged over acoustic periods is important.

Figs. 3 and 4 are contour plots of the product concentration in the reacting mixing layer for runs 1 and 3. The only difference in these two simulations is the amount of heat release (Ce = 0, Ce = 5), all other parameters being equal. The development of the layer into the now widely recognized large coherent structures and the pairing process of these structures is clearly evident. The main difference observed in these two cases is the amount of product formed. The effect of heat release has been to significantly reduce the amount of product produced in the layer. Concentration profiles averaged horizontally across the layer are shown in Fig. 5 for runs 1, 2, and 3. Here we see the reduction in product with the degree of heat release. Averaged temperature profiles are displayed in Fig. 6. The thickness of the layer, based on the point at which either the average product or temperature approach free stream values, is seen to remain approximately the same, with a possible slight decrease indicated. Because of the decrease in density caused by exothermic chemical reactions, the heat release and resulting density changes thus act to decrease the rate of mass entrainment into the layer, since the overall layer growth is approximately unchanged from the cold flow case. This is in qualitative agreement with the experimental findings of Wallace[10], who conducted an experimental study of mixing layers that included a chemical reaction with weak heat release.

Fig. 7 shows the computed velocity profiles across the mixing layer for runs 1, 2, and 3 at a time of t=24. The layer thickness, as defined by the point at which the average velocity attains one half of the free stream value, is seen to decrease with increasing heat release. The interesting feature apparent in these plots is the inflection point in the profile for the runs with heat release. This can be explained in terms of the vorticity dynamics. For a two-dimensional mixing layer the vorticity equation may be written as

$$\frac{D\vec{\omega}}{Dt} + \vec{\omega}\nabla\cdot\vec{v} = \frac{1}{\rho^2}(\nabla\rho \times \nabla p) + \frac{1}{Re}\nabla\times(\nabla\cdot\bar{\tau}) \quad .$$

The first term on the right hand side is referred to as the baroclinic torque and the second term on the left hand side represents a change in vorticity

resulting from thermal expansion. In the simulations discussed here the action of the baroclinic torque was the main source of vorticity generation. If there are no heat sources present in the flow, $\nabla \cdot \vec{v} = 0$ and ρ = constant so that aside from diffusion effects, vorticity is conserved along streamlines. Fig. 8 shows the vorticity contours at times of t = 8, 16, and 24 for a reacting mixing layer without heat release. The vorticity is of the same sign throughout the flow field and the large scale structures of the flow are clearly apparent. The vorticity field for a mixing layer with heat release (run 3, Ce = 5) is shown in Fig. 9. The heat release has resulted in the generation of vorticity which changes sign at the outer edges of the layer. This indicates a change in the sign of the velocity gradient, i.e., an inflection point. The generation of vorticity is caused mainly by the action of the baroclinic torque term in the vorticity equation. This we have plotted in Fig. 10. A qualitative explanation for this complicated looking plot is as follows. The direction of the pressure gradient is roughly radially outward from the center of the vortex structures, and is monotonic across the reaction front. The density gradient, however, changes sign across the reaction front, resulting in a change in sign of the baroclinic torque in the reaction zone. As the layer rolls up, the reaction zone becomes highly distorted, and the complicated structure of the baroclinic torque shown in Fig. 10 results†.

Another effect of heat release in reacting flows will generally be to raise the viscosity, thus lowering the Reynolds number. It can be argued that this will tend to have a stabilizing effect on the flow. If the Reynolds number is large enough the dynamics of the mixing layer, however, do not depend strongly on the Reynolds number. In the simulations presented here the viscosity has been held constant. In other flow configurations, where the instability or other important features of the flow are more dependent on Reynolds number (for example, boundary layer flows), ignoring Reynolds number dependence could give quite misleading results.

5. Conclusions

The application of the approximate set of equations derived here for low Mach number flows has resulted in a significant reduction in computer costs compared with solutions to the exact, fully compressible equations of motion. The computer time needed to integrate the governing equations has been reduced by a factor of approximately 1/M using the low Mach number approximation. Excellent agreement with the exact equations has been obtained for the cases presented in this paper.

Preliminary simulation results in two spatial dimensions of a chemically reacting mixing layer indicate that the amount of mass entrained into the layer is reduced as the rate of heat release increases. The thickness of the layer is also reduced when exothermic chemical reactions occur. This is in qualitative agreement with mixing layer experiments with low rates of heat release.

These simulations demonstrate the effectiveness of the direct numerical simulation approach as a predictive tool in studying complex reacting flows with heat release. An extension of this work to three spatial dimensions should provide insight into the more complex problem of the interactions between turbulence and heat release in reacting flows.

Acknowledgements

This work has been sponsored by NASA Lewis Research Center under contract NAS3-24229. All simulations were run on the NASA Lewis Cray-1 computer.

References

1. A. Roshko, 1976, "Structures of Turbulent Shear Flows: A New Look," AIAA Journal, 14:1349-1357.

2. J. J. Riley and R. W. Metcalfe, 1983, "Direct Simulations of Chemically Reacting Turbulent Mixing Layers," Flow Research Report No. 274.

3. B.-C. Chu and L. S. G. Kovasznay, 1958, "Non-linear Interactions in a Viscous Heat-Conducting Compressible Gas," J. Fluid Mech. 3:494-514.

4. C. D. Winant and F. K. Browand, 1974, "Vortex Pairing, the Mechanism Of Turbulent Mixing-Layer Growth at Moderate Reynolds Number," J. Fluid Mech. 63:237-255.

5. J. J. Riley and R. W. Metcalfe, 1980, "Direct Numerical Simulation of a Perturbed, Turbulent Mixing Layer," AIAA Pap. No. 80-0274.

6. R. G. Rehm and H. R. Baum, 1978, "The Equations of Motion for Thermally Driven, Buoyant Flows," J. Research, Nat. Bureau of Standards, 83:297-308.

7. E. S. Oran and J. P. Boris, 1981, "Detailed Modelling of Combustion Systems," Prog. Energy Comb. Sci., 7:1-72.

8. R. Peyret and T. D. Taylor, 1983, Computational Methods for Fluid Flow, Springer-Verlag, pp. 160-169.

9. A Michalke, 1964, "On the Inviscid Instability of the Hyperbolic Tangent Velocity Profile," J. Fluid Mech., 19:543-556.

10. A. K. Wallace, 1981, "Experimental Investigation on the Effects of Chemical Heat Release in the Reacting Turbulent Plane Shear Layer," Ph.D. Thesis, University of Adelaide, Adelaide, Australia.

† This qualitative picture benefited from a discussion with Professor F. A. Williams of Princeton University.

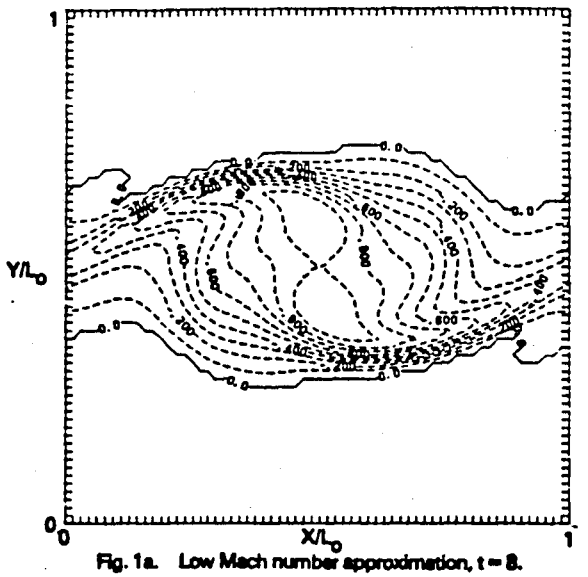

Fig. 1a. Low Mach number approximation, t = 8.

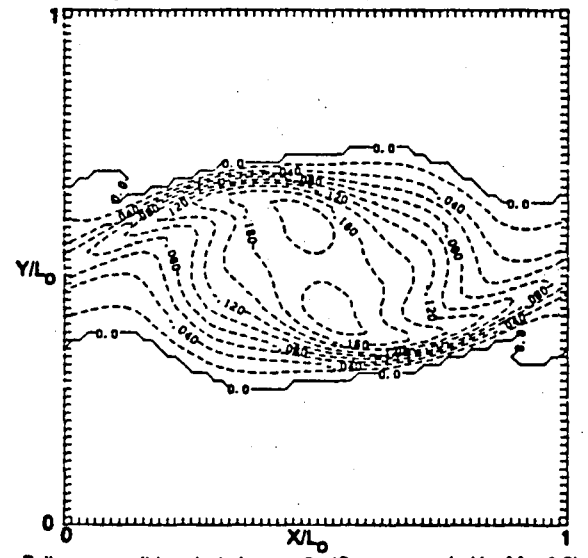

Fig. 1b. Full compressible calculation, t = 8. (Contours scaled by M = 0.2)

Figure 1. Vorticity contours comparing simulation results for the low Mach number approximation and the exact, fully compressible equations of motion, Ce = 2.0.

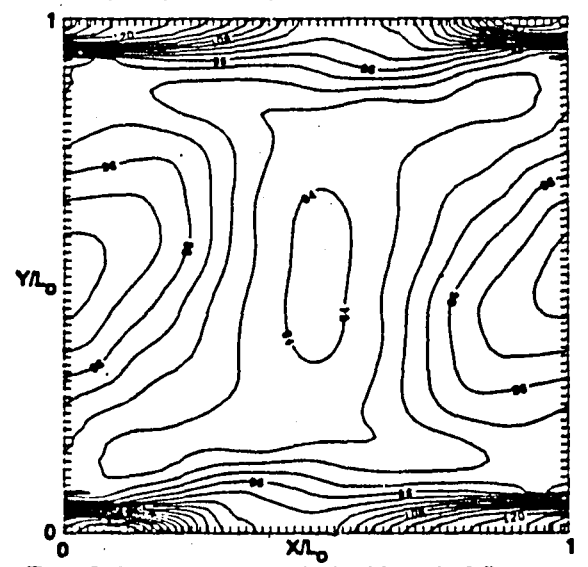

Figure 2. Pressure contours obtained from the fully compressible equations of motion, t = 8.

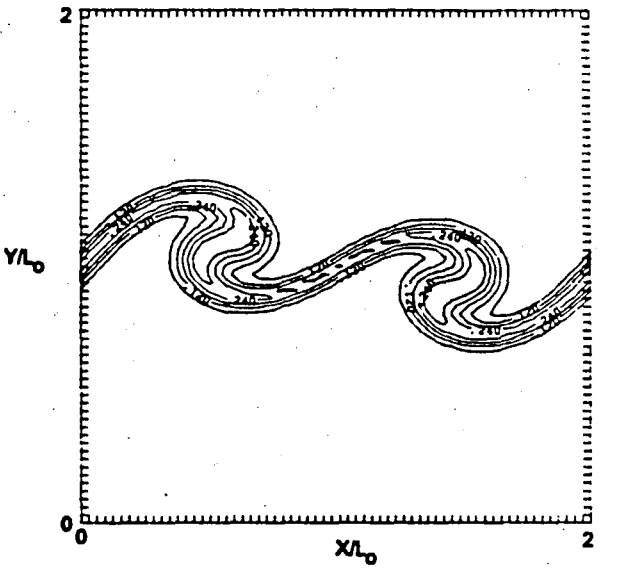

Fig. 3a. t = 8.

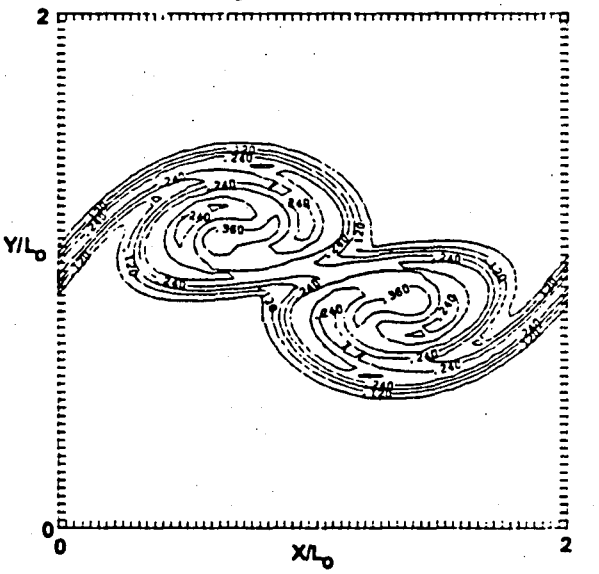

Fig. 3b. t = 16.

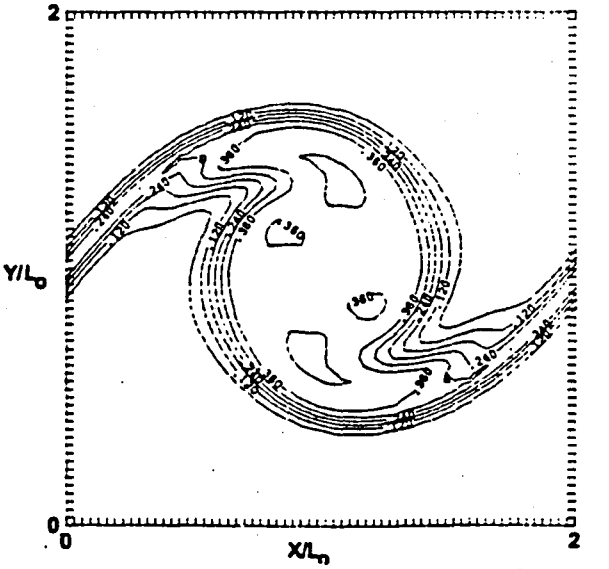

Fig. 3c. t = 24.

Figure 3. Chemical product contours plot, no heat release (Ce = 0).

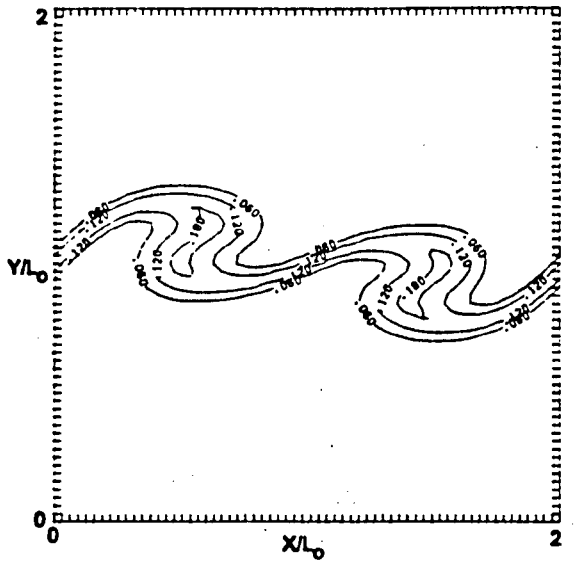

Fig. 4a. t = 8.

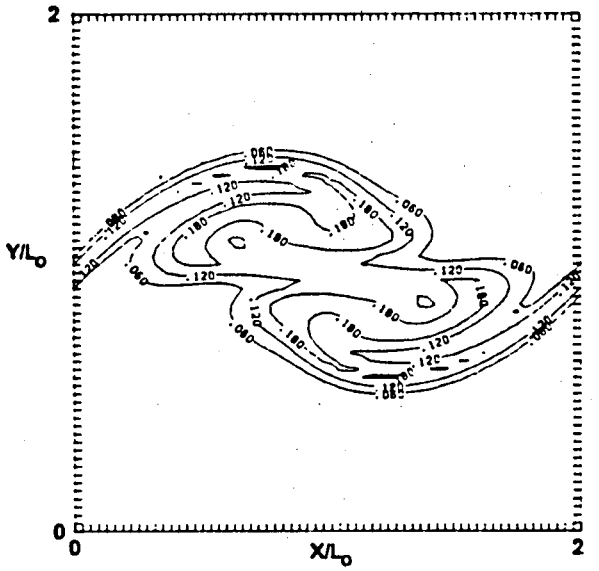

Fig. 4b. t = 16.

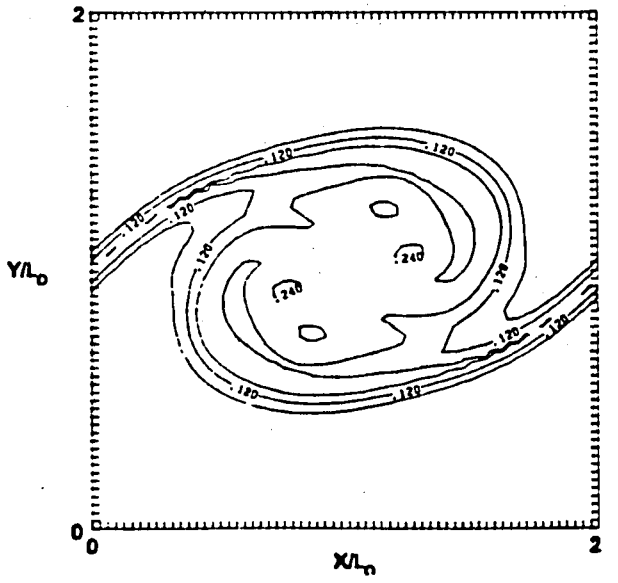

Fig. 4c. t = 24.

Figure 4. Chemical product contour plot, with heat release (Ce = 5).

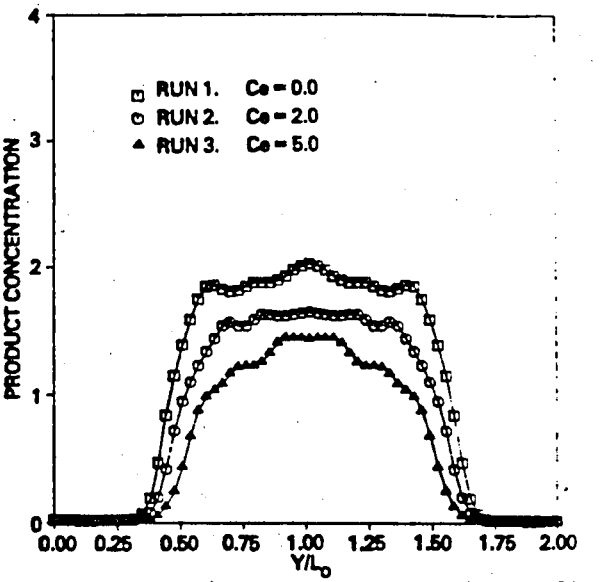

Figure 5. Average product concentration across mixing layer. t = 24.

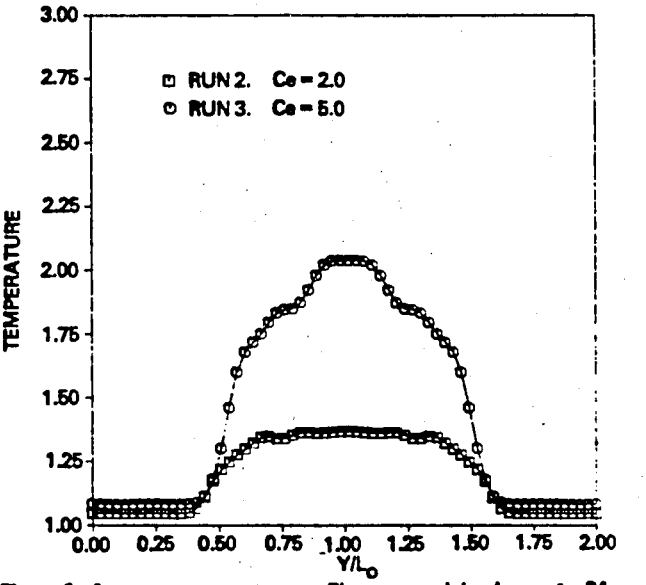

Figure 6. Average temperature profile across mixing layer. t = 24.

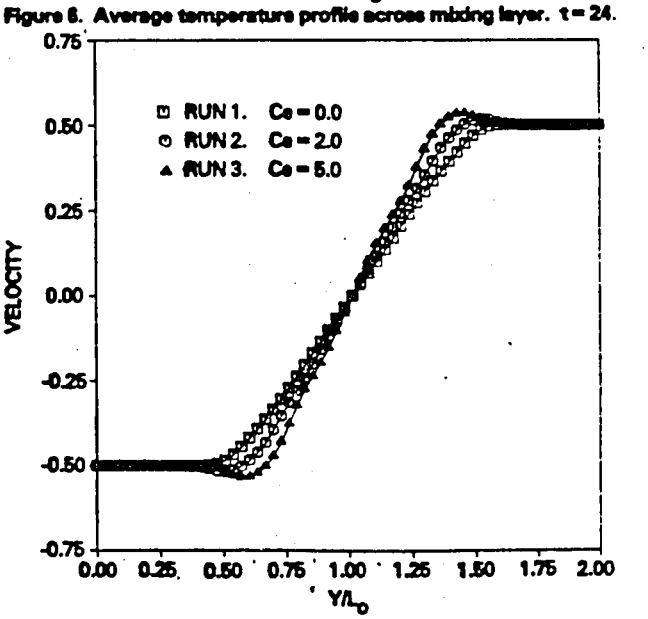

Figure 7. Velocity profile across mixing layer. t = 24.

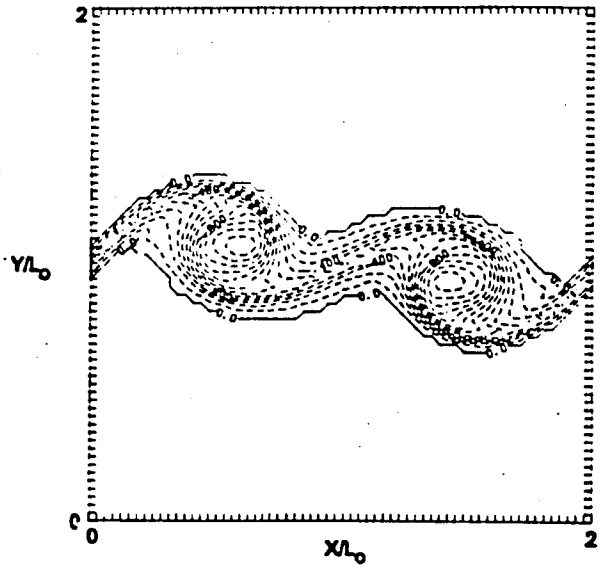

Fig. 8a. t = 8.

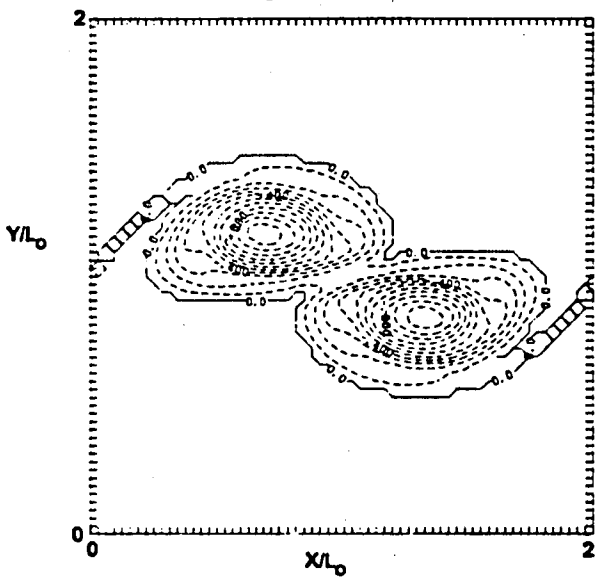

Fig. 8b. t = 16.

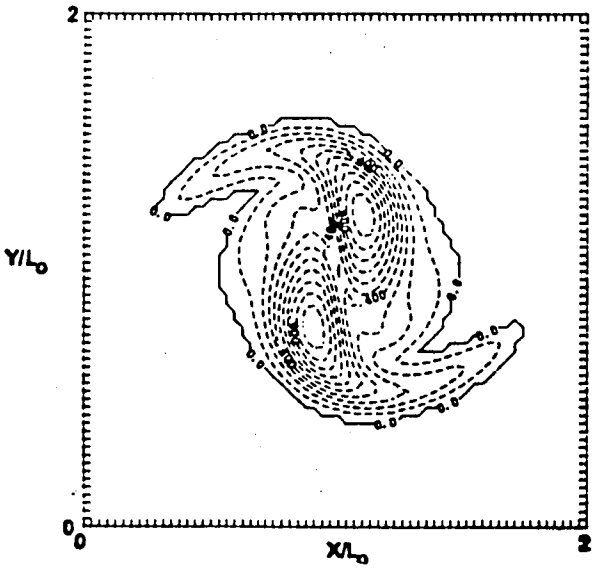

Fig. 8c. t = 24.

Figure 8. Vorticity contour plots, no heat release (Ce = 0).

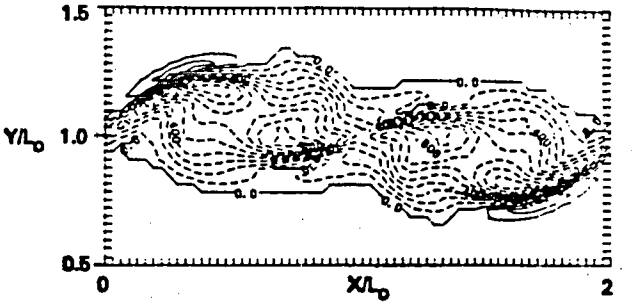

Fig. 9a. t = 8.

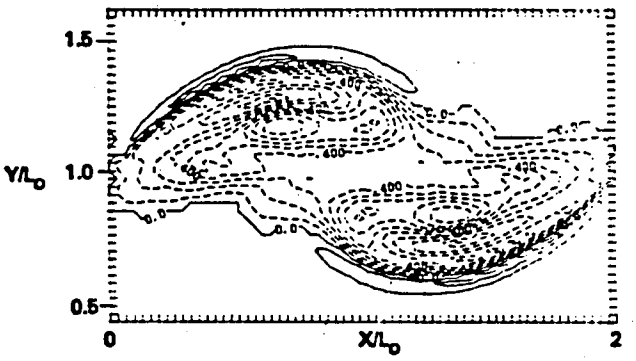

Fig. 9b. t = 16.

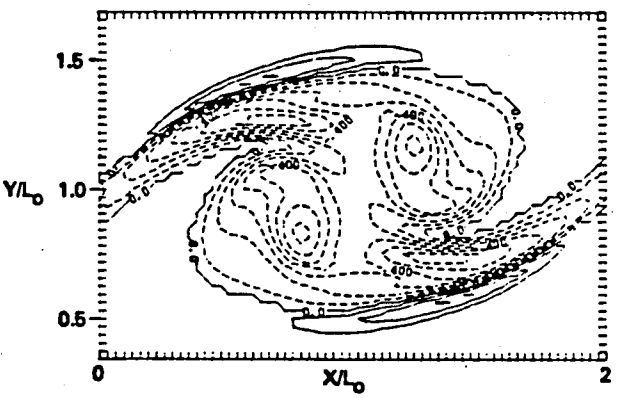

Fig. 9c. t = 24.

Figure 9. Vorticity contour plots, with heat release (Ce = 5).

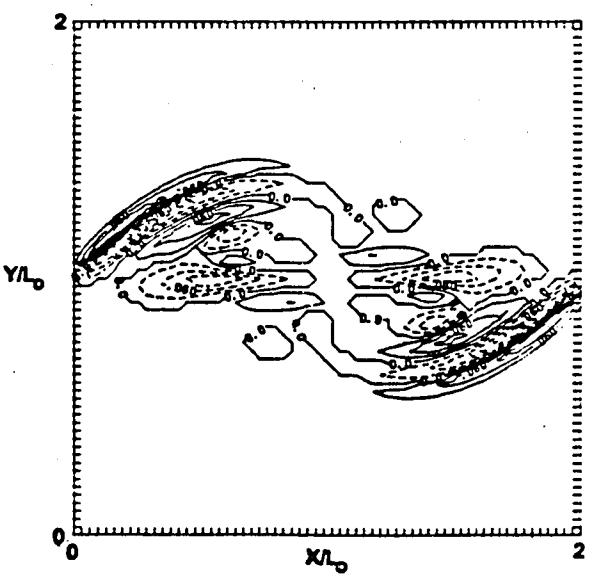

Figure 10. Baroclinic torque, Ce = 5, t = 16.

APPENDIX B

MECHANISMS BY WHICH HEAT RELEASE AFFECTS THE FLOW FIELD IN A CHEMICALLY REACTING, TURBULENT MIXING LAYER

P.A. McMurtry* and J.J. Riley**
University of Washington
Seattle, Washington

and

R.W. Metcalfe†
Flow Research Company
Kent, Washington

Abstract

The mechanisms by which heat release affects the fluid dynamics in a turbulent reacting mixing layer are studied by direct numerical simulation. In agreement with previous laboratory experiments, the heat release is observed to lower the rate at which the mixing layer grows and to reduce the rate at which chemical products are formed. The baroclinic torque and thermal expansion in the mixing layer are shown to produce changes in the flame vortex structure that act to produce more diffuse vortices than in the constant density case, resulting in lower rotation rates of fluid elements. Previously unexplained anomalies observed in the mean velocity profiles of reacting jets and mixing layers are shown to result from vorticity generation by baroclinic torques. The density reductions also lower the generation rates of turbulent kinetic energy and the turbulent shear stresses, resulting in less turbulent mixing of fluid elements.

Calculations of the energy in the various wave numbers shows that the heat release has a stabilizing effect on the growth rates of individual modes. A linear stability analysis of a simplified model problem confirms this, showing that low density fluid in the mixing region will result in a shift of the frequency of the unstable modes to lower wave numbers (longer wavelengths). The growth rates of the unstable modes decrease, contributing to the slower growth of the mixing layer.

1. Background

The interactions between chemical heat release and fluid dynamics are one of the least understood aspects of chemically reacting flows. To increase our predictive capability of reacting flows and develop more reliable and efficient combustion models there is a need to understand more fully the fundamental physical processes occurring in such flows. In the work presented here these processes are studied in a temporally growing mixing layer by the technique of direct numerical simulation.

Many chemically reacting flows are turbulent in nature and are characterized by large amounts of energy release, resulting in large density changes. If the Damkohler number of the flow is large (fast chemistry), the reaction rate will be controlled by molecular diffusion and fluid dynamical mixing. Properly treating the turbulent behavior is then clearly an essential part of any predictive method for this type of flow. In a mixing layer, for example, product formation is augmented by stretching and wrinkling of the reaction zone. A highly strained flow field develops, which increases the area of the reaction interface and produces an inflow of reactants to this interface. For reactions that are accompanied by large amounts of heat release, the fluid dynamics of the flow will be coupled to the chemistry through the nonhomogeneous density field that results. The main objective of this work is to investigate the effects of exothermic chemical reactions on the turbulent flow field and to explain these observations by studying the basic physical mechanisms that are involved.

To achieve this purpose, direct numerical simulations of two- and three-dimensional chemically reacting mixing layers have been performed. An exothermic chemical reaction between initially unmixed chemical species is included. Numerical simulations can supplement laboratory experiments well and have the advantage that they can give much more information about the flow, since the entire flow field is known at every time step. In particular, properties that are difficult or impossible to measure experimentally can easily be obtained and studied in the simulations. In addition, initial conditions are easily controlled, and flow field parameters can easily be varied to study their effect on the flow. Unfortunately, computer time and storage requirements limit full simulation to flows with moderate Reynolds and Damkohler numbers.

A mixing layer is formed when two initially separated parallel flowing fluids of different velocities come into contact and mix (figure 1). This fairly simple free shear flow has been extensively studied and has proven very useful in understanding the nature of turbulent flows. Laboratory experiments have shown that, at least in its early stages, the mixing layer is dominated by large-scale, quasi-two-dimensional vortices,[1] with the growth of the mixing layer dominated by the pairing of these vortices.[2] Two-dimensional simulations have been shown to accurately portray the characteristic large scale-rollup and vortex-pairing process.[3] Implications of heat releasing chemistry on this process can thus be meaningfully addressed with two-dimensional simulations.

* Graduate Student, Mechanical Engineering
** Professor, Mechanical Engineering, Member AIAA
† Senior Research Scientist, Member AIAA

However, since all turbulent flows are inherently three-dimensional, some potentially important physics will be lost by restricting the simulations to two spatial dimensions. For example, secondary instabilities can develop into streamwise vortices or "ribs",[4] which can increase mixing and enhance product formation. Three-dimensional simulations are necessary to study this type of behavior and to realistically treat the turbulent behavior of the flow.

A large amount of work in the area of turbulent reacting flows has been directed at trying to understand the effects of the fluid dynamics on mixing and on reaction rates. A number of experiments have been performed on chemically-reacting constant density mixing layers to study the process of mixing and entrainment.[5-9] In these experiments the chemistry had no influence on the development of the velocity field due to the small amount of heat released. The results of these studies consistently showed that chemical reaction products were concentrated in large, spanwise-coherent structures that, at least initially, dominate the turbulent transport. In addition, three-dimensional effects are present and can be important. Breidenthal[6] notes a significant increase in product formation rate coinciding with the development of three-dimensional motions in the flow.

Previous direct numerical simulations of an incompressible reacting mixing layer[10] focussed on how the turbulent flow field affects the chemical reaction rate. This work has given physical insight into how vortex rollup and three-dimensional turbulence affect the chemical reaction. Furthermore, comparisons of these simulations with laboratory data have led to an increased confidence in the application of the direct numerical simulation methodology to this class of problems.

Effects of heat release in turbulent reacting mixing layers have been studied experimentally by Wallace[11] and Hermanson.[12] Wallace utilized a nitric oxide - ozone reaction to attain temperature rises of 400°K. Hermanson used a hydrogen - fluorine reaction to produce temperature rises to 940°K. Large-scale structures were observed to persist over these temperature ranges. The results that were obtained in these experiments all indicated that the heat release resulted in a slower growth rate of the layer and a decrease in the total amount of mass entrained into the layer. Hermanson suggested that the decrease in mass entrainment could be attributed to a reduction in the turbulent shear stresses that was observed in the high heat release experiments. In both sets of experiments the streamwise pressure gradients were small. Hermanson performed additional experiments while imposing a favorable streamwise pressure gradient. These experiments showed an additional thinning of the layer.

McMurtry et al.[13] performed direct numerical simulations of a two-dimensional temporally growing mixing layer that included effects of chemical heat release. A low Mach number approximation was used which allowed them to study the effects of density changes while eliminating the numerical stability requirements for computing the high frequency acoustic waves. Qualitative agreement with the experimental results of Wallace and Hermanson was obtained.

Higher heat release experiments have been performed by Keller and Daily.[14] Cold premixed reactants carried in a high velocity stream were ignited by hot, low density combustion products which were carried in a low speed stream. Results were reported for a range of equivalence ratios. In these experiments a large, favorable pressure gradient existed in the streamwise direction and the reaction was not diffusion limited. The mixing layer thickness was observed to increase with increasing heat release, a result different from what Hermanson and Wallace reported in their experiments with a diffusion limited reaction and an initially uniform freestream density. The thickening of the layer with heat release was attributed to downstream acceleration of the low speed, low density fluid. Large scale, two-dimensional vortices were again observed to persist over all heat release ranges.

Two-dimensional numerical simulations of combustion at a rearward facing step performed by Hsiao et al.[15] and Ghoniem et al.[16] gave qualitative agreement with similar experiments[17]. Chorin's[18] random vortex method was used and expansion effects due to heat release were modeled by a set of distributed volume sources.

Visual studies of diffusion flames in jets[19-21] have shown that the existence of flames (heat release) retards the transition from laminar to turbulent flows. More recent turbulence measurements[22,23] show lower turbulence levels near the jet exit in jets with flames and an increase in turbulence downstream. Velocity profiles are steeper in the heat release runs and Yule[23] reports humps (i.e., more than one inflection point) in the profiles that are not seen in the cold jets. Also, the frequencies of the most energetic instabilities (vortices at the fuel-air interface) were observed to decrease as heat release increased.

Some theoretical work performed by Marble and Broadwell[24] and Karagozian[25] is helpful in interpreting the results of our simulations. Marble and Broadwell studied the deformation of a constant density diffusion flame by turbulent motions. Karagozian examined the deformation of laminar diffusion flames in the flow field of two- and three-dimensional vortex structures, and also studied the effects of heat release on a laminar diffusion flame interacting with an inviscid vortex. The presence of density changes in the core caused the entire flow field to be shifted radially outward. The braids, or "flame arms" of the vortex were thus translated to a region of lower total straining (further from the point where the vortex was imposed), reducing the rate at which reactants were consumed by the flame. The effect of the reduction of the density in the core of the vortex structures was shown to reduce the rate at which reactants are consumed by the flame.

These previous investigations have shown that there can be a very significant influence of combustion on the velocity field in reacting flows. The objective of the work presented in this paper is to use the simulation results to understand the mechanisms that produce these observed heat release effects.

The Temporally Developing Mixing Layer

The simulation results discussed here are of a temporally growing mixing layer which is taken to be statistically homogeneous in the streamwise (x) and spanwise (z) directions. This is not the same flow as the spatially developing layer that is usually studied experimentally, but is an approximation if one follows the flow at the mean velocity. By studying a temporally growing layer, the requirement of specifying inflow-outflow boundary conditions, which are difficult to correctly implement for the spatial layer, is avoided. In this work periodic boundary conditions are used in the homogeneous directions and pseudo-spectral numerical methods are used to solve the governing equations of motion. (See Gottlieb and Orszag[51] for a description of these methods.) There are many dynamical features common to the two mixing layers,[26] so that a study of a temporal mixing layer can reveal important information about the spatial layer. Some of the differences between the two have been pointed out by Corcos and Sherman.[27] In the spatially developing layer, events that occur downstream can induce changes in the flowfield upstream, whereas in the temporally developing layer, obviously no event can affect the flow at previous times. Also, the spatially developing layer has no symmetries around any spanwise axis so that entrainment rates of fluid into the layer from the two streams will not necessarily be the same. These points should be kept in mind when comparing experiments to simulations. For co-flowing mixing layers the differences between the two become small when the parameter $\xi=(U1-U2)/(U1+U2)$ becomes small. U1 and U2 are the velocities on the high- and low-speed sides of the layer (figure 1). To address these differences, simulations of a spatially growing layer should be performed.

In the following section, a summary of the numerical approach used is discussed. Selected results that illustrate some of the effects of heat release on the flow are presented in section 3. These effects are explained in section 4 by studying different aspects of the flow including the turbulent shear stress and turbulent kinetic energy distribution, the vorticity dynamics, and stability considerations. Section 5 summarizes the results and includes a discussion of how the different aspects of the flow discussed in section 4 are related.

2. Methodology

Performing numerical studies specifically directed at investigating the basic interactions between the chemistry and the flow field calls for an approach in which the basic physical processes are an inherent part of the methodology. The method used in this work is termed direct numerical simulation and involves solving the three-dimensional, time-dependent governing equations for the detailed development of the flow field. This method of studying turbulent flows was developed by Orszag and Patterson[29] and first applied to homogeneous, isotropic turbulence. This technique uses no closure modeling and no assumptions pertaining to the turbulent behavior of the fluid are made. However, due to finite computer resources, the range of temporal and spatial scales that can accurately be resolved is limited. This limitation restricts these simulations to flows with moderate Reynolds and Damkohler numbers, although a conserved scalar approach can be used[28] to treat the limit of infinite Damkohler number. At the present time, direct numerical simulations have been limited to fairly simple geometries and are used only in research applications. These applications mainly consist of trying to understand the physics of simple flows with the idea that the information obtained can then be applied to predicting the behavior of more complicated flows.

Direct numerical simulations have been used successfully in many fluid mechanical applications including homogeneous turbulence,[29-31] turbulent channel flow,[34] mixing layers,[3] reacting mixing layers without heat release,[10] turbulent wakes,[32,33] and turbulent boundary layers.[35] Extending the use of direct numerical simulations to reacting flows with chemical heat release has been justified by two-dimensional simulations performed by McMurtry et al.[13] In this paper, results of three-dimensional simulations are presented to study the mechanisms by which heat release affects the flow.

Low Mach Number Approximation

To solve for the development of the flow field, a set of approximate equations valid for low Mach number flows is utilized. This approximation has previously been presented, in various forms, by Rehm and Baum,[36] Sivashinsky,[37] Buckmaster,[38] Majda and Sethian,[39] and McMurtry et al.[13] The general idea behind this approximation is that for low Mach number flows, the acoustic waves generated by the turbulence and the combustion process have a much higher frequency and much faster propagation velocity than the motions characterizing convection processes. In the asymptotic limit, the speed of sound becomes infinite and any disturbances in thermodynamic pressure will be felt instantaneously throughout the fluid. This approximation allows one to study effects of density changes due to heat release while avoiding the numerical stability problems of resolving acoustic wave propagation.

Starting with the exact equations of combustion gas dynamics and applying a low Mach number expansion, a set of ordered approximate equations is obtained. In this work, the equations solved include conservation equations for mass, momentum, energy, chemical species, and an equation of state. In the limit of low Mach number flows, these equations take the following (nondimensional) form:

$$\frac{\partial \rho^{(0)}}{\partial t} + \nabla\cdot\left[\rho^{(0)}\vec{v}^{(0)}\right] = 0 \qquad (1a)$$

$$\nabla p^{(0)} = 0 \qquad (1b)$$

$$\rho^{(0)}\frac{D^{(0)}}{Dt}T^{(0)} = -(\gamma-1)p^{(0)}\nabla\cdot\vec{v}^{(0)} + \frac{1}{PrRe}\nabla\cdot\vec{q}^{(0)} + DaCe\dot{Q} \qquad (1c)$$

$$\frac{\partial c_i^{(0)}}{\partial t} + \nabla\cdot\left[c_i^{(0)}\vec{v}^{(0)}\right] = DaR_i + \frac{1}{Pe}\nabla^2 c_i^{(0)} \qquad (1d)$$

$$p^{(0)} = \rho^{(0)}T^{(0)} . \qquad (1e)$$

The momentum equation, to the lowest order (eq. 1b) simply describes the variation of the thermodynamic pressure $p^{(0)}$. To complete the description of the velocity field the first order momentum equation must also be retained, and is given by

$$\rho^{(0)} \frac{D^{(0)}}{Dt} \vec{v}^{(0)} = -\nabla p^{(1)} + \frac{1}{Re} \nabla \cdot \bar{\tau}^{(0)} \quad . \qquad (1f)$$

The nondimensional parameters appearing in these equations are the Damkohler number, $Da = k_o C_o L_o / U_o$, Peclet number, $Pe = L_o U_o / D_o$, and Reynolds number, $Re = U_o L_o / \nu$. The parameter Ce, a nondimensional number characterizing the amount of heat release, is given by $Ce = C_o \Delta H / \rho_o C_v T_o$.

D_o, ν, C_o, ρ, and T_o are the free stream molecular diffusivity, kinematic viscosity, chemical species concentration, density, and temperature. U_o is the velocity difference across the layer, ΔH is the heat of reaction, and C_v is the specific heat at constant volume. For computational convenience, the length scale L_o is chosen such that the nondimensional wavelength of the most unstable mode is 2π ($L_o = \lambda / 2\pi$, where λ is the dimensional wavelength).

The distinction between the two pressures that appear, $p^{(0)}$ and $p^{(1)}$, is essential both from a theoretical point of view and in the numerical solution procedure. The thermodynamic pressure, $p^{(0)}$, is constant in space, but may vary in time due to heat addition. $p^{(1)}$ is the dynamic pressure associated with the fluid motion and does not participate directly in thermodynamic processes.

These equations have previously been successfully applied to a two-dimensional problem.[13] Comparisons of simulations using the exact equations and the low Mach number approximation were performed for a flow with a Mach number of 0.2 and confirmed the validity of the approximation in studying this type of flow. Details of the derivation of the equations and the numerical solution procedure are also discussed in reference 13.

Boundary Conditions and Numerical Methods

Since a temporally developing mixing layer is studied here, periodic boundary conditions can be applied in the streamwise (x) and spanwise (z) direction. In the transverse (y) direction, a free-slip, adiabatic boundary condition is applied. With these boundary conditions, very accurate pseudo-spectral numerical methods can be efficiently implemented. All dependent variables are expanded in Fourier Series in the streamwise and spanwise directions. In the transverse direction a Fourier cosine series is used for all dependent variables except for the transverse velocity component, v, which is expanded in a Fourier sine series. Spatial derivatives are then computed by differentiating the series term by term. A second order accurate Adams-Bashforth time-stepping scheme is used to advance the equations in time.

The pseudo-spectral technique as implemented here exhibits very small phase errors and numerical diffusion compared to finite difference techniques. The only errors that are of any consequence are truncation errors due to the finite wave number cut off and time stepping errors. Care has been taken to minimize these errors by using small time steps and transport coefficients (viscosity, molecular diffusion coefficient) that are high enough to ensure accurate resolution. The lack of phase and diffusion errors is a very desirable property in simulations of reacting flows, where steep gradients of reacting species can develop and where reaction rates are controlled by molecular diffusion. However, truncation errors can become significant if gradients become too steep.

Flow Field Initialization

The computational domain for the simulations is chosen to be large enough to contain the most unstable mode and its subharmonic (as determined from linear stability theory for an incompressible flow[50]). The velocity field is initialized by adding a hyperbolic tangent velocity profile (figure 2) to a low level, three-dimensional, broad band background perturbation. In addition, in certain simulations a perturbation in the form of the most unstable mode and its subharmonic are added. The spatially periodic "forcing" in the temporally developing layer is analogous to periodic (in time) forcing of a spatially growing layer.

To specify the background perturbation we use a method similar to that discussed by Orszag and Pao.[32] (Also discussed in more detail in Riley and Metcalfe.[33]) Energy is assigned to each wave number component as specified by a selected three-dimensional energy spectrum. A random phase is then given to each component which results in a random velocity field with a specified energy spectrum. The actual shape of the spectrum is not critical as long as energy is contained in a fairly wide range of wave numbers. The spectrum used in these simulations is given by

$$E_u(k) = \epsilon_{3d} \Lambda \frac{k^4 \Lambda^4}{(1+k^2\Lambda^2)^3}$$

This is a fairly broad banded, isotropic spectrum. Λ is the integral length scale, k is the magnitude of the wave number, and ϵ_{3d} is a coefficient that determines the level of the perturbation. This spectrum is multiplied by a "form function" in physical space to give a turbulence intensity profile characteristic of mixing layers.[3] For simulations that start with a low enough initial amplitude (in the linear range), the most amplified frequencies will ultimately dominate.

The chemical reactant fields are initially two-dimensional and are given by the following functional relationships:

$$C_1(\vec{x},0) = \frac{1}{y_o\sqrt{\pi}} \int_{-\infty}^{y} \exp(-\zeta^2/y_o^2) d\zeta$$

$$C_2(x,y,z,0) = 1 - C_1(x,y+\delta,z,0)$$

δ is a value by which the two species fields have been offset so that there is initially no overlap between the two (figure 2). These functions are easily resolvable using spectral methods and are not unlike those measured experimentally. The particular chemical reaction used is a single step,

irreversible reaction.

$$C_1 + C_2 \rightarrow \text{Products} + \text{Heat}$$

The reaction rate is a function only of the reactant concentrations and does not depend on temperature. Although some important features of real reacting flows are lost with this simple reaction, many important features of the effects of energy release on the dynamics of the flow can still be studied.

Summary of Approximations

The following is a summary of the major simplifications and approximations used in the numerical simulations.

A. Low Mach number approximation.
To ease stability requirements in the numerical calculation a low Mach number approximation is used. This allows acoustic waves to be filtered out of the equations. The validity of the approximation has been illustrated for these simulations in reference 13 by comparing results from the complete set of full compressible equations with the results from the low Mach number approximation.

B. Temporally developing mixing layer.
The simulations are all for a mixing layer that develops in time and is spatially periodic. As pointed out earlier, this is not the same flow as the spatially growing layer that is encountered in practice. However, many dynamic similarities exist between the two so the temporally growing case is of relevence. Also, a more efficient and accurate computer code can be written for the temporally growing mixing layer for a given amount of computer resources.

C. Simple chemistry.
A single step, irreversible reaction between two species to form a product is used. The reaction is taken to be a function only of the reactant concentrations and does not depend on temperature. This does not represent any real chemical reaction but does allow for details of the effects of energy release in the flow to be studied.

D. Constant transport coefficients.
The viscosity, thermal and molecular diffusivities, and the specific heats are taken to be temperature independent constants. Again, this is not a realistic feature of general combusting flows, but in addition to simplifying matters from a numerical point of view, it allows other effects on the flow to be isolated and studied in a simpler environment.

E. The amount of heat release is restricted.
This restriction is necessary to ensure that large velocities will not be generated by the combustion that may violate the low Mach number approximation. The condition that must be statisfied is $DaCe \quad 1/M$.

3. Simulation Results

Results are reported for two different values of the heat release parameter, Ce: one with no heat release (Ce=0), and the other giving a density decrease of $\rho/\rho_0 = 0.5$. Runs 1 (Ce=0) and 2 (Ce=5) were initialized with random perturbations only. Runs 3 (Ce=0) and 4 (Ce=5) included, in addition, a two-dimensional perturbation corresponding to the most unstable wavelength and its subharmonic. In the following, runs 3 and 4 will be referred to as the "forced" cases. These runs are analogous to laboratory experiments in which well defined harmonic perturbations are applied to the flow at selected frequencies. The parameters used in these runs are given in table 1. Additional simulations have been run using different random initializations. The results presented here are representative of all these runs.

All simulations were carried out on the CRAY X-MP computer at NASA Lewis Research Center. The three-dimensional computations were performed on a 64 x 65 x 64 array and required 12 seconds of cpu time per time step. Each simulation presented here required between 600 and 1200 time steps to complete.

The initial three-dimensional random perturubations added to the velocity field were identical for all three-dimensional runs. The initial energy spectrum for runs 1 and 2 (three-dimensional random perturbations only) and runs 3 and 4 (which includes the two-dimensional forcing) is shown in figure 3. The energy contained in the fundamental wavelength (wavenumber = 1) is approximately an order of magnitude higher in the forced cases, although the energy in the higher modes is the same. The initial streamwise rms velocity profile is shown in figure 4 for the forced runs (run 3 and 4). The initial turbulence levels for these runs is low, approximately 3% of the velocity difference across the layer. For the unforced runs (runs 1 and 2), the maximum turbulence levels were approximately 2.2% .

Higher heat release cases can be run, but since the boundary conditions used here imply constant volume combustion, the equivalent of a significant downstream pressure gradient would develop (the background pressure would rise with time). Test cases with a computational domain twice as large in the transverse (y) direction (reducing the effective pressure gradient by a factor of two) were performed to verify that pressure gradient effects were not significant for the values of the paramters studied here.

The growth of mixing layers is strongly influenced by large-scale two-dimensional vortices, and to understand the development of the flow field, the dynamics of these structures must be understood. Figure 5 is a contour plot of the instantaneous spanwise vorticity field obtained from a previous, constant density, two-dimensional simulation[13]. The development of the most unstable mode and the pairing of two vortices to form a single larger one is apparent. In this simulation the velocity field was initialized with perturbations corresponding to the most unstable mode and its subharmonic. One purpose of this present investigation is to examine the influence of heat release on this process and the influence this has on the product formation rate.

Some aspects of the three-dimensional nature of the flow can be seen in a three-dimensional perspective plot of the total vorticity. In figure 6, surfaces having a value of 50% of the maximum of the sum of the absolute values of all three vorticity components are plotted ($|\omega_x| + |\omega_y| + |\omega_z| = \text{constant}$).

This is a result from run 1 (initial random velocity perturbations, no heat release) after one pairing. In addition to the approximately two-dimensional spanwise vorticity associated with the large-scale structure, tubes aligned in the streamwise direction are also apparent. These structures have been recognized as counter-rotating vortices[4] and have been modeled by Lin and Corcos[40] and computed in constant density mixing layers by Metcalfe et al.[26] The effect of these structures on the flow field is to induce a velocity field that acts to pump fluid between the two layers, thereby further convoluting the reaction interface. This tends to increase mixing between the two streams and enhance chemical reactions.

The effect of heat release on the chemical product formation for runs 1 and 2 is shown in figure 7, where the total product (integrated over the entire computational domain) is plotted as a function of time. In agreement with previous two-dimensional results,[13] the total product is seen to be lower for the case with heat release. Since the instantaneous reaction rate (the slope of these curves) is only a function of the joint species concentrations, this again indicates that one effect of the heat release has been to reduce the amount of mixing between the two streams. An increase in the rate of product formation is seen to occur at about t = 40 in the constant density case (run 1) and at t = 60 in the heat release case. This is due to the rollup of the subharmonic mode, which engulfs large amounts of fluid into the vortex structures. Figure 8 shows the amount of product formed when the layer is forced at its most unstable wavelength and subharmonic in addition to the random three-dimensional perturbations. The overall rate of product formation is greater when the layer is forced, but again the decrease in the product with heat release is apparent.

The total product from a two-dimensional simulation with the same level of forcing as runs 3 and 4 ($A_{1,0} = 0.01$ and $A_{1/2,0} = 0.01$) is also plotted in figure 8. During the rollup and pairing process, the three-dimensional growth is inhibited, giving nearly identical results for the two- and three-dimensional simulations. Other studies[26] have shown rollup and pairing has a stabilizing effect on the three-dimensional growth when the amplitudes of the three-dimensional modes are small, while absence of pairing can enhance the growth of the three-dimensional modes. After saturation of the two-dimensional modes (at a time of about t=35) the product formation in the three-dimensional runs continues to grow rapidly due to enhanced three-dimensional mixing, while in the two-dimensional simulations the product formation drops off rapidly.

One measure of the layer growth is the vorticity thickness, defined as the inverse of the maximum slope of the velocity profile. The velocity profiles for runs 1 and 2 (figure 9) at a time of t=72 and runs 3 and 4 (figure 10) at a time of t=36 show a steeper profile for the heat release runs, indicating a slower rate of the layer growth. Note also the overshoot in the velocity profile that occurs in the heat release runs. These observations are similar to those obtained from previous two-dimensional calculations,[13] except the overshoot in the velocity profile is not as pronounced in the unforced three-dimensional simulations (runs 1 and 2) as in the simulations with two-dimensional forcing. This is because of the greater spanwise variation and lack of coherence that exists in the three-dimensional simulations. These overshoots seen in the velocity profile are similar to those seen in the jet flame experiments of Yule et al.[23] and have also been seen in reacting mixing layer experiments.[48]

Plots of the vorticity thickness and velocity half-width (the location where the average streamwise velocity component attains one half of its free stream value) as a function of time reveal another interesting feature (figures 11 - 14). Initially, the growth of the layer given by these two measures is slightly greater in the heat release case; up to t=30 in the unforced runs (runs 1 and 2, figures 11 and 12) and up to t=15 in the forced runs (runs 3 and 4, figures 13 and 14). At later times the layer thickness is less in the heat release runs. In addition, the initial difference in the growth rates with heat release is not as great in the forced runs as in the unforced runs. The initial increase in the layer growth rate is a result of thermal expansion, which shifts the whole flowfield outward. Explanations for the smaller thickness seen in the heat release runs at the later times, as well as the differences seen in the forced and unforced cases are given in the next section.

To summarize, the most obvious macroscopic effects of heat release on the mixing layer dynamics revealed in these numerical simulations and similar experiments are a decrease in the product formation and, after a small initial increase, a decrease in the layer growth rate. These results are qualitatively similar to those obtained experimentally by Wallace[11] and Hermanson,[12] and are consequences of lower rates of fluid entrainment into the mixing region when exothermic chemical reactions occur. In the following section, physical mechanisms responsible for these observations are made.

4. Effects of Heat Release

In this section, the evolution of the flow and the influence of heat release is discussed in terms of the shear stress distribution, the turbulent kinetic energy balance, vorticity dynamics, and stability considerations. Since each of these aspects of the flow must be consistent with the others, they are not interpreted as separate mechanisms, but instead they provide different viewpoints from which the effects of heat release can be explained.

Turbulent Stresses

Hermanson[12] suggests that most of the observed heat release effects can be accounted for as a result of a decrease in the turbulent shear stresses. Velocity and density profiles obtained experimentally as well as the measured layer growth rate were used to compute the turbulent shear stress profiles in his experiments.

To understand the significance of the turbulent stress distribution it is instructive to look at the averaged momentum conservation equation:

$$\frac{\partial}{\partial t}(\bar{\rho}\tilde{U}_i) + \frac{\partial}{\partial x_k}(\bar{\rho}\tilde{U}_k\tilde{U}_i) = \frac{\overline{\partial p}}{\partial x_i} + \frac{\partial}{\partial x_k}(\tau_{ik} - \widetilde{\rho u_k'' u_i''}) \quad (2)$$

The above equation is written in its Favre averaged (density weighted) form. The wavy overbar denotes Favre averaged quantities, which are defined as

$$\tilde{U} = \overline{\rho U}/\bar{\rho}$$

The fluctuating quantities are then given by

$$u'' = u - \tilde{U} .$$

The straight overbar refers to conventional Reynolds averaging. In the temporal calculations this is an average over a horizontal plane. The turbulent stresses, $\widetilde{\rho u_k'' u_i''}$, which appear in the averaged momentum equation represent a transport of mean momentum (per unit volume). The Favre averaged stresses contain momentum exchange mechanisms due to turbulent transport, interactions between the mean flow and volumetric changes, and fluctuation-fluctuation interactions ($\overline{\rho' u_i' u_k'}$).[41] In the numerical simulations performed here, it was possible to compute the Favre averaged turbulent shear stresses directly.

The computed Favre (density weighted) averaged turbulent shear stress profiles ($\widetilde{\rho u_1'' u_2''}$) for runs with and without heat release are shown in figures 15 and 16. Figure 15 is for a three-dimensional calculation without forcing (runs 1 and 2) and figure 16 is the profile computed for a three dimensional calculation that includes forcing at the most unstable mode and its subharmonic (runs 3 and 4). The suppression of the shear stress in the heat release runs is clearly indicated.

The lower turbulent stresses in the heat release case imply a lower transport of momentum to the turbulence. In the following sections it will be shown that this also indicates that less energy is being transferred from the mean flow to the turbulence. In addition, the turbulent shear stresses can be directly related to the stability characteristics of the mixing layer, providing explanations for the lower growth rates.

Turbulent Kinetic Energy

Another aspect of the flow that is useful to examine and is also closely related to the turbulent shear stresses is the turbulent kinetic energy. This can give another way to interpret the effects of heat release on the turbulent motions and account for some of the observations in the heat release runs. Furthermore, the turbulent kinetic energy and its production, redistribution, and viscous dissipation are important aspects of the flow that must be treated in many of the models currently used to describe turbulent flows.

Statistical information related to the turbulent kinetic energy was computed for all the simulations. Qualitatively, the heat release effects were the same for the cases with and without two-dimensional forcing. Therefore, to simplify the discussion, only the runs with the initial random velocity perturbations (runs 1 and 2) are discussed below.

The turbulent kinetic energy profile ($\widetilde{\rho u_i'' u_i''}$) for runs with and without heat release is shown in figure 17 at a nondimensional time of t=48. (Time is nondimensionalized by L_o/U_o.) This corresponds to a time after the rollup of the most unstable mode and before the rollup of its subharmonic is complete. From this figure it can be seen that the total turbulent kinetic energy is less for the heat release run. This is consistent with the earlier observations of less product formation and lower growth rates, since lower turbulence levels imply lower (turbulent) transport rates, resulting in a lower exchange of mass, momentum, and energy among fluid elements.

To understand how a lower turbulent kinetic energy profile results, it is useful to examine its transport equation. In the Favre averaged form, the transport equation for the turbulent kinetic energy is given by

$$\frac{\partial}{\partial t}(\bar{\rho}q) + \frac{\partial}{\partial x_1}(\bar{\rho}\tilde{U}_1 q) = -\widetilde{\rho u_k'' u_i''}\frac{\partial \tilde{U}_i}{\partial x_k} - \frac{\partial}{\partial x_k}(\widetilde{\rho u_i'' u_i'' u_k''}) - \overline{u_i''\frac{\partial p'}{\partial x_i}} - \overline{\tau_{ki}\frac{\partial u_i''}{\partial x_k}} \quad (3)$$

where $q = 1/2\ \widetilde{u_i'' u_i''}$ is the turbulent kinetic energy per unit mass.

From equation 3 we can see that a number of different mechanisms contribute to the kinetic energy balance.

The first term on the right hand side is the production term and accounts for the exchange of energy between the mean flow and the fluctuating motion. The production of kinetic energy is proportional to the average velocity gradient and the turbulent stresses. In the mixing layer simulated here, the only nonzero contribution of this term is for i=1 and k=2. The profile of the turbulent production is shown in figure 18 at t=48. Production is greatest at the center of the mixing layer where the velocity gradient and turbulent stresses are the largest. (In the following plots, negative values indicate a production of turbulent energy). Although it was shown that the velocity gradient is steeper in the cases with heat release, the total turbulent kinetic energy production is less with heat release due to the smaller turbulent stress term, $\widetilde{\rho u_1'' u_2''}$, as shown in the previous section. The slope of the velocity profile is plotted in figure 9 and the Favre averaged turbulent stress profile for this run is shown in figure 15.

The next term, $\frac{\partial}{\partial x_k}(\widetilde{\rho u_i'' u_i'' u_k''})$ is conservative (in general, any term of the form $\nabla\cdot\phi\vec{v}$ is conservative for a variety of boundary conditions) and describes the transport of turbulent kinetic energy by the fluctuating velocity field. From figure 19 we see that turbulent transport tends to convect kinetic energy away from the center of the mixing layer, where the turbulent intensity is highest, to the outer regions. The magnitude of this term is less for the heat release runs since the turbulent fluctuations are lower.

The term $\overline{u_i'' \frac{\partial p'}{\partial x_i}}$ describes the effects of pressure fluctuations on the turbulent kinetic energy distribution. The value of this term is plotted in figure 20 at t=48. This term is of the same order of magnitude as the production term. It has an opposite sign, however, and does not appear to be as greatly affected by the heat release, although a decrease in the magnitude is apparent. The physical interpretation of this contribution can be clarified somewhat by writing this term as

$$\overline{u_i'' \frac{\partial p'}{\partial x_i}} = \frac{\overline{\partial u_i'' p'}}{\partial x_i} - \overline{p' \frac{\partial u_i''}{\partial x_i}} \qquad (4)$$

The first term on the right hand side is a conservative term and represents the redistribution of kinetic energy by pressure fluctuations. The second term, which is zero for constant density flows, is a source of kinetic energy resulting completely from the combustion. The contribution of these two terms for the heat release run is shown in figure 21. The transport due to the pressure fluctuations is not much changed between the runs with and without heat release, although the peak magnitude is somewhat less in the heat release run. In both cases pressure fluctuations act to transport energy from the center of the mixing layer to the outer regions. The contribution due to the velocity divergence leads to a production of kinetic energy in the center of the vortices. In this respect the heat release acts to increase the turbulence level, although this effect is dominated by the decrease in the mean flow production term. In the outer regions, the pressure-divergence correlation changes sign and acts to decrease the turbulence level.

From the results presented here (figures 17-21) it is seen that the most important effects of heat release are significant reductions in the turbulence production and turbulent transport. In the case of the production term, the lower density resulting from the combustion is directly responsible for most of this change. Transport by the fluctuating motion decreases in the heat release runs simply because the turbulence levels are lower. The heat release results in a production of turbulent kinetic energy along the center of the mixing layer through the expansion part of the velocity-pressure gradient correlation. However, the production is small in these simulations compared with the decrease in the exchange of energy with the mean flow, yielding an overall lower turbulent kinetic energy profile. As heat release is increased, the term $\partial u_i/\partial x_i$ would also increase, resulting in more internal energy being converted to kinetic energy. With significantly higher heat release, this could possibly result in an overall increase in the kinetic energy.

Vorticity Dynamics

The numerical simulations can provide us with much more information about the flow than is revealed in the turbulent stress profiles and turbulent kinetic energy profiles, which only give integrated effects and do not reveal much about the physical mechanisms at work. It is more instructive to relate the heat release effects directly to the dynamics of the large-scale structures.

Another approach to studying the flow and interpreting the effects of heat release on the flow field is in terms of vorticity dynamics. In a two-dimensional flow without heat release or diffusion, the vorticity is conserved following particle paths. Therefore, observing the vorticity field allows a direct visualization of the flow field. In a three-dimensional flow, or a flow with density variations or expansion, the vorticity no longer serves as a reliable fluid marker. However, the dynamics of the flow field can still be understood and interpreted by studying the vorticity field. In this section, the effects of heat release on the flow field are discussed and explained in terms of the vorticity dynamics.

Vorticity Equation

The vorticity equation is derived by taking the curl of the momentum equation. In a general three-dimensional flow, the vorticity equation can be written in the following form:

$$\frac{D\vec{\omega}}{Dt} = (\vec{\omega}\cdot\nabla)\vec{v} - \vec{\omega}(\nabla\cdot\vec{v}) + (\nabla\rho \times \nabla p)/\rho^2 + \frac{1}{Re}(\nabla^2\vec{\omega}) \qquad (5)$$

Four different mechanisms can be identified that alter the development of the vorticity field: vortex stretching $(\vec{\omega}\cdot\nabla)\vec{v}$, thermal expansion, $\omega(\nabla\cdot v)$, baroclinic torques, $(\nabla\rho \times \nabla p)/\rho^2$, and viscous diffusion. For a low Mach number flow without heat release, the expansion and baroclinic torque terms will be zero. When density changes due to heat release do occur, these two mechanisms can be important in the vorticity dynamics. For a two-dimensional flow, the vortex stretching term is identically zero, and if no heat is released equation 5 becomes

$$\frac{D\vec{\omega}}{Dt} = \frac{1}{Re}(\nabla^2\vec{\omega}) \qquad (6)$$

showing that vorticity follows fluid particle paths in the absence of diffusion.

The instantaneous spanwise component of vorticity (ω_3) at times of t=48 and 72 is shown in figures 22 and 23 for runs 1 and 2 (three-dimensional perturbations, no forcing). In the following figures, dashed contour lines indicate negative vorticity (local rotation of fluid elements in the clockwise direction) and solid lines indicate positive vorticity. One of the most apparent differences between these two figures is that, for the simulations with heat release, the maximum amplitude of the vorticity, which occurs in the vortex cores, has decreased substantially. Furthermore, the vorticity is not as concentrated in the center of the large structures as in the constant density case. Also note the regions of positively signed vorticity that appear at the outer edges of the vortex structures for the case with heat release. This same behavior has been seen in previous two-dimensional calculations.[13] The results of the cases with and without forcing are again qualitatively similar so only the results with the initial random velocity field (runs 1 and 2) are discussed below. In the following, the mechanisms responsible for these effects and their influence on the flow field development are discussed.

Thermal Expansion and Baroclinic Torque

In an expanding flow, $\nabla \cdot v$ is positive; therefore, the effect of thermal expansion results in a decrease in the magnitude of vorticity (see equation 5). This can also be understood by angular momentum considerations, since as a fluid element expands due to heat release, the magnitude of vorticity must decrease to conserve angular momentum.

The instantaneous value of the spanwise component of the expansion term is shown in figure 24 at two different times. Thermal expansion occurs as heat is released by the chemical reaction so that this term also gives a good indication of the reaction zone. The rate of reaction is highest where the inflow of reactants is the highest. This occurs in the regions of highest strain, which are located in the braids. The result of the expansion is a decrease in the magnitude of vorticity, which in part explains the changes in the vorticity field that result when exothermic chemical reactions occur. (For a temperature dependent reaction, the high dissipation rates in the braids can cause local quenching of the flame so that the reaction rate is not necessarily highest in the regions where the inflow of reactants is the highest.[44,45] This effect is not addressed here.)

Another mechanism that affects the vorticity distribution in the mixing layer is the baroclinic torque, $(\nabla\rho \times \nabla p)/\rho^2$. This results from nonaligned pressure gradients and density gradients. Plots of the spanwise component of this term at specific spanwise locations show an alternating sign across the reaction surface and no contribution in the vortex cores (figure 25). This can be understood by recognizing that the density gradient changes sign across the reaction surface and the pressure gradient vector points approximately radially outward from the vortex cores. In the vortex cores the pressure and density gradients are small and are also approximately aligned, so there is no contribution of this term here. As the layer rolls up and winds around itself, the baroclinic torque takes on the complicated structure shown in figure 25b. Comparisons with the results of two-dimensional simulations show that these effects are dominated by two-dimensional dynamics.

Comparing figures of the spanwise vorticity component (figure 22) and the instantaneous baroclinic torque (figure 25) shows that the regions of positively signed vorticity at the outer regions of the vortices, and also the appearance of multiple extrema in the vorticity field, are a result of the baroclinic torque. The overshoot in the velocity profile seen in the previous section (figures 9 and 10) is a result of the generation of positive vorticity in this region by the baroclinic torque. This is also the mechanism that produces the previously unexplained inflection points seen in the velocity profile at the outer edges of jet diffusion flames.[23]

In an attempt to understand the relative importance of the expansion and baroclinic torque terms on the development of the flow, average values of these two terms are plotted as a function of the height across the mixing layer for a sequence of times (figure 26). (Negative values of the expansion term indicate a decrease of vorticity while negative values of the baroclinic torque indicate an increase.) The magnitude of the expansion term is seen to be initially stronger than the baroclinic torque term. At later times, the amplitude of the two terms are comparable. Note that the expansion term consistently produces a net decrease in vorticity. The baroclinic torque tends to decrease the vorticity near the upper and lower limits of the dynamically active region, at least during the initial stages when the two-dimensional modes dominate the flow. This is consistent with the generation of regions of positive vorticity at the edges of the cores (figure 25). Note also that the baroclinic vorticity generation on the centerline is occurring in the braids rather than the cores.

The baroclinic torque and thermal expansion have shown to result in weaker and more diffuse vortex structures. This will result in a slower rollup of the layer, thus reducing the straining of the reaction interface and decreasing the mass entrainment into the layer. This accounts for the decrease seen in the overall product formation and the changes in the layer growth rate. In section 3 it was shown (figures 11-14) that with heat release, the layer growth rate initially increases, and then decreases compared with the constant density case. The initial increase was explained to be due to thermal expansion, which tends to shift the whole layer outward. Later in the development of the mixing layer, however, the growth is dominated by the large scale rollup and pairing process. Since this process is inhibited by heat release, the constant density mixing layer will then grow faster. Note also that this behavior is more apparent between runs 1 and 2 (unforced) than between runs 3 and 4 (forced). In runs 3 and 4, the effects of two-dimensional rollup are felt sooner, since the flowfield was initialized with coherent perturbations (in addition to the random background noise) corresponding to the most unstable wavelengths. The initial rms amplitudes of the velocity perturbations were approximately 25% higher in runs 3 and 4 than in runs 1 and 2, due to the addition of the coherent two-dimensional perturbations.

The relative importance of the expansion and the baroclinic torque on the flow field development depends on the geometry of the mixing layer. Experiments and simulations have shown that, in a reacting mixing layer, combustion products are concentrated in the vortex cores. This implies that the density changes in the cores will be responsible for most of the observed heat release effects. Since the baroclinic torque is weakest in the cores, it might be expected that thermal expansion alone can account for most of the significant changes of the altered vorticity field. Furthermore, from figure 25 it can be seen that regions of strong vorticity generation due to the baroclinic torque are located adjacent to corresponding regions of vorticity destruction. This is due to the change in sign of the density gradient across the reaction surface as explained above. Therefore, although the magnitude of the baroclinic torque may be quite large, the effect on the flow field falls off rapidly with distance from these regions. This may cause local changes in the flow field, but the global effects on the large scale structures will not be as strong as those due to thermal expansion. However, as the vorticity generated by the baroclinic torque is convected in the layer and engulfed into the large scale structures, the integrated effects over time of the baroclinic torque and thermal expansion become

difficult to isolate. Since the local magnitudes of these two terms are of the same order both effects should be accounted for.

The effects of heat release on the three-dimensional, spanwise variation in the reactant concentrations presented in section III can also be interpreted in terms of the vorticity dynamics. Secondary instabilities in the flow are characterized by counterrotating streamwise vortices.[4] The flow field induced by these vortices enhances mixing and increases the surface area of the interface between the two reacting chemical species, as shown in figures 27 and 28. In figure 27 the streamwise component of vorticity at a time of t=72 is plotted at the streamwise location x = π. Comparing this with a similar plot of run 2 (figure 28) shows a less intense streamwise component of vorticity when heat release accompanies the chemical reaction. The changes seen between these two figures are typical of any streamwise cut. Undoubtedly, mechanisms similar to those discussed for primary instabilities also work to reduce the growth of secondary instabilities in the presence of heat release.

Stability Considerations

A question that arises in these simulations is 'how are the stability characteristics of the mixing layer affected by heat release?' There are both physical and numerical reasons for addressing this question. If the unstable modes shift to other frequencies, or if the growth rates change as a result of density changes, this certainly can affect the growth of the mixing layer and the rate at which chemical products are formed.

From a computational point of view, it is not possible to look at a continuous distribution of frequencies. Because of the periodic boundary conditions employed here, only disturbances of wavelengths that divide exactly into the computational domain are allowed (λ=domain size/n). Therefore, if the most unstable modes shift to different wavelengths, dynamically important effects may be overlooked.

To address this question, a linear stability analysis of a simplified model problem was carried out in conjunction with the simulations. This analysis involved a shear layer with a piece-wise linear velocity profile with a low density in the velocity transition region (figure 29). The velocity and density in the free stream were constant, and the density in the transition zone was also constant and given by $\rho(1-\beta)$, $0<\beta<1$. Although this does not exactly describe the conditions in the simulations reported here, the basic characteristics of the two are similar, so that the general trends indicated by the analysis are expected to be true of the simulations. Details of the analysis are given in McMurtry.[45]

The results of this analysis are plotted in figure 30, which shows the growth rate of any individual unstable mode (specified by its wave number) for a given value of β. As the density decreases (increasing β), the most unstable mode, represented as the maximum value on each curve, shifts to a lower wave number (longer wavelength). The growth rates of the unstable modes are also seen to decrease as the density is lowered, a result consistent with the lower growth rates discussed in section 3.

The energy, $E(k_x,k_z)$ contained in various modes as a function of time is shown in figures 31 and 32 for runs 1 and 2 (initial random perturbation velocity field). The energies are defined here as

$$E(k_x,k_z) = \int_{-\infty}^{\infty} |\vec{v}(k_x,k_z,y)|^2 dy$$

where

$$\vec{v}(k_x,k_z,y) = \sum_{k_y=0}^{N} \vec{u}(k_x,k_z,k_y,t)X(k_y,y)$$

and $\vec{u}(\vec{k},t)$ are the Fourier components of the velocity and X is either $\sin(k_y y)$ or $\cos(k_y,y)$, depending on the component of the velocity under consideration. In the following discussion, we analyze the temporal behavior of the energies in these Fourier modes. Although we refer to the modes $E_{1,0}$ and $E_{1/2,0}$ as the fundamental and subharmonic respectively, it is important to note in the interpretation of these results that this correspondence is not exact. For example, the subharmonic mode by itself does develop higher wavenumber components as it rolls up. Thus, the Fourier mode $E_{1,0}$, while being dominated by the energy of the fundamental, can also contain some energy of the subharmonic mode.

In figure 31, the the fundamental ($E_{1,0}$) grows until a time of t = 40, at which point it reaches a quasi-equilibrium, saturated state.[3,26] The subharmonic ($E_{1/2,0}$) continues to grow until it reaches its saturation level at t = 65. The behavior of these two modes changes significantly when heat release occurs. The growth of the fundamental drops off at a level well below the incompressible saturation level and at a much earlier time (figure 33), although the initial growth before much density change occurs (up to about t=7) is the same in the two cases. The subharmonic remains unstable but grows at a lower rate and reaches saturation at a later time than in the constant density case (figure 34). The energy in the three-dimensional modes (the sum of $E(k_x,k_z)$ for all $k_x$and $k_z \neq 0$) is also decreased due to the heat release as shown in figure 35.

The results of the simplified linear analysis for the linear profiles compare favorably with the simulation results. The density changes occurring in run 2 correspond to a β of 0.5. With this amount of heat release, the most unstable mode in the constant density case is predicted to be stable, which is consistent with the modal behavior in the simulations (figure 33). The actual most unstable mode shifts to a wave number of 0.3, which is fairly close to the wave number of the subharmonic of the most unstable mode in the constant density case (0.22). From figure 34, the growth rate of the subharmonic is shown to reduce from 0.18 to 0.13, while in the simulations the computed growth rate of the subharmonic decreased from 0.12 to 0.09 in the heat release case. In figure 34 this lower growth rate of the subharmonic is indicated by the smaller slope.

The temporal behavior of the various modes when the layer is initially forced at the fundamental and subharmonic (runs 3 and 4) is shown in figures 36

and 37. With these levels of forcing, the growth of the fundamental is not suppressed by the heat release nearly as dramatically as in the case with no forcing. The fundamental stabilizes at a slightly earlier time in the heat release case (at t=18 vs. t=21 for the constant density case) and the energy contained in this mode is only a factor of two lower. This observation may be a result of the time it takes for the density decreases to develop in the simulations. During this time, the instabilities will grow. With high enough levels of forcing, substantial rollup can occur before the stabilizing effects of heat release are strongly felt.

The laboratory experiments on mixing layers, although clearly showing lower growth rates as heat release is increased, do not conclusively show anything regarding the total supression of some modes or a shift in the wavelengths of the most unstable modes. This particular aspect has not been carefully investigated in the experiments, although Hermanson[12] suggests there is little change in the spacing (wavelengths) of the vortex cores when heat release occurs. This has been observed, however, in experiments on jets (Yule et al., 1981) which showed the value of the most energetic frequencies decreased as heat release increased.

There are a number of possible reasons for why this behavior may not be as apparent in laboratory experiments as in the simulations. First, the suppression of higher wave number components in the simulations could in part result from the thicker reaction zone that exists in the simulations compared to the experiments. This is a consequence of a lower Damkohler number in the simulations, which is necessary to achieve accurate resolution of the reaction zone structure. Secondly, in the experiments, the turbulence levels in the boundary layer at the splitter plate are often much higher than in the simulations presented here, so that the flow instabilities may not be governed by linear stabity theory. Finally, any laboratory experiment on mixing layers is extremely sensitive to any type of external forcing. This forcing is often applied purposely, or can result from any disturbances or resonances associated with the experimental setup. Such resonances exist in any experimental facility, and even extremely low levels of facility generated coherent disturbances can result in large variations in the development of the shear layer.[47] The simulations performed here (runs 3 and 4) also show that even low levels of coherent forcing have a significant impact on the growth of the unstable modes. This problem of how heat release affects the growth rates and wavelengths of the unstable modes is an area that calls for further experimental work.

5. Summary

The simulations performed as a part of this work and similar laboratory experiments have shown that, when heat release accompanies the chemical reaction, the mixing layer grows at a lower rate and the amount of product formed decreases. In addition, an overshoot in the velocity profile appears. In the previous section, four different aspects of the flow were studied to explain the observed effects of heat release: the turbulent shear stresses, the turbulent kinetic energy, vorticity dynamics, and stability considerations. These different considerations must be consistent with each other and, therefore, only provide different viewpoints from which the flow can be studied.

The study of the flow in terms of the vorticity dynamics explored the two actual mechanisms that do not act in constant density flows: the baroclinic torque and thermal expansion. The action of these mechanisms was shown to result in more diffuse and weaker vortices when heat release accompanies the chemical reaction. At the largest scales (which dominate the dynamics of the flow and account for most of the turbulent transport), the altered vorticity distribution resulted in slower rollup of the most unstable modes, giving lower growth rates and less entrainment of unmixed fluid. This was indicated by the lower energies and growth rates of the unstable modes computed in the simulations and confirmed by a stability analysis of a simplified model problem similar to the mixing layer flow simulated here. The appearance of "humps" in the velocity profile were shown to be the result of vorticity generation in the outer regions of the vortices by baroclinic torques.

The turbulent kinetic energy and the turbulent stresses are closely related, since the turbulent stresses are a direct indication of the kinetic energy transfer from the mean flow to or from the turbulence. Lower values of both the turbulent kinetic energy and the turbulent stresses were observed in the heat release runs. This can be related directly to the vorticity dynamics by realizing that in turbulent flows, the largest eddies (vortices) are responsible for most of the transport of momentum and scalar variables. The weaker large-scale vortices that result when heat release occurs transport less momentum, which is exactly what the lower values of the turbulent shear stresses indicate. The transport rates of the chemical reactants will also result in less product formation, as observed in the simulations and similar experiments.

Acknowledgements

This work was supported by the NASA Lewis Research Center under contract NAS3-24229. All computer simulations were perfomed on the CRAY X-MP at NASA Lewis. This work benefitted from many discussions with Mr. Russ Claus. The substantial efforts of Dr. W.-H. Jou concerning both physical interpretations and aspects of the numerical solution are greatly appreciated.

References

1. Brown, G. L. and Roshko, A. (1974) "On Density Effects and Large Structure in Turbulent Mixing Layers", J. Fluid Mech., Vol. 91 pp. 319-335.

2. Winant, C.D. and Browand, F.K., (1974) "Vortex Pairing, The Mechanism of Turbulent Mixing-Layer Growth at Moderate Reynolds Number," J. Fluid Mech., Vol. 63, pp. 237-255.

3. Riley, J.J. and Metcalfe, R.W., (1980) "Direct Numerical Simulations of a Perturbed, Turbulent Mixing Layer," AIAA Paper No. 80-0274.

4. Bernal. L. P. (1981) "The Coherent Structure Of Turbulent Mixing Layers. I. Similariity of the Primary Vortex Structures. II. Secondary Streamwise Vortex Structure", Ph.D Thesis, Calif. Inst. of Technology, Pasadena.

5. Konrad, J.H. (1976) "An Experimental Investigation of Mixing in Two-Dimensional Turbulent Shear Flows With Application to Diffusion Limited Chemical Reactions", Ph.D Thesis, Calif. Inst. of Technology, Pasadena.

6. Breidenthal,R.E. (1981) "Structure in Turbulent Mixing Layers and Wakes Using a Chemical Reaction," J. Fluid Mech., Vol. 109, pp. 1-24.

7. Koochesfahani, M.M. (1984) "Experiments On Turbulent Mixing And Chemical Reactions in a Liquid Mixing Layer", Ph.D Thesis, Calif. Inst. of Technology, Pasadena.

8. Mungal, M.G. and Dimotakis, P.E., (1984) "Mixing and Combustion With Low Heat Release in a Turbulent Shear Layer" J. Fluid Mech., Vol. 148, pp. 349-382.

9. Masutani, S.M. (1985) "An Experimental Investigation of Mixing and Chemical Reaction in a Plane Mixing Layer", Ph.D Thesis, Stanford University, California.

10. Riley, J.J. and Metcalfe, R.W., and Orszag, S.A. (1986), "Direct Numerical Simulations of Chemically Reacting Mixing Layers," The Physics of Fluids, Vol. 29, 2 pp. 406-422.

11. Wallace, A.K. (1981) "Experimental Investigation on the Effects of Chemical Heat Release on Shear Layer Growth and Entrainment", Ph.D Thesis, University of Adalaide, Australia.

12. Hermanson,J.C. (1985) "Heat Relelase Effects in a Turbulent Shear Layer," Ph.D Thesis, California Institute of Technology.

13. McMurtry, P.A., Jou, W.-H., Riley, J.J. and Metcalfe, R.W. (1986) "Direct Numerical Simulations of a Reacting Mixing Layer With Chemical Heat Release," AIAA Journal, Vol. 24 (6).

14. Keller, J.O. and Daily, J.W. (1985) "The Effects of Highly Exothermic Chemical Reaction on a Two-Dimensional Mixing Layer," AIAA Journal, Vol. 23 (12).

15. Hsiao, C.C., Oppenheim, A.K., Ghoniem, A.F. and Chorin, A.J. (1984) "Numerical Simulation of a Turbulent Flame Stabilized Behind a Rearward-Facing Step," Twentieth Symposium (International) on Combustion, The Combustion Institute.

16. Ghoniem, A.F., Chorin, A.J., and Oppenheim, A.K. (1981) "Numerical Modeling of Turbulent Coombustion in Premixed Gases," Eighteenth Symposium (International) on Combustion, The Combustion Institute.

17. Pitz, R.W., and Daily, J.W., (1983) "Combustion In A Turbulent Mixing Layer Formed At A Rearward-Facing Step," AIAA Journal, Vol.21, pp. 1565-1570.

18. Chorin, A.J. (1973) "A Numerical Study of Sligthly Viscous Flows", J. Fluid Mech., Vol. 57, p. 785.

19. Whol, K., Gazley, C., and Kapp, A.J., (1949) "Diffusion Flames", Third Symposium on Combustion Flame and Combustion Phenomena, Combustion Institute, Pittsburgh, Pa.

20. Hottel, H.C., and Hawthorne, W.R., (1953) Third Symposium (International) on Combustion, Williams and Wilkens, p. 254.

21. Takeno, T. and Kotani, Y., (1975) Acta Astronatica, Vol. 2, p. 999.

22. Takagi, T., Shin, H.-D., and Ishio, A. (1980) "Local laminarization in Turbulent Diffusion Flames," Combustion and Flame, Vol. 37 pp. 163-170.

23. Yule, A.J. Chiger, N.A., Ralph, S. Boulderstone, R., and Ventura, J. (1981) "Combustion-Transition Interaction in a Jet Flame," AIAA Journal, Vol. 19, 6, pp, 752-760.

24. Marble, F.E. and Broadwell, J.E. (1977) "The Coherent Flame Model Furbulent Chemical Reactions", Project SQUID Technical Report, TRW-9-PU.

25. Karagozian, A. (1982) "An Analytical Study Of Diffusion Flames In Vortex Structures", Ph.D Thesis, Calif. Inst. Of Technology, Pasadena.

26. Metcalfe, R.W., Orszag, S.A., Brachet, M.E., Menon, S., and Riley, J.J., (1986) "Secondary Instability of a Temporally Growing Mixing Layer," Submitted to J. Fluid Mech.

27. Corcos, G.M. and Sherman, F.S. (1984) "The Mixing Layer: Deterministic Models of a Turbulent Flow. Part 1. Introduction and the Two-dimensional Flow", J. Fluid Mech., Vol. 139, pp. 29-65.

28. Bilger,R.W. (1980) in Turbulent Reacting Flows, P.A. Libby and F.A. Williams, ed., Springer-Verlag, New York.

29. Orszag, S.A. and Patterson, G.S., (1972) "Numerical Simulation of Turbulence," in Statistical Models And Turbulence, p. 127, Springer-Verlag.

30. Mansour, N.N, Moin, P., Reynolds, W.C., and Ferziger, J.H., (1979) "Improved Methods For Large Eddy Simulation of Turbulence," in Turbulent Shear Flows I, Springer-Verlag.

31. Rogallo, R.S., (1981) "Numerical Experiments In Homogeneous Turbulence," NASA Technical Memorandom 81315, Ames Research Center, Moffett Field, California.

32. Orszag, S.A. and Pao, Y. (1974) " Numerical Computation of Turbulent Shear Flows", Advances In Geophysics, Vol. 18, pp. 225-236.

33. Riley, J.J. and Metcalfe, R.W., (1978) "The Direct Numerical Simulations of the Turbulent Wakes of Axisymmetric Bodies", Flow Research Report No. 135, Flow Research Co., Kent, WA.

34. Moin, P. and Kim, J. (1982) "Numerical Investigation of Turbulent Channel Flow," J. Fluid Mechanics, Vol. 118, pp. 341-377.

35. Patera, A.T. and Orszag, S.A. (1981) in Proceedings Of The Seventh Conference On Numerical Methods In Fluid Mechanics, Springer-Verlag, Berlin, p.386.

36. Rehm, R.G. and Baum, H.R., (1978) "The Equations of Motion For Thermally Driven, Buoyant Flows," Journal Of Research, National Bureau of Standards, Vol. 83, pp. 297-308.

37. Sivashinsky, G.J. (1979) "Hydrodynamic Theory of Flame Propogation in an Enclosed Volume," Acta Astronautica, Vol 6, pp. 631-645.

38. Buckmaster, J.D., (1985) " An Introduction To Combustion Theory," in The Mathematics Of Combustion, J. Buckmaster, ed. SIAM.

39 Majda, A. and Sethian, J. (1985) "The Derivation and Numerical Solution of the Equations For Zero Mach Number Combustion," Combust. Sci. and Tech., Vol.42, pp. 185-205.

40. Lin, S.J. and Corcos, G.M. (1984) "The Mixing Layer: Derterministic Models of a Turbulent Flow. Part 3. The Effect of Plain Strain on the Dynamics of Streamwise Vortices," J. Fluid Mech., Vol. 141, pp. 139-178.

41. Libby, P.A. and Williams, F.A. (1980) "Fundamental Aspects of Turbulent Reacting Flows," in Turbulent Reacting Flows, Libby and Williams, Eds. Springer Verlag.

42. Oster, D., and Wygnanski, I. (1982) "The Forced Mixing Layer Between Parallel Streams," J. Fluid Mech., Vol. 123 pp. 91-130.

43. Ho, C.M. and Huang, L.S. (1982) "Subharmonics and Vortex Merging In Miixing Layers", J. Fluid Mech., Vol. 119, pp. 443-473.

44. Peters, N. (1983) "Local Quenching Due to Flame Stretching and Non-Premixed Turbulent Combustion," Combustion Science And Tech., Vol. 30 pp 1-17.

45. Givi, P., Jou, W.-H., and Metcalfe, R.W. (1986) "Flame Extinction in a Temporally Developing Mixing Layer," Twentyfirst Symposium (International) on Combustion, The Combustion Institute.

46. McMurtry, P.A. (1987) "Direct Numerical Simulations of a Reacting Mixing Layer With Chemical Heat Release," Ph.D. Thesis, University of Washington, Seattle, WA.

47. Gutmark, E., and Ho, C.-H. (1983) "Preferred Modes and the Spreading Rates of Jets," Phys. Fluids, Vol. 26, 10, p2932.

48. Hermanson, J. Personal communication and unplublished data.

49. Tennekes, H. and Lumley, J.L., (1972) A First Course In Turbulence, MIT Press, Cambridge, Mass.

50. Michalke, A. (1964) "On the Inviscid Instability of The Hyperbolic Tangent Velocity Profile", J. Fluid Mech., Vol. 19, pp. 543-556.

51. Gottlieb, D. and Orszag, S.A. (1977) Numerical Analysis of Spectral Methods, SIAM, Philadelphia.

TABLE 1

THREE-DIMENSIONAL SIMULATION PARAMETERS

Run No.	Domain	Re	Da	$A_{1,0}$	$A_{1/2,0}$	ϵ_{3D}	Ce	Λ
1	4π	500	2	0.0	0.0	0.00003	0	2
2	4π	500	2	0.0	0.0	0.00003	5	2
3	4π	500	2	0.01	0.01	0.00003	0	2
4	4π	500	2	0.01	0.01	0.00003	5	2

$A_{1,0}$ and $A_{1/2,0}$ are the amplitude of most unstable mode and its subharmonic as determined from a linear stability analysis of the hyperbolic tangent velocity profile.[50]

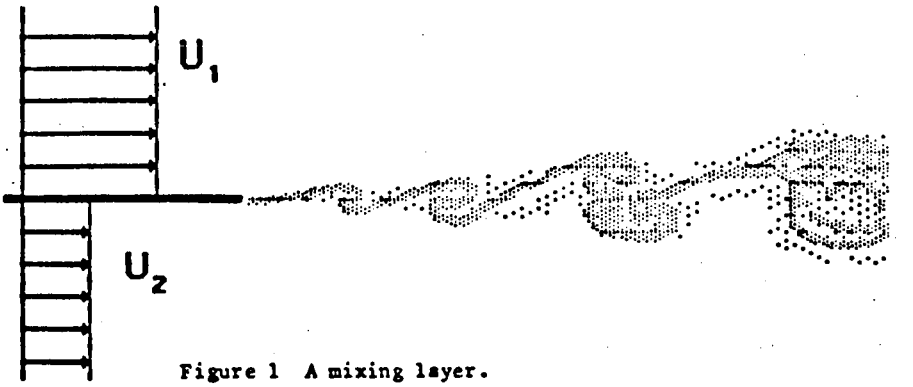

Figure 1 A mixing layer.

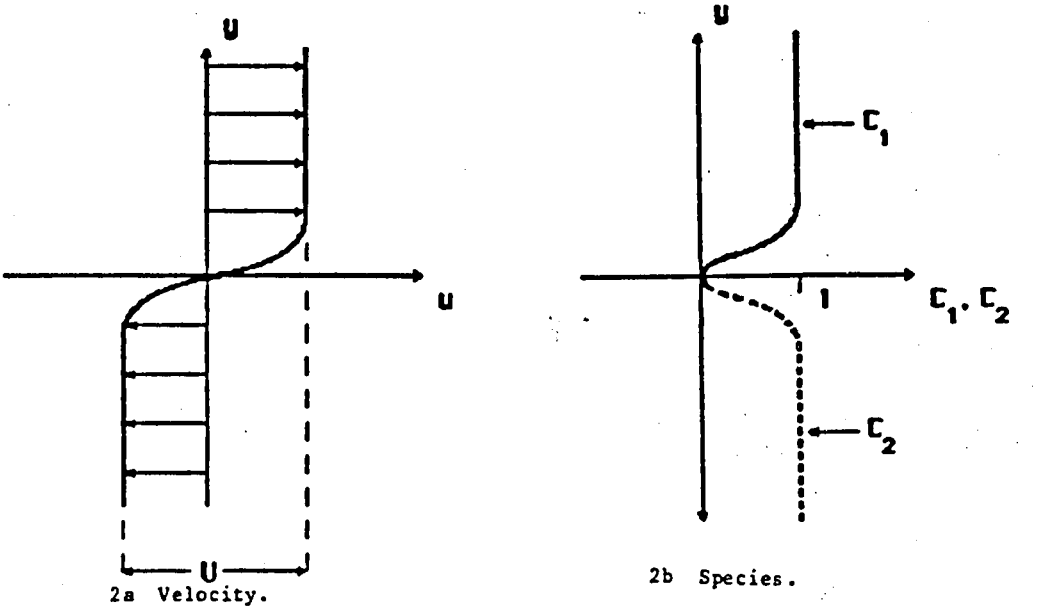

Figure 2 Initial mean velocity and chemical species field.

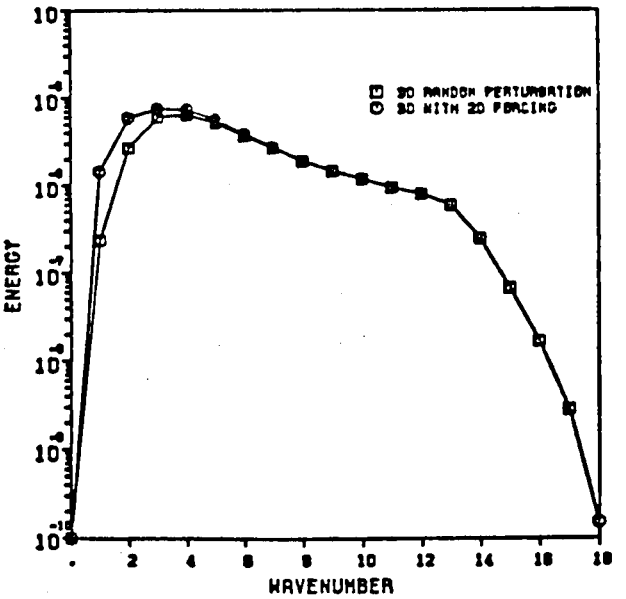

Figure 3 Initial energy spectrum for runs 1 and 2 (no two-dimensional forcing) and runs 3 and 4(forcing at most unstable wavelength and subharmonic).

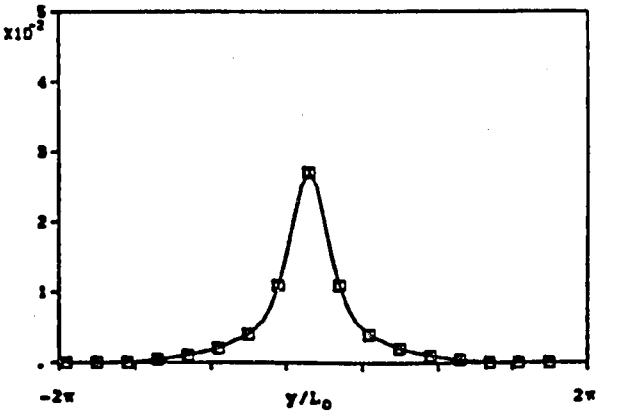

Figure 4 Initial rms velocity profile for runs 3 and 4.

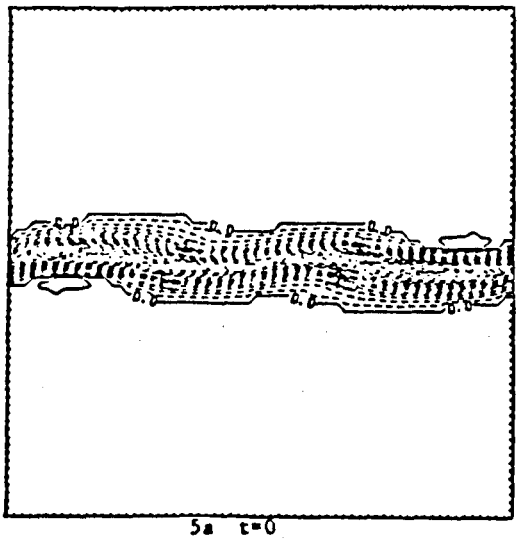

5a t=0

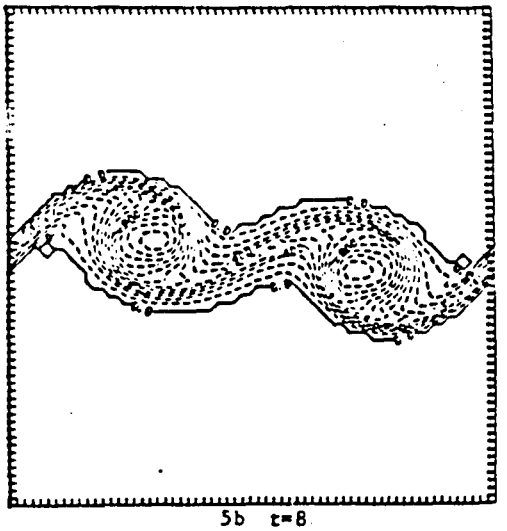

5b t=8

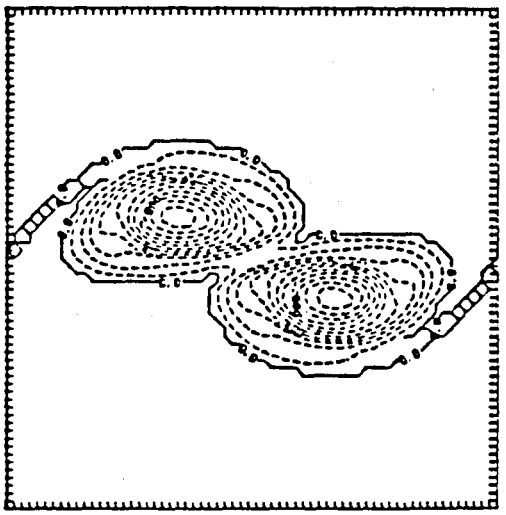

5c t=16

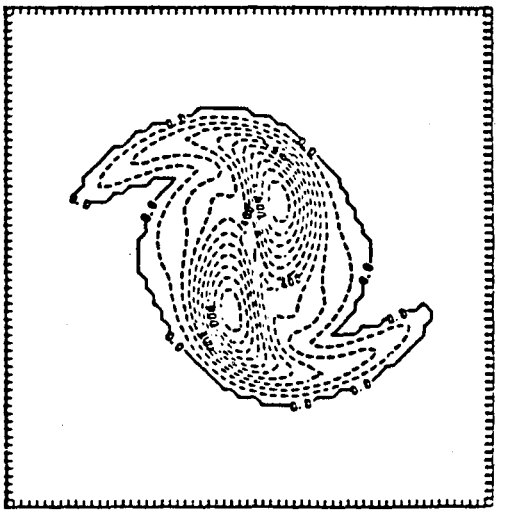

5d t=24

Figure 5 Spanwise component of vorticity. Two-dimensional simulation, no heat, run1.

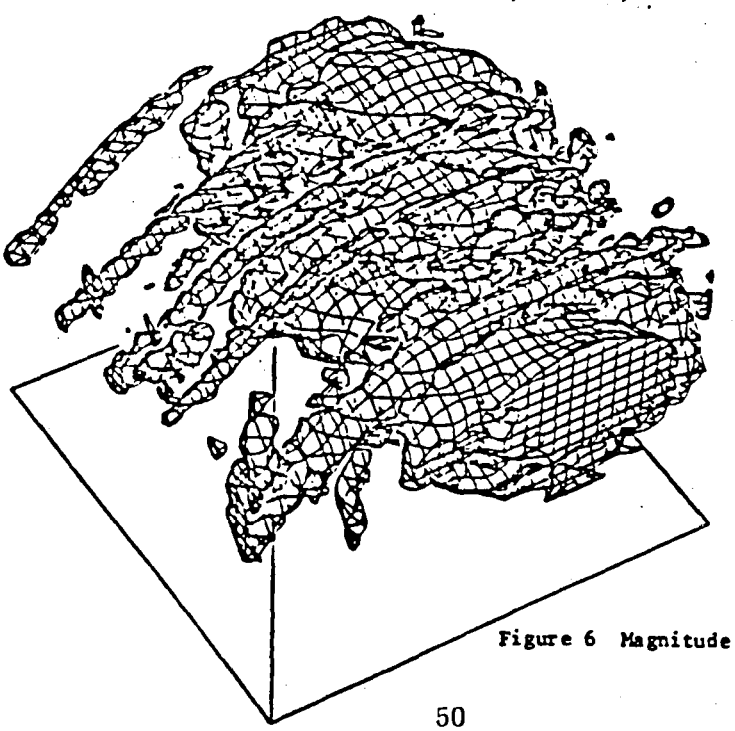

Figure 6 Magnitude of total vorticity, run1.

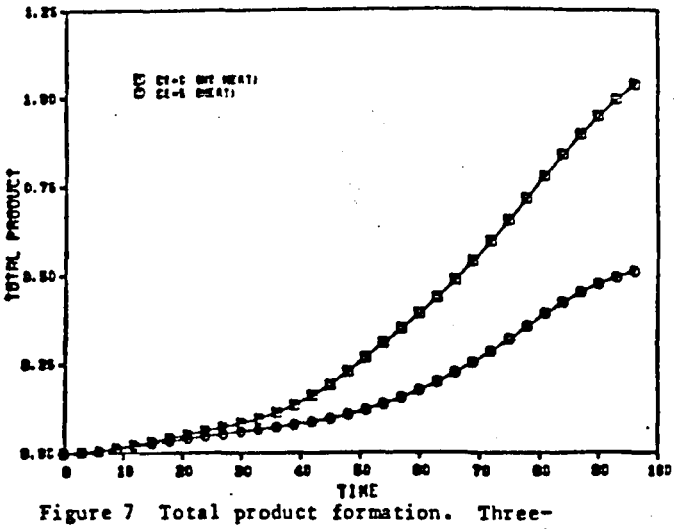

Figure 7 Total product formation. Three-dimensional simulation, no forcing, run1 (no heat), run2 (heat release).

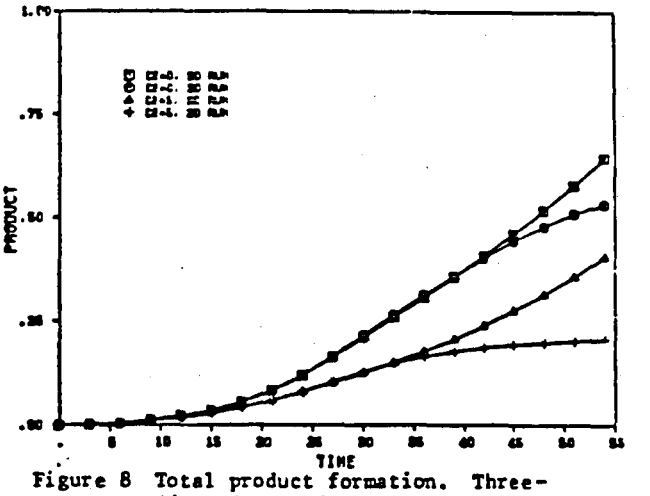

Figure 8 Total product formation. Three-dimensional simulation, forcing at fundamental and subharmonic, run3 (no heat), run4 (heat release) and two-dimensional simulation.

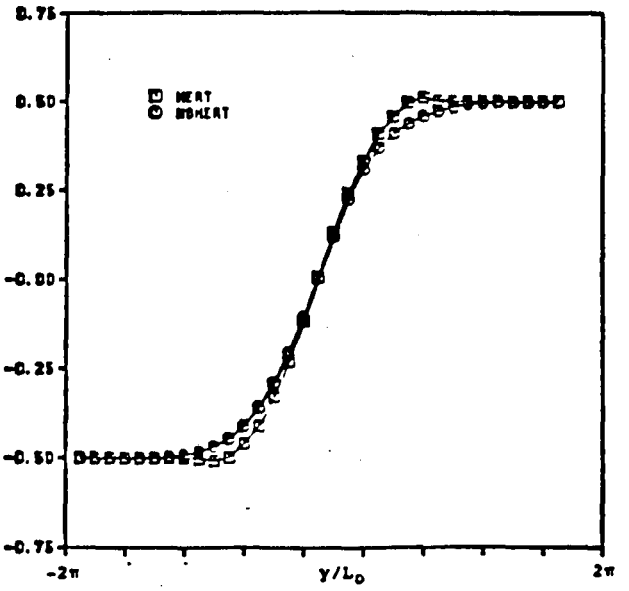

Figure 9 Velocity profile. Three-dimensional simulation, run1 (no heat, Ce=0), run2 (heat release, Ce=5), no forcing, t=72.

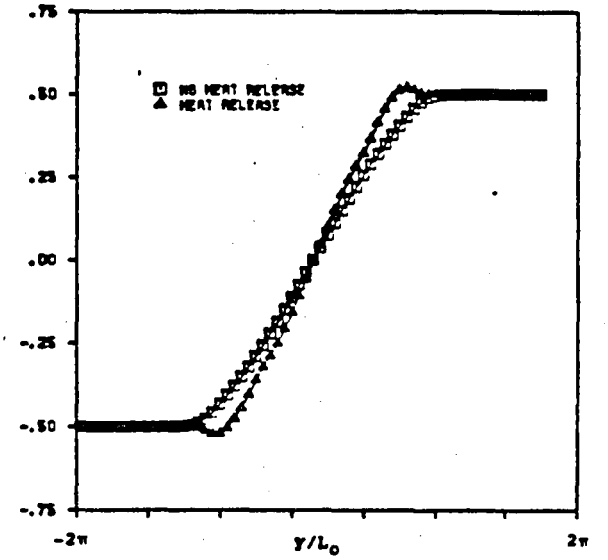

Figure 10 Velocity profile. Three-dimensional simulation, run3 (no heat, Ce=0), run4 (heat release, Ce=5), t=36.

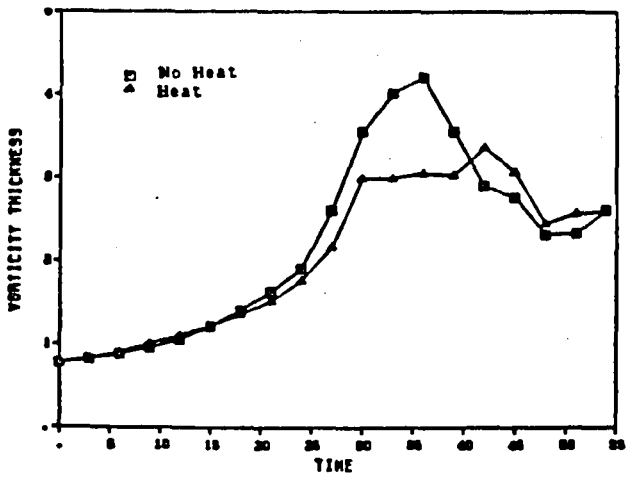

Figure 11 Vorticity thickness, three-dimensional simulation, run3 (no heat), run4 (heat release).

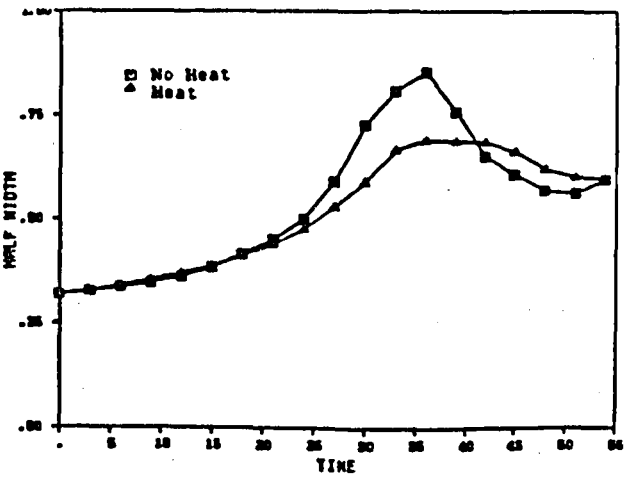

Figure 12 Velocity half width, three-dimensional simulation, run3 (no heat), run4 (heat release).

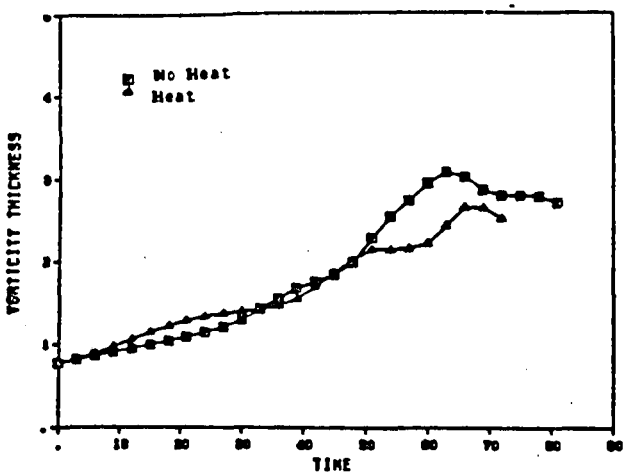

Figure 13 Vorticity thickness, three-dimensional simulation, run1 (no heat), run2 (heat release).

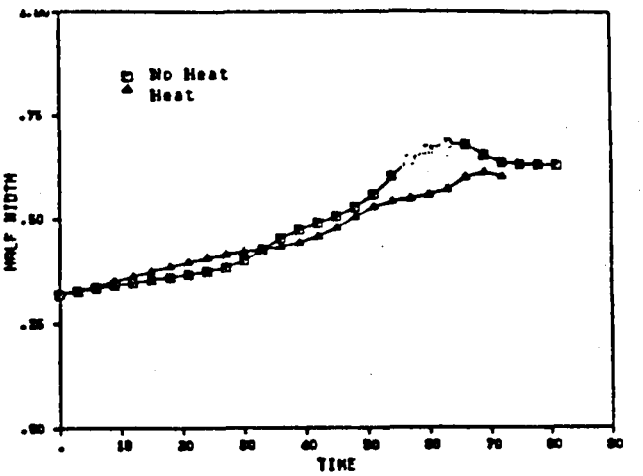

Figure 14 Velocity half width, three-dimensional simulation, run1 (no heat), run2 (heat release).

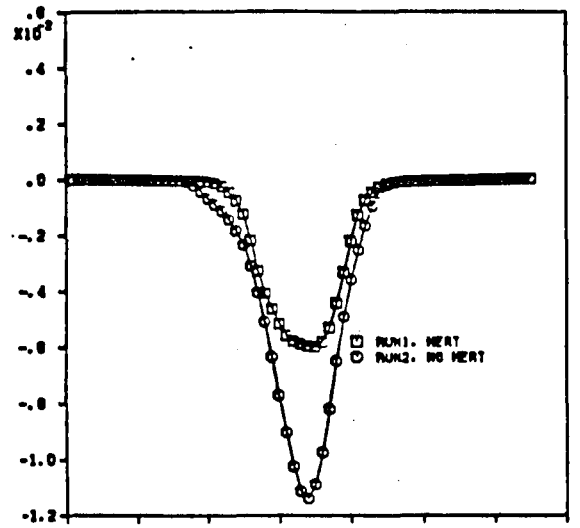

Figure 15 Favre average turbulent shear stress profile, runs 1 and 2, t=48.

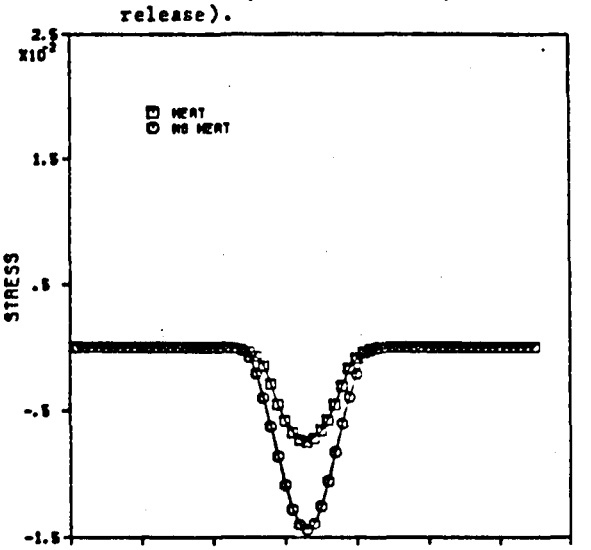

Figure 16 Favre average turbulent shear stress profile, runs 3 and 4, t=48.

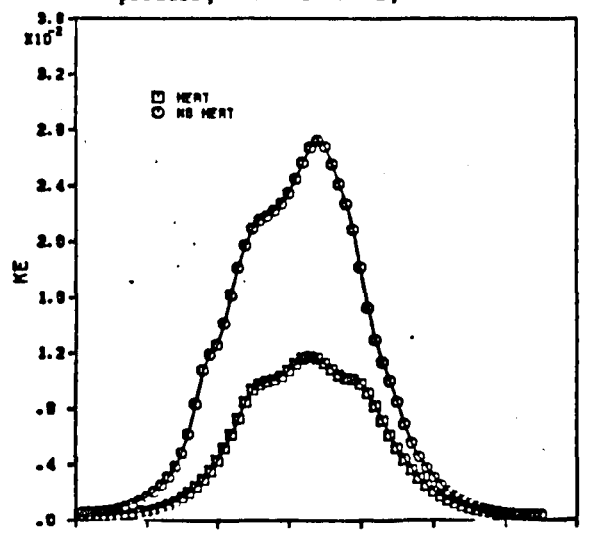

Figure 17 Turbulent kinetic energy profile, run1 (no heat), run2 (heat release), t=48.

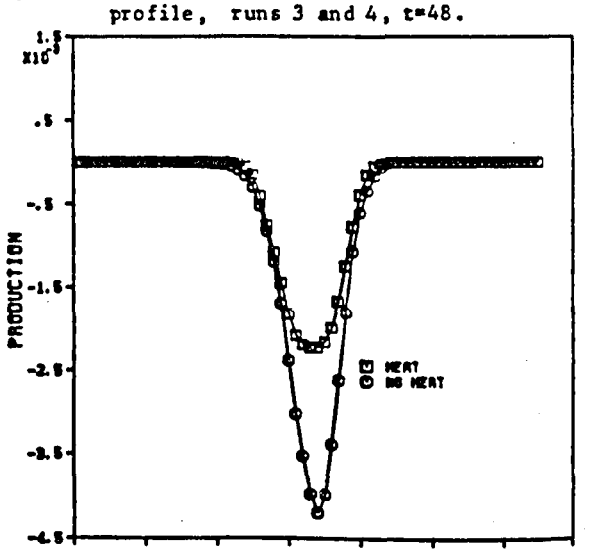

Figure 18 Production term in Favre averaged turbulent kinetic energy equation, run1 (no heat), run2 (heat release), t=48.

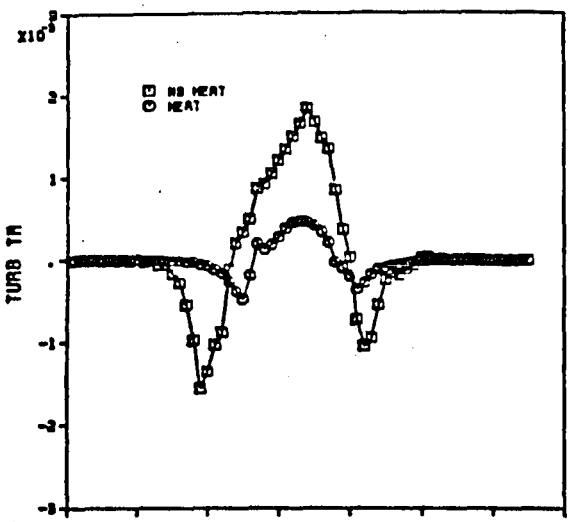

Figure 19 Turbulent transport term in kinetic energy equation, run1 (no heat), run2 (heat release), t=48.

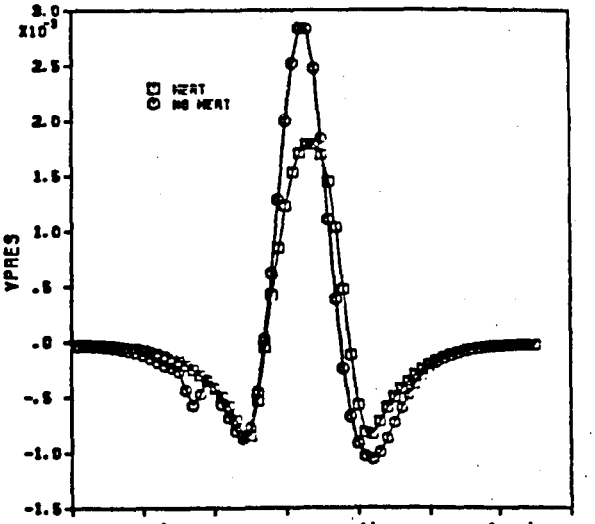

Figure 20 Velocity-pressure gradient correlation, run1 (no heat), run2 (heat release), t=48.

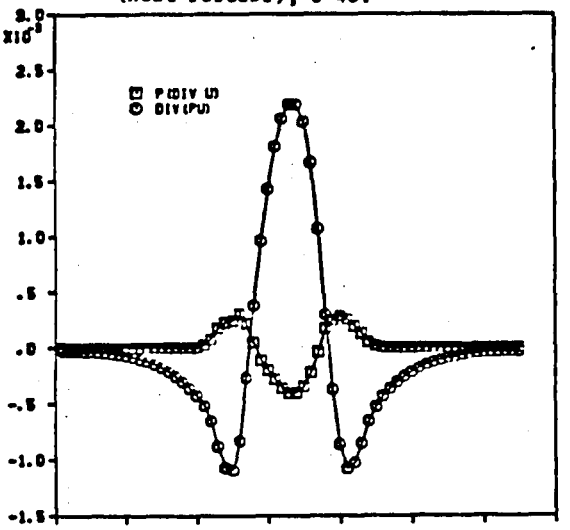

Figure 21 Contribution of of expansion and pressure fluctuations to velocity-pressure correlation.

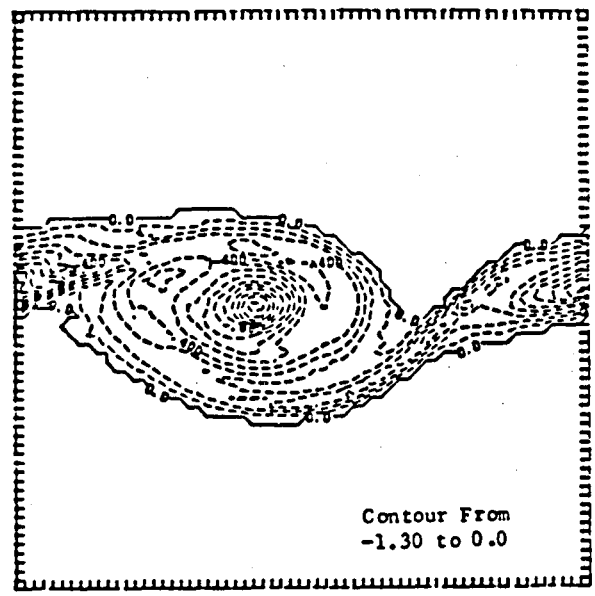

22a t=48.

Figure 22 Spanwise component of vorticity. Three-dimensional simulation, no heat, run1.

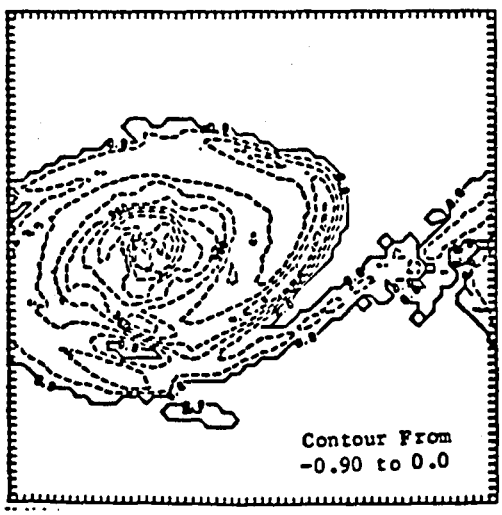

22b t=72.

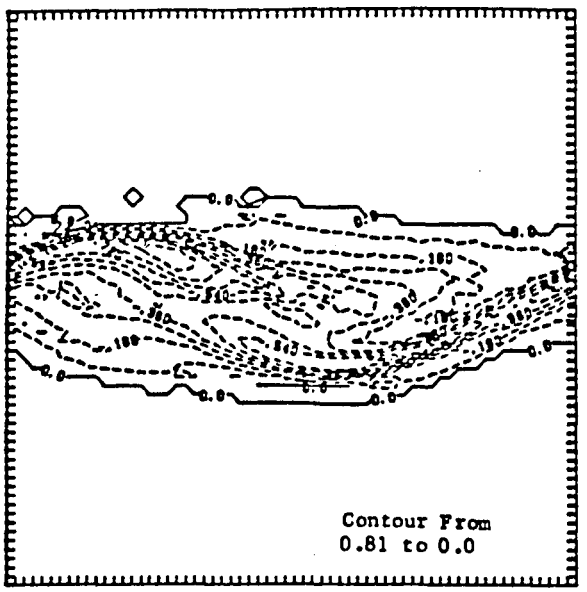

23a t=48.

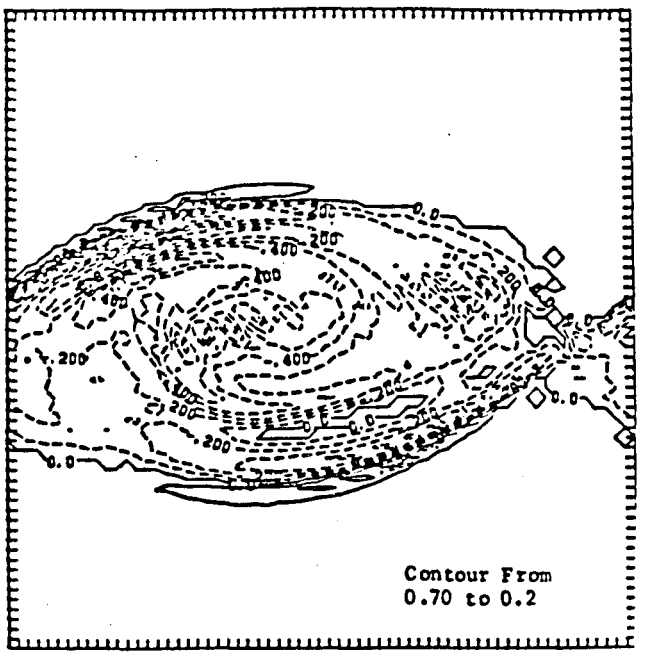

23b t=72.

Figure 23 Spanwise component of vorticity. Three-dimensional simulation, heat release, run2.

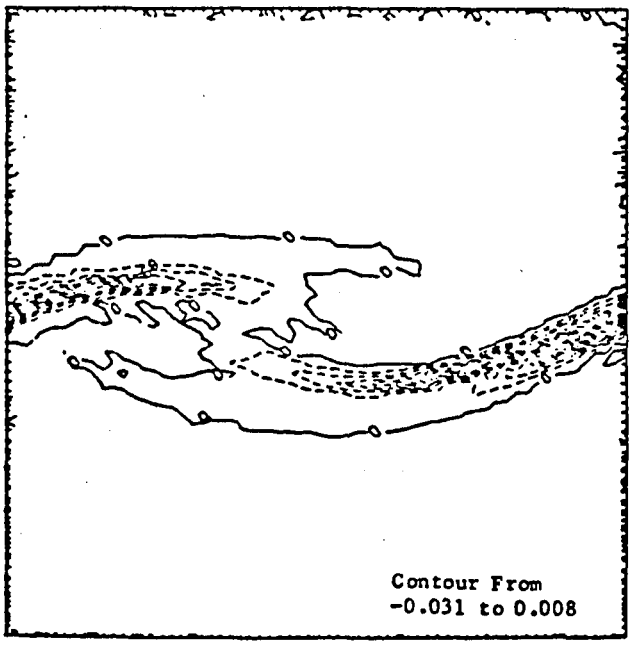

24a t=24.

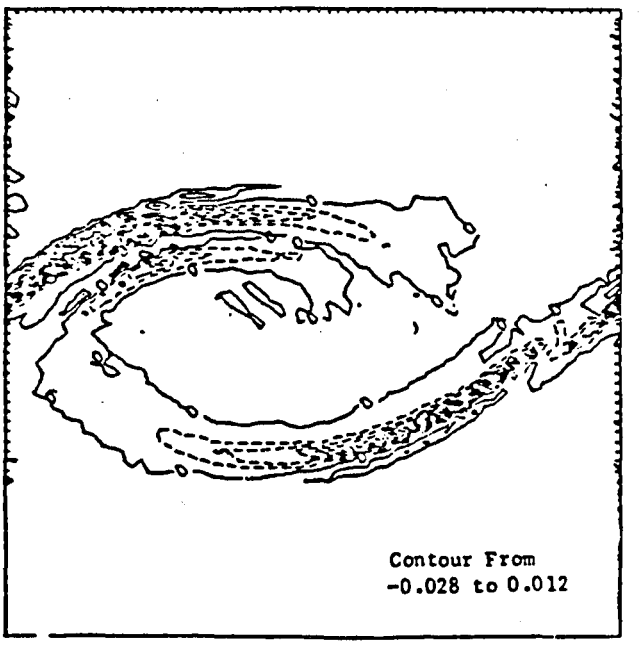

24b t=72.

Figure 24 Instantaneous value of expansion term in vorticity equation, run1, z=0.

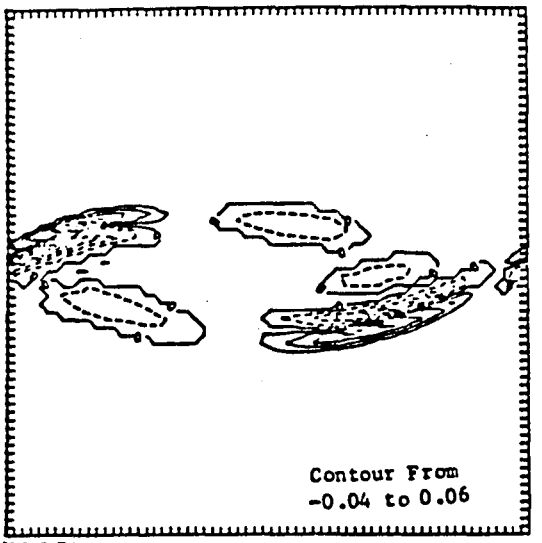

25a t=48.

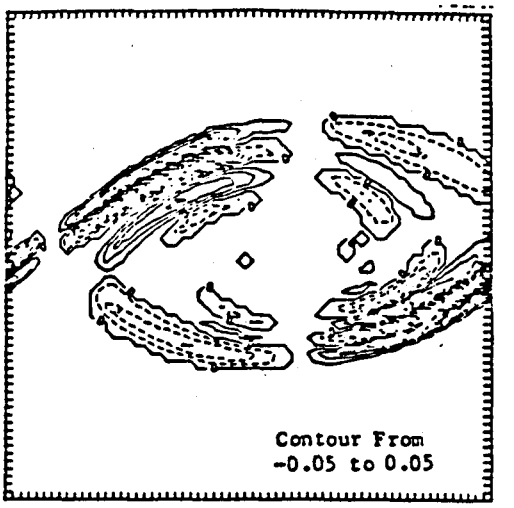

25b t=72.

Figure 25 Instantaneous value of baroclinic torque. Three-dimensional simulation, run2.

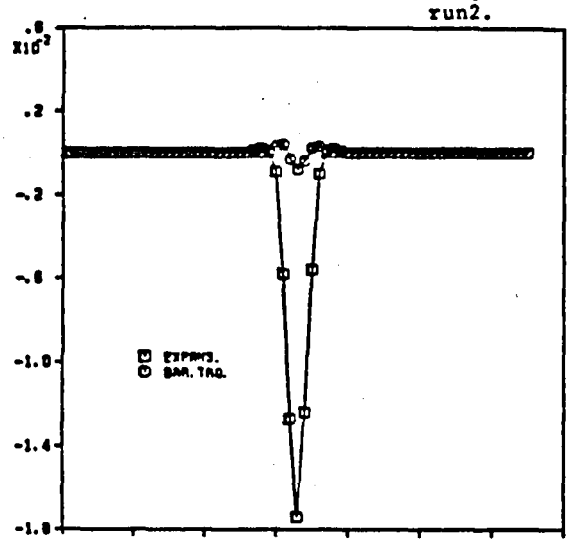

26a t=12.

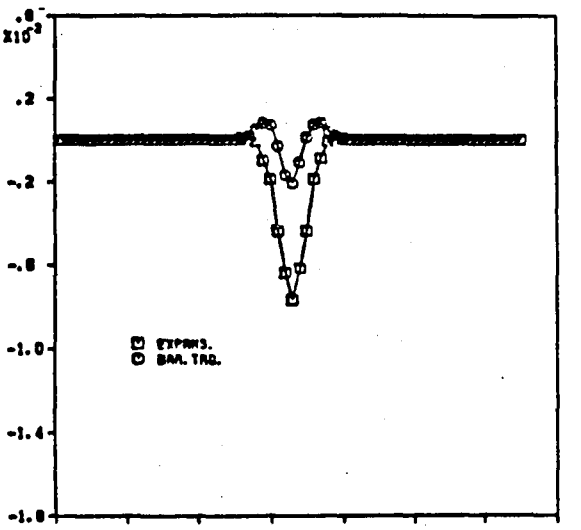

26b t=24.

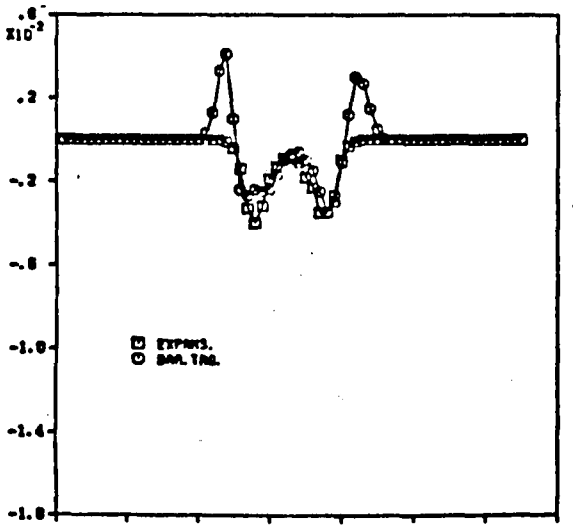

26c t=48.

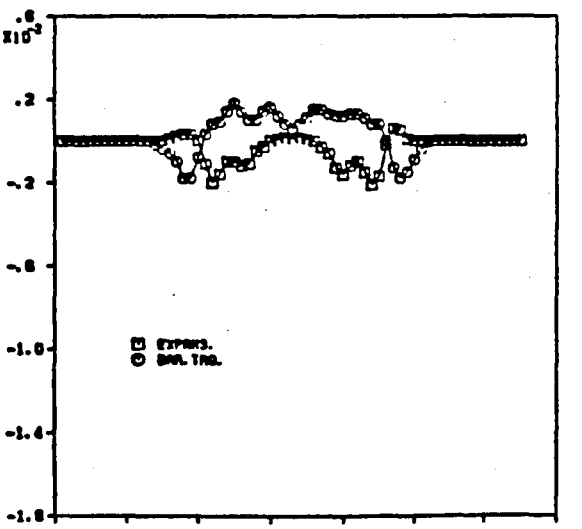

26d t=72.

Figure 26 Average value of baroclinic torque and expansion terms plotted across the mixing layer, run2.

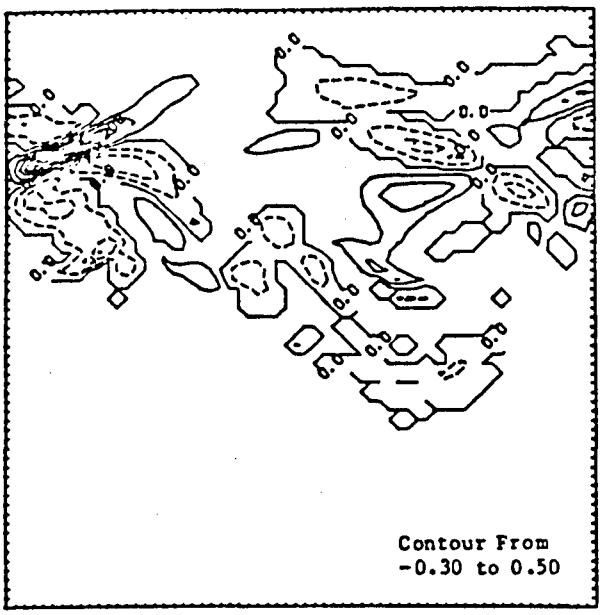

Figure 27 Streamwise component of vorticity, run2 (heat release) streamwise location x=π, t=72.

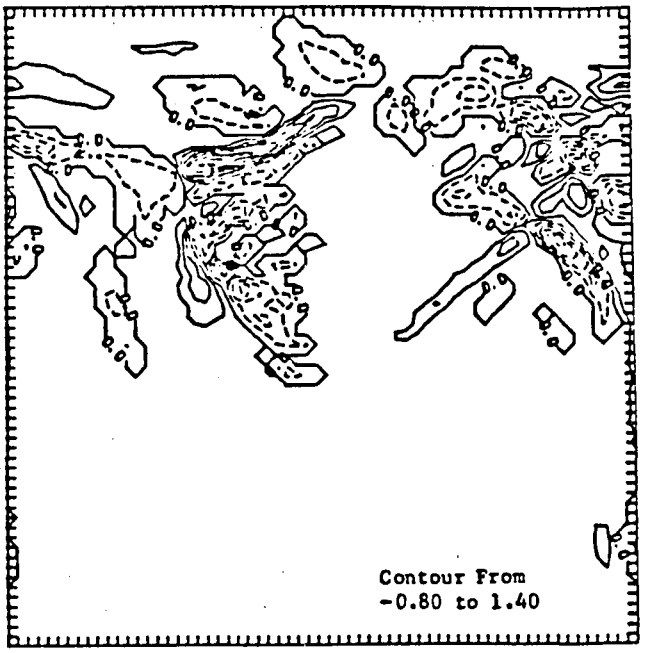

Figure 28 Streamwise component of vorticity, run1 (no heat release), streamwise location x=π, t=72.

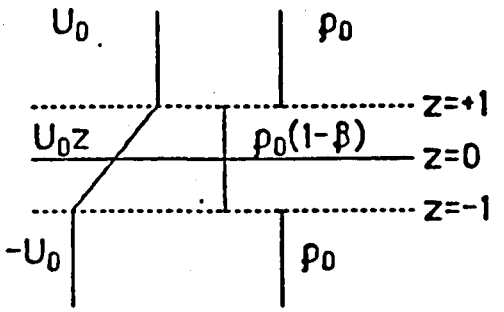

Figure 29 Configuration for stability analysis.

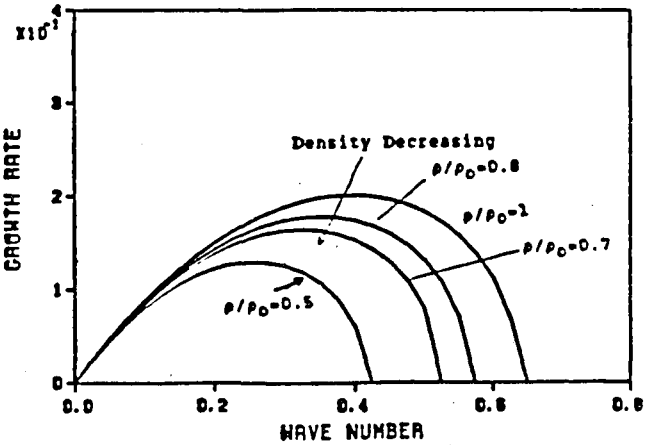

Figure 30 Stability anaysis results.

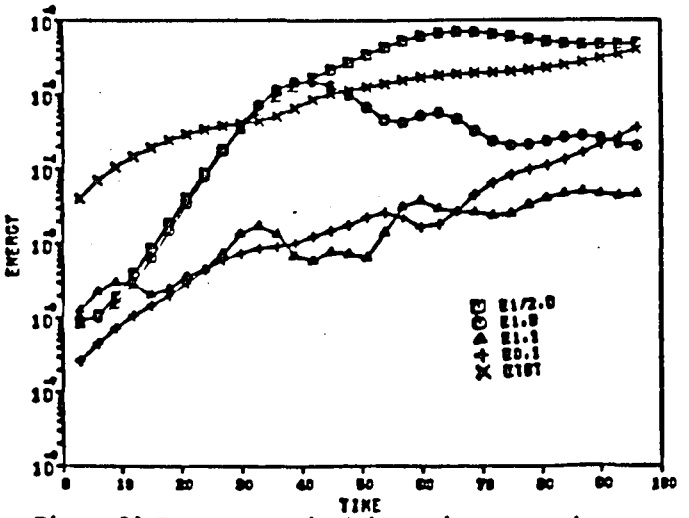

Figure 31 Energy contained in various wavnumbers, run1 (no heat).

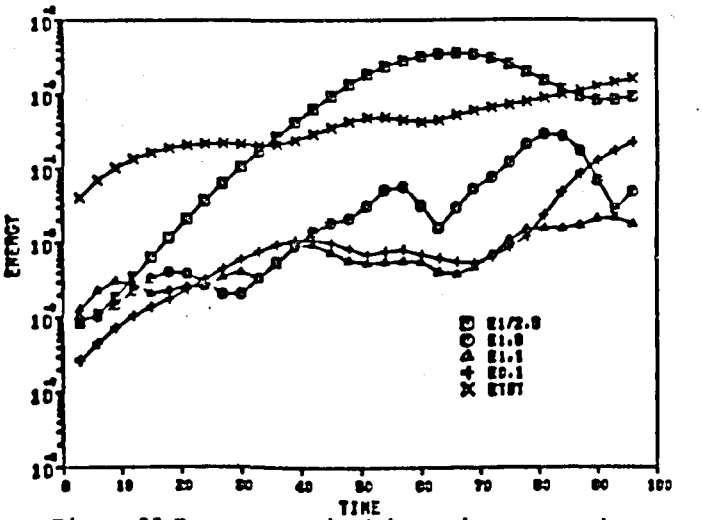

Figure 32 Energy contained in various wavenumbers, run2 (heat).

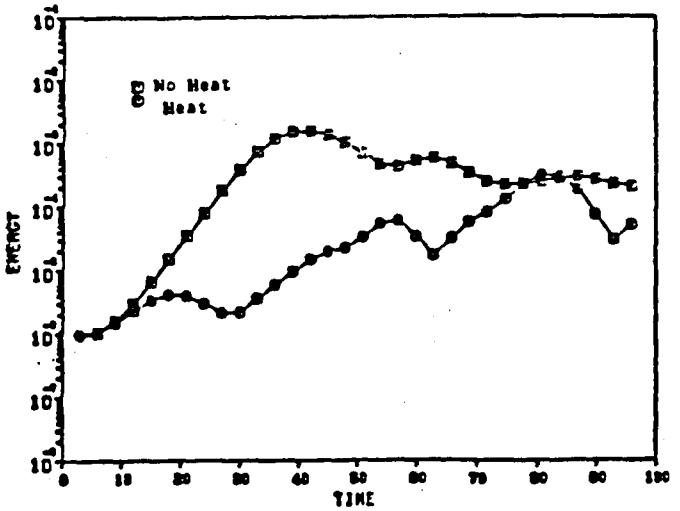

Figure 33 Comparison of energy in fundamental mode, runs 1 and 2.

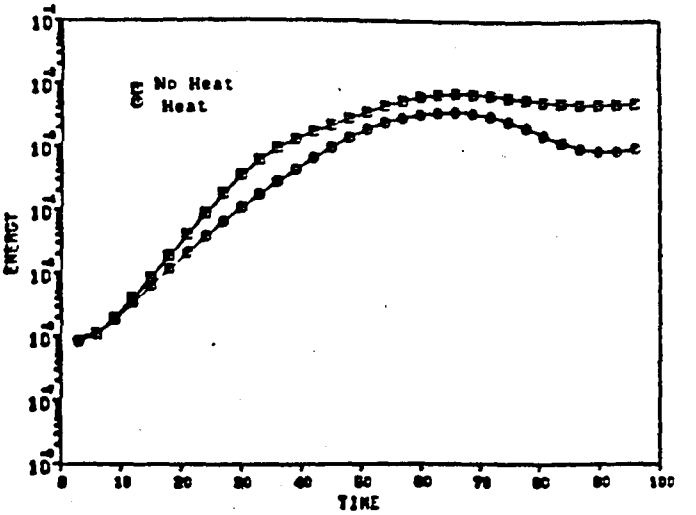

Figure 34 Comparison of energy in subharmonic, runs 1 and 2.

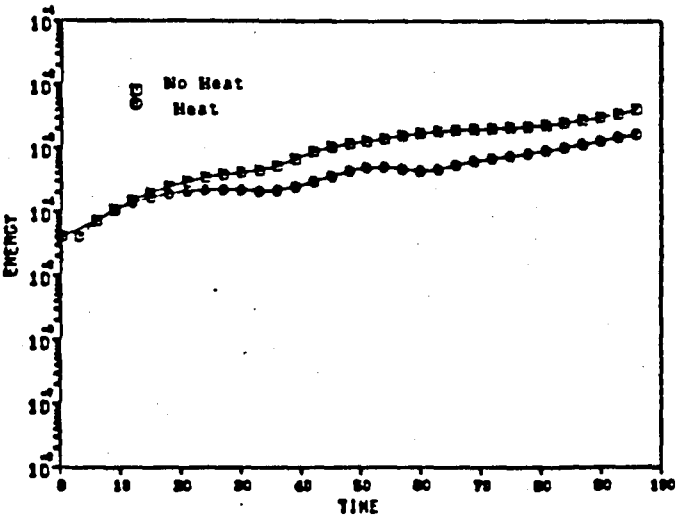

Figure 35 Comparison of energy in three-dimensional modes, runs 1 and 2.

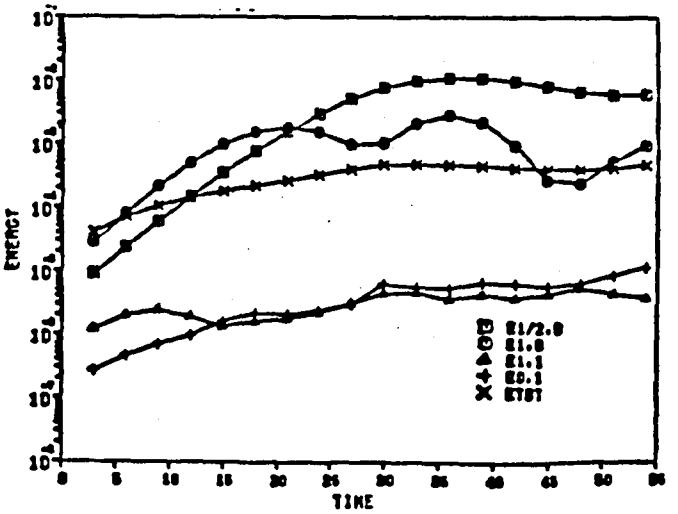

Figure 36 Energy contained in various wavenumbers, run3 (no heat).

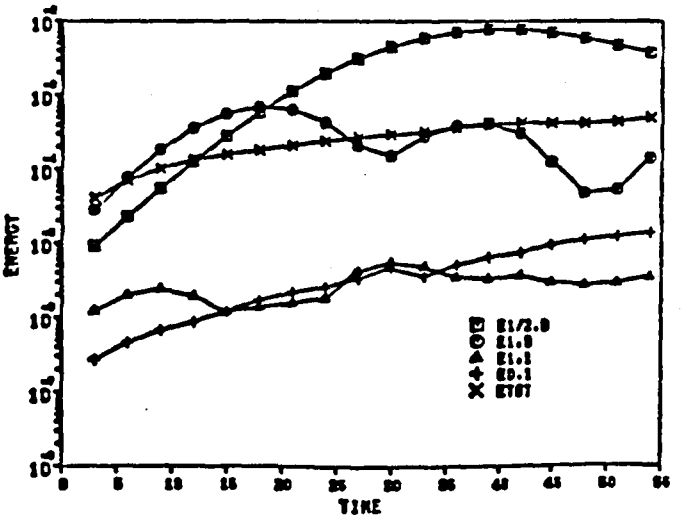

Figure 37 Energy contained in various wavenumbers, run4 (heat).

NASA
National Aeronautics and Space Administration

Report Documentation Page

1. Report No.	2. Government Accession No.	3. Recipient's Catalog No.
NASA CR-180853		

4. Title and Subtitle

Direct Simulations of Chemically Reacting Turbulent Mixing Layers - Part II

5. Report Date

June 1988

6. Performing Organization Code

7. Author(s)

Ralph W. Metcalfe, Patrick A. McMurtry, Wen-Huei Jou, James J. Riley, and Peyman Givi

8. Performing Organization Report No.

Flow Research Report No. 425

10. Work Unit No.

505-32-32

9. Performing Organization Name and Address

Flow Research Company
21414 68th Avenue South
Kent, Washington 98032

11. Contract or Grant No.

NAS3-24229

13. Type of Report and Period Covered

Contractor Report
Final

12. Sponsoring Agency Name and Address

National Aeronautics and Space Administration
Lewis Research Center
Cleveland, Ohio 44135-3191

14. Sponsoring Agency Code

15. Supplementary Notes

Project Manager, Russell W. Claus, Internal Fluid Mechanics Division, NASA Lewis Research Center.

16. Abstract

This report presents the results of direct numerical simulations of chemically reacting turbulent mixing layers. This is an extension of earlier work to a more detailed study of previous three-dimensional simulations of cold reacting flows plus the development, validation, and use of codes to simulate chemically reacting shear layers with heat release. Additional analysis of earlier simulations showed good agreement with self-similarity theory and laboratory data. Simulations with a two-dimensional code including the effects of heat release showed that the rate of chemical product formation, the thickness of the mixing layer, and the amount of mass entrained into the layer all decrease with increasing rates of heat release. Subsequent three-dimensional simulations showed similar behavior, in agreement with laboratory observations. Baroclinic torques and thermal expansion in the mixing layer were found to produce changes in the flame vortex structure that act to diffuse the pairing vortices, resulting in a net reduction in vorticity. Previously unexplained anomalies observed in the mean velocity profiles of reacting jets and mixing layers were shown to result from vorticity generation by baroclinic torques.

17. Key Words (Suggested by Author(s))	18. Distribution Statement
Turbulent flow Chemical reaction Direct simulation	Unclassified - Unlimited Subject Category 34

19. Security Classif. (of this report)	20. Security Classif. (of this page)	21. No of pages	22. Price*
Unclassified	Unclassified	59	A04

NASA FORM 1626 OCT 86

*For sale by the National Technical Information Service, Springfield, Virginia 22161

End of Document